

FINITE ELEMENT ANALYSIS AND LIFE ESTIMATION OF A PERMANENT
CYLINDRICAL MOLD WITH ANSYS AND COFFIN-MANSON APPROACH

Except where reference is made to the work of others, the work described in this thesis is my own or was done in collaboration with my advisory committee. This thesis does not include proprietary or classified information.

Ajay K Roy

Certificate of Approval:

Dr. J T. Black
Professor Emeritus
Industrial and Systems Engineering

Dr. Lewis N. Payton, Chair
Assistant Research Professor
Industrial and Systems Engineering

Dr. Ruel A. Overfelt
Associate Professor
Materials Engineering

Dr. Winfred A. Foster Jr.
Professor
Aerospace Engineering

Dr. Jerry Davis
Assistant Research Professor
Industrial and Systems Engineering

Steven L. McFarland
Acting Dean
Graduate School

FINITE ELEMENT ANALYSIS AND LIFE ESTIMATION OF A PERMANENT
CYLIDRICAL MOLD WITH ANSYS AND COFFIN-MANSON APPROACH

Ajay K Roy

A Thesis

Submitted to

the Graduate Faculty of

Auburn University

in Partial Fulfillment of the

Requirements for the

Degree of

Master of Science

Auburn, Alabama

May, 2005

FINITE ELEMENT ANALYSIS AND LIFE ESTIMATION OF A PERMANENT
CYLINDRICAL MOLD WITH ANSYS AND COFFIN-MANSON APPROACH

Ajay K Roy

Permission is granted to Auburn University to make copies of this thesis at its discretion, upon request of individuals or institutions and at their expense. The author reserves all publication rights.

Signature of Author

Date

Copy sent to:

Name _____ Date

VITA

Ajay K. Roy, son of Baikunth Roy and Kalawati Devi, was born October 1977, in Patna, Bihar, India. He graduated from St. Xavier's High School in 1993. He attended Science College in Patna, Bihar, India for two years. After working as a sales supervisor for two years, he entered Pune University, College of Engineering (Sangamner)'s Department of Production Engineering in July 1997 and graduated with distinction with a Bachelor of Engineering degree in Production Engineering, 2001. After working for one year as a Service and Manufacturing Engineer in Alfa Laval India Ltd., he entered the Graduate School at Auburn University, Department of Industrial and Systems Engineering, in August 2002.

THESIS ABSTRACT

FINITE ELEMENT ANALYSIS AND LIFE ESTIMATION OF A PERMANENT CYLINDRICAL MOLD WITH ANSYS AND COFFIN-MANSON APPROACH

Ajay K Roy

Master of Science, Industrial and Systems Engineering
Auburn University, 2005
(B.E. Pune University, 2001)

Directed by: Dr. Lewis Payton

Thermal fatigue is the most severe problem encountered by a permanent mold, leading to heat checking and cracking which affects the dimensional stability of the mold. Developing a methodology to determine the optimal diameter to thickness ratio to ensure the dimensional stability of a permanent cylindrical mold exposed to cyclic thermal loading is the focus of this work. In this research, thermal stress analysis was performed for multilayered cylindrical molds made up of 2 ¼ % Cr 1% Mo steel and 99% pure copper and cylindrical molds made up of 2 ¼ % Cr 1% Mo steel. Heating and cooling cycles of 10 and 25 seconds were applied to the inside surface, while the outside surface was water cooled. A 2-D (Plane strain) coupled-field analysis was performed using a thermal-elastic-plastic model accounting for the elastic, as well as, the plastic deformation with ANSYS. The Coffin-Manson equation was then used to

calculate fatigue life utilizing the strain amplitude was obtained from the finite element analysis. The results of the finite element analysis and the calculated fatigue life were validated against a widely accepted mathematical model's result and empirical industrial data. The method estimated the actual fatigue life observed in industry conservatively (within 5%).

ACKNOWLEDGMENTS

I wish to express my sincere appreciation to my committee members Dr. J T. Black, Dr. Lewis N. Payton, Dr. Ruel A. Overfelt, Dr. Winfred A. Foster and Dr. Jerry Davis.

Special recognition, however, goes to Dr. J T Black for encouraging and supporting me to start my career at Auburn University. I also thank him for his valuable guidance throughout my studies and for giving me the opportunity to gain some teaching experience. My gratitude extends as well to Dr. Lewis N. Payton for his constant interest and guidance.

I am most grateful to my parents for their support throughout all my endeavors. They have always been my source of inspiration. I am thankful to my friends and family members for always supporting me and boosting my confidence when my spirits were low.

Style manual or journal used: SME (Society of Manufacturing Engineers)

Computer software used: Microsoft Word, ANSYS, Microsoft Excel, Maple 9.5

TABLE OF CONTENTS

LIST OF FIGURES	x
LIST OF TABLES	xiv
NOTATIONS	xv
CHAPTER 1: INTRODUCTION	1
CHAPTER 2: LITERATURE REVIEW	5
CHAPTER 3: ANSYS 9.0 FEATURES AND SYNTAX	16
CHAPTER 4: METHODOLOGY, MODELS AND PARAMETERS.....	35
CHAPTER 5: RESULTS AND DISCUSSION.....	45
CHAPTER 6: CONCLUSIONS AND FUTURE WORK	57
REFERENCES	59
APPENDIX A (MATERIAL PROPERTIES).....	63
APPENDIX B (LOG FILE, ANSYS INPUT FILE).....	71
APPENDIX C (RESULTS FOR MONOLAYER CYLINDER, T=0.52”	91
APPENDIX D (RESULTS FOR MONOLAYER CYLINDER, T=0.95”.....	97
APPENDIX E (RESULTS FOR VALIDATION, OLIVER 1988)	103

LIST OF FIGURES

- Figure 1.1 Schematic of centrifugal casting
- Figure 2.1 Interaction between material, function, shape and process
- Figure 3.1 Geometry of Plane13 element
- Figure 3.2 Types of hardening rules
- Figure 3.3 Stress-strain behavior of multilinear isotropic plastic material
- Figure 3.4 Uniaxial behavior
- Figure 4.1 30.00 foot long mold
- Figure 4.2 2-D drawing of multilayer cylinder
- Figure 4.3 Cross section of cylinder showing dimensions
- Figure 4.4 Load curve
- Figure 4.5 Load and boundary conditions
- Figure 4.6 Stress-strain curve of steel (2¼% Cr 1% Mo) at different temperature
- Figure 4.7 Stress-strain curve of oxygen free high conductivity copper at different temperature
- Figure 5.1 Radial temperature (C) in multilayer cylinder at time 1,10 and 35 second
- Figure 5.2 Radial stress (Pa) in multilayer cylinder at time 1,10 and 35second
- Figure 5.3 Tangential stress (Pa) in multilayer cylinder at time 1,10 and 35 second
- Figure 5.4 Axial stress (Pa) in multilayer cylinder at time 1,10 and 35 second
- Figure 5.5 Equivalent stress (Pa) in multilayer cylinder at time 1,10 and 35 second
- Figure 5.6 Net displacement (m) in multilayer cylinder at time 1,10 and 35 second
- Figure 5.7 Equivalent plastic strain in multilayer cylinder at time 1,10 and 35 second
- Figure 5.8 Equivalent plastic strain in multilayer cylinder over time
- Figure 5.9 Total strain in multilayer cylinder over time
- Figure 5.10 Total strain difference in multilayer cylinder over time
- Figure 5.11 Fatigue life of mold vs thickness of mold

Figure A.1 Density of steel (2 ¼ % Cr 1% Mo) vs temperature
Figure A.1 Specific heat of steel (2 ¼ % Cr 1% Mo) vs temperature
Figure A.3 Elastic modulus of steel (2 ¼ % Cr 1% Mo) vs temperature
Figure A.4 Poisson's ratio of steel (2 ¼ % Cr 1% Mo) vs temperature
Figure A.5 Coefficient of expansion of steel (2 ¼ % Cr 1% Mo) vs temperature
Figure A.6 Thermal conductivity of steel (2 ¼ % Cr 1% Mo) vs temperature
Figure A.7 Density of copper vs temperature
Figure A.8 Specific heat of copper vs temperature
Figure A.9 Elastic modulus of copper vs temperature
Figure A.10 Poission ratio of copper vs temperature
Figure A.11 Coefficient of expansion of copper vs temperature
Figure A.12 Thermal conductivity of copper vs temperature
Figure C.1 Radial temperature (C) in monolayer cylinder at time 1,10 and 35 second
Figure C.2 Radial stress (Pa) in monolayer cylinder at time 1,10 and 35 second
Figure C.3 Tangential stress (Pa) in monolayer cylinder at time 1,10 and 35 second
Figure C.4 Axial stress (Pa) in monolayer cylinder at time 1,10 and 35 second
Figure C.5 Equivalent stress (Pa) in monolayer cylinder at time 1,10 and 35 second
Figure C.6 Net displacement in monolayer cylinder at time 1,10 and 35 second
Figure C.7 Equivalent plastic strain in monolayer cylinder at time 1, 10 and 35 second
Figure C.8 Equivalent plastic strain in monolayer cylinder over time
Figure C.9 Total strain in monolayer cylinder over time
Figure C.10 Total strain difference in monolayer cylinder over time
Figure D.1 Radial temperature (C) in monolayer cylinder at time 1,10 and 35 second
Figure D.2 Radial stress (Pa) in monolayer cylinder at time 1,10 and 35 second
Figure D.3 Tangential stress (Pa) in monolayer cylinder at time 1,10 and 35 second
Figure D.4 Axial stress (Pa) in monolayer cylinder at time 1,10 and 35 second
Figure D.5 Equivalent stress (Pa) in monolayer cylinder at time 1,10 and 35 second
Figure D.6 Net displacement in monolayer cylinder at time 1,10 and 35 second
Figure D.7 Equivalent plastic strain in monolayer cylinder at time 1, 10 and 35 second

- Figure D.8 Equivalent plastic strain in monolayer cylinder over time
- Figure D.9 Total strain in monolayer cylinder over time
- Figure D.10 Total strain difference in monolayer cylinder over time
- Figure E.1 Radial temperature profile in a composite tube with a 6 mm Steel OD layer – 18 mm Cu middle layer – 6 mm Steel ID Layer at 10 second
- Figure E.2 Radial stress in a composite tube with a 6 mm Steel OD layer – 18 mm Cu middle layer – 6 mm Steel ID Layer at 10 second
- Figure E.3 Tangential stress in a composite tube with a 6 mm Steel OD layer – 18 mm Cu middle layer – 6 mm Steel ID Layer at 10 second
- Figure E.4 Axial stress in a composite tube with a 6 mm Steel OD layer – 18 mm Cu middle layer – 6 mm Steel ID Layer at 10 second
- Figure E.5 Equivalent stress in a composite tube with a 6 mm Steel OD layer – 18 mm Cu middle layer – 6 mm Steel ID Layer at 10 second
- Figure E.6 Equivalent plastic strain in a composite tube with a 6 mm Steel OD layer – 18 mm Cu middle layer – 6 mm Steel ID Layer at 10 second
- Figure E.7 Radial temperature profile in a composite tube with a 6 mm Steel OD layer – 18 mm Cu middle layer – 6 mm Steel ID Layer at 10 second
- Figure E.8 Radial stress in a composite tube with a 6 mm Steel OD layer – 18 mm Cu middle layer – 6 mm Steel ID Layer at 10 second
- Figure E.9 Tangential stress in a composite tube with a 6 mm Steel OD layer – 18 mm Cu middle layer – 6 mm Steel ID Layer at 10 second
- Figure E.10 Axial stress in a composite tube with a 6 mm Steel OD layer – 18 mm Cu middle layer – 6 mm Steel ID Layer at 10 second
- Figure E.11 Equivalent stress in a composite tube with a 6 mm Steel OD layer – 18 mm Cu middle layer – 6 mm Steel ID Layer at 10 second
- Figure E.12 Equivalent plastic strain in a composite tube with a 6 mm Steel OD layer – 18 mm Cu middle layer – 6 mm Steel ID Layer at 10 second
- Figure E.13 Radial temperature in a composite tube with a 6 mm Steel OD layer – 18 mm Cu middle layer – 6 mm Steel ID Layer at 10 second
- Figure E.14 Radial stress in a composite tube with a 6 mm Steel OD layer – 18 mm Cu middle layer – 6 mm Steel ID Layer at 10 second

Figure E.15 Tangential stress in a composite tube with a 6 mm Steel OD layer – 18 mm Cu middle layer – 6 mm Steel ID Layer at 10 second

Figure E.16 Axial stress in a composite tube with a 6 mm Steel OD layer – 18 mm Cu middle layer – 6 mm Steel ID Layer at 10 second

Figure E.17 Equivalent stress in a composite tube with a 6 mm Steel OD layer – 18 mm Cu middle layer – 6 mm Steel ID Layer at 10 second

Figure E.18 Equivalent plastic strain in a composite tube with a 6 mm Steel OD layer – 18 mm Cu middle layer – 6 mm Steel ID Layer at 10 second

Figure E.19 Total strain in a composite tube with a 6 mm Steel OD layer – 18 mm Cu middle layer – 6 mm Steel ID Layer at 10 second

Figure E.20 Total strain difference in a composite tube with a 6 mm Steel OD layer – 18 mm Cu middle layer – 6 mm Steel ID Layer at 10 second

LIST OF TABLES

Table 3.1	Summary of multilinear isotropic plastic option	25
Table 5.1	Results for multilayer cylinder analysis.....	46
Table 5.2	Results available in Appendix C	46
Table 5.3	Results available in Appendix D.....	47
Table 5.4	Calculation and validity of fatigue life.....	55

NOTATIONS

Variable	Definition
$\{\epsilon_{el}\}$	elastic strains
ρ	density (DENS)
C	specific heat (C)
EX	elastic modulus (E)
$PRXY$	poisson ratio (ν)
$ALPX$	coefficient of expansion (α)
T	temperature (Temp)
t	Time
$\{\epsilon_{pl}\}$	plastic strains
$\{\epsilon_{tr}\}$	trial strain
$\{\epsilon_{th}\}$	thermal strain
$\{\epsilon_{cr}\}$	creep strain
$\{\epsilon_{sw}\}$	swelling strain
$\{\epsilon\}$	total strain
$\hat{\epsilon}^{pl}$	equivalent plastic strain
$\{\sigma\}$	Stresses
σ_e	equivalent stress
σ_y	material yield parameter
σ_m	mean stress
$\hat{\sigma}_e^{pl}$	equivalent stress parameter
λ	plastic multiplier

Variable	Definition
$\{\alpha\}$	yield surface translation
κ	plastic work
C	translation multiplier
[D]	stress-strain matrix
ET	tangent modulus
F	yield criterion
N	stress ratio
Q	plastic potential
$\{S\}$	deviatoric stress
q	heat flux (heat flow)
	heat generation rate per unit volume
$\{L\}$	vector operator
v	Velocity
K	thermal conductivity
h_f	film coefficient

CHAPTER 1: INTRODUCTION

Casting is the process wherein molten material is poured into a mold and allowed to solidify. Centrifugal casting (Figure 1.1) is one of the casting methods commonly used to make parts, in particular axi-symmetrical parts, hollow parts and structures with large diameters such as pipes, pressure vessels and cylindrical liners. Centrifugal force is exerted on liquid molten metal by spinning the mold, whereupon liquid metal solidifies on the inner wall of mold producing a sound casting. The mold is generally a long, hollow tube lined with a centrifugally applied refractory material in a slurry form, which is subsequently dried and baked.

This study focuses on the permanent cylindrical mold, its thermal management, thermal fatigue life and dimensional stability. Thermal fatigue is encountered by molds leading to heat checking and cracking. The time taken to develop the crack determines the life of the mold. The size and thickness of the mold determines the thermal and mechanical load it can withstand and cooling rate or cycle time it requires for a given material. Thus selecting the optimal diameter to thickness ratio or inside diameter to thickness ratio is a vital step in the customization of a cylindrical mold. A methodology is developed to determine the optimal diameter to thickness ratio to ensure the dimensional stability of a permanent cylindrical mold that will be exposed to a cyclic thermal loading on the inner surface with cooling on the outer surface.

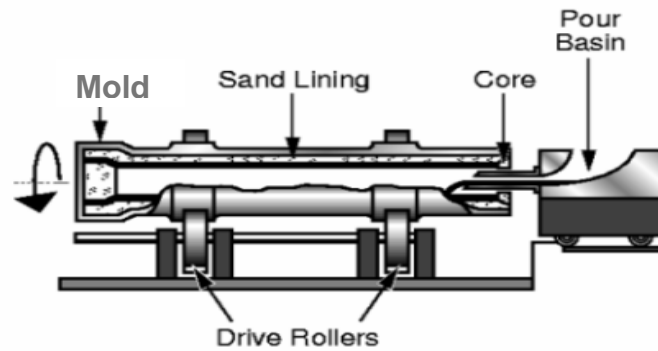


Figure 1.1 Schematic of centrifugal casting (Janco, 1988)

To improve the method used to select the most appropriate mold material and estimate the location of failure and the life of the mold, a two step approach was used in this study. The steps are listed below and discussed briefly in the following paragraphs:

- 1). Finite element analysis
- 2). Prediction of fatigue life

In the finite element method, a structure is broken down into many small, simple blocks or elements. The behavior of the individual elements can be described with a relatively simple set of equations. Just as the set of elements would be joined together to build the whole structure, the equations describing the behavior of individual elements are joined into an extremely large set of equations that describes the behavior of the whole structure. A computer can then be used to solve this large set of equations.

There are many software packages available for finite element analysis. In this study, the ANSYS FEA package was used. ANSYS is a general purpose finite element modeling package that can be used to numerically solve a wide variety of mechanical problems. The centrifugal casting process involves rapid changes of the mold temperature with time and because of this temperature variation, steep thermal gradients

and high stresses are generated. When stresses pass the elastic limit or yield stress, the body experiences an irreversible strain (plastic strain). If this load is cyclic it accumulates enough plastic strain over time, to initiate failure or cracking. A coupled-field analysis using ANSYS was performed, which takes into account the interaction (coupling) between two or more fields of engineering. Thermal-stress analysis and fluid-structure analysis are both examples of coupled field analysis. This analysis provides detailed results, including information on the deformation, radial stress, tangential stress, equivalent stress, elastic strain, plastic strain, thermal strain, heat flow, temperature distribution, thermal gradient and stress ratio. These results were validated against results reported in literature. Using the results obtained from the finite element analysis, the life of the mold was estimated using the Coffin-Manson equation. Coffin and Manson worked independently on the thermal fatigue problem and proposed a characterization of fatigue life based on plastic strain amplitude (low cycle fatigue) (Suresh 1991).

Chapter 2 reviews the literature on stress analysis, fatigue life determination, finite element analysis and methods to improve the life of structures. Chapter 3 gives a brief overview of the finite element method and the ANSYS features used for modeling and describe the formulation of the system equation for the features. Chapter 3 also highlights the method followed by ANSYS to obtain the solution (implementation). Chapter 4 describes the methodology for this study and gives details of the model and parameters used for the finite element analysis. Chapter 5 contains the results and discussion of the multilayer (steel-copper-steel) cylinder as well as results of the monolayer (steel) cylinder of thickness 0.52” and 0.95”.

CHAPTER 2: LITERATURE REVIEW

Thermal fatigue is a severe problem encountered in permanent molds. It results from the cyclic, rapid and asymmetric heating and cooling experienced by molds and is one of the major causes of poor quality casting and mold failures. Cyclic temperatures induce stress and strain conditions due to the thermal expansion or contraction of a section that is restrained by the surrounding material. Thermal stress develops as the result of the thermal gradient across a section. This thermal gradient arises because of the heating and cooling of the surface during the pouring, cooling, ejecting, lubricant coating and spraying stages of casting cycle. When the molten material is poured into the mold, the mold surface heats up considerably more than the inner section of the mold, setting up a steep thermal gradient. As a result, the outer surface expands more than the inner section, but as the interior is more massive, it prevents the outer surface from expanding. Plastic deformation will occur when these stresses exceed the yield strength of the mold material, and with sufficient cycling, micro-cracks will nucleate. Cracking starts after a number of cycles, but once initiated the cracks will propagate at a very fast rate. Heat checking also affects the surface, leading to defective castings and mold failure. This is a thermal fatigue phenomenon resulting from the rapid cyclic expansion of the mold surface layer as it comes into contact with the molten metal and

the constraint of the surface by the much cooler inner portion of the mold (Tanka, et al. 1993).

In order to understand the physics behind plastic deformation, heat checking and the life of the mold, it is necessary to study the subject in detail. This study applied the finite element method to analyze a cylindrical mold subjected to a thermal and mechanical load. This chapter reviews the literature on the stresses generated in cylindrical shapes subjected to thermal and mechanical loads. The critical factors affecting the life of cylindrical structures and the methods and techniques used to analyze the phenomenon are discussed along with the measures to prevent or delay the crack initiation, so that the life of the mold can be extended.

Duhamel conducted the first study on a long circular cylinder with a symmetrical temperature distribution about the axis in 1838 and proposed a method to calculate the elastic stress. Timoshenko and Goodier (1970) also reported the elastic solutions for several cases of thermal loading of cylindrical shapes. Both these studies calculated the values of the displacement (U), stresses (σ), and elastic strain, but these solutions are valid only in the elastic region, where the applied stresses do not exceed the yield strength of the material. Unfortunately in many real-world cases, the applied stress exceeds the yield strength of the material, at this point the plastic deformation occurs, and any value of stress calculated based on elasticity theory will be in error.

Wohler conducted systematic investigations of fatigue failure during the period 1852-1869 in Berlin (Suresh 1991). His work led to the characterization of fatigue behavior in terms of stress amplitude life (S-N) curves, which many fatigue life predictions used today are based on.

To better approximate the stresses and strains when yielding occurs, Mendelson and Manson (1956) developed a technique which accounts for plastic deformation due to thermal loading. Their technique consists of deriving strain equations in terms of temperature and plastic yielding from the equilibrium, compatibility, and stress-strain relationships for the geometric shape and materials under investigation. The strains are then calculated by an iterative technique, taking into account the plastic flow of the material being analyzed. Stresses are then calculated from the general stress- strain equations.

Coffin (1954) studied cyclic strain and fatigue failure arising from cyclic thermal stresses. A cyclic temperature was experimentally imposed on a thin, tubular 347 stainless steel (annealed) test specimen subjected to longitudinal constraint. The studies examined the effect of thermal stress cycling on strain hardening and life to failure for a fixed mean temperature, effect of degree and kind of previous cold work on strain hardening and cycles to failure, effect of mean temperature on thermal stress cycling, effect of period of cycles on cycles to failure and effect of prior strain cycling on stress-strain characteristics. Coffin concluded that strain hardening is not an important factor in the problem and discussed the concept of total plastic strain. Coffin and Manson established a notion that plastic strains are responsible for cyclic damage (Suresh 1991). They noted that when the logarithm of the plastic strain amplitude, $\Delta \epsilon_p / 2$ was plotted against the logarithm of the number of load reversals to failure, $2N_f$, a linear relationship resulted for metallic materials, i.e.

$$\Delta \epsilon_p / 2 = \epsilon_f' (2N_f)^c \quad 2-1$$

Where ϵ_f' is the fatigue ductility coefficient and c is the fatigue ductility exponent. In general, ϵ_f' is approximately equal to the true fracture ductility ϵ_f in monotonic tension, and c is in the range of -0.5 to -0.7 for most metals.

Hanson (1958) used the Mendelson and Manson technique to compare the deformation and incremental theories of plasticity in the solution of two boundary value problems. The deformation theory assumes that the state of stress and strain existing in the body depends only on the current load. Thus, this theory does not account for the prior plastic strain due to prior loading and is therefore load-path independent. Using the incremental theory, the loading and unloading cycle is divided into several small load increments. Stresses and strains are then calculated based on these small load increments, and any plastic strains that occur during a load increment or during prior load increments has a accumulative effect on the stress-strain state. The incremental theory's ability to account for plasticity due to small changes in load makes stress strain calculations load path dependent.

The first problem Hanson addressed concerned the stress analysis of a solid cylindrical rod of 18-8 stainless steel quenched from 538° C. A stress analysis was performed using both the deformation and incremental theories of plasticity, and the results of each analysis were compared. The second problem in the study was the stress analysis, again applying both the deformation and incremental theories of plasticity, of a thin circular disc when heated on the outside diameter. Hanson found that the results of the analyses from both the deformation and incremental theories were in agreement until unloading occurred. Upon unloading however, the values of stress calculated from

each theory differed. Hanson's experimental evidence indicated that the incremental theory was more predictive of stress-strain state than was the deformation theory.

Manson and Robert (1981) extended the Mendelson and Manson (1956) technique in order to determine the thermal fatigue life of a rotating solid disc when subjected to thermal loading. The load conditions were similar to those experienced by discs in jet engines. Strain range values were calculated based on the mechanical and thermal loading cycles and a thermal fatigue life was predicted.

Gene Oliver (1988) analyzed and optimized a multilayer tube's thermal fatigue life when subjected to cyclic thermal loading on the inside surface. In this study the thermal load was taken as a constraint and held constant. The thermal gradient, on the other hand, could be reduced, either by the selection of a high thermal conductivity material or by thinner shell design. To achieve a lower thermal gradient, enhance the dimensional stability and increase the abrasion resistance, a three layered sandwich design was proposed. Total strain equations expressed in terms of temperature and plastic strain for a cylindrical tube were derived. An equation to determine the radial temperature profile as a function of time, heat input, interface heat transfer coefficients, alloy thermal properties and thickness of the layers was also derived. The finite difference method and incremental theory was used to solve the derived equation for a multilayered cylinder. The temperature profile obtained for the inside surface of the hollow cylinder by Oliver (1988) was used in this work to describe the load curve applied on the inside surface of the cylinder as discussed and plotted in Chapter 3.

Givens (1996) developed a method for a detailed stress/strain analysis of a coker burner pressurized vessels and the laminated cylindrical shells with multi-

directional lay-up angles. To accomplish this method he first developed and tested finite element models for use with ANSYS program, then obtained the stress/strain response of burner vessels subjected to internal pressure and laminated shells subjected to an internal pressure and axial load. The analysis reported here used the cut boundary displacement method to develop a finite element model and the appropriate submodels to analyze the entire burner vessel including all major openings. The peak stress was compared with the far-field stresses determined using the finite element results for internal pressure simulation and found to be 50% lower than those found from physical experiments.

Wang (2000) used the finite element method to estimate the life of the dies used in casting, namely the number of thermal cycles before the die surface reached a failure level. He performed a thermal-visco-elastic stress analysis using FEM for a 1-D simple die casting model and a more complex 3-D dumbbell die casting structure. Wang used MMO software for his analysis and evaluated the effective plastic strain at the die surface. The point where the maximum effective plastic strain increment occurred was assumed to be the point of failure in the die. The Coffin-Manson equation was used to estimate the life of the die, which was composed of H13 steel and Aluminum 380. Elements with 8 nodes and 20 nodes were developed and compared for accuracy of result obtained, when the developed elements are used for mesh generation. The interactions between the thermal and mechanical processes are included by coupling the thermal and stress analysis.

Sirinterlikci (2000) focused on the thermal and structural issues to develop an analytical approach, diagnosing the areas susceptible to heat checking in order to

estimate the number of shots before the onset of heat checking. He also attempted to identify the critical factors associated with the structural state (stress/strain) within the die tool itself. Spray tests were conducted to determine the heat transfer coefficient during the lubricating spray phase. He examined factors such as the tempering, cyclic loading, elevated temperature material properties, temperature cycling and influence of mechanical loading on the structural state within the tooling. His thermal and structural analysis yielded acceptable results, although the fatigue calculations overestimated the number of cycles to produce heat checking. However, the structural and fatigue analyses were successful in the diagnosis of critical tooling areas which are prone to heat checking. Structural analysis was identified as the most effective approach to reduce the structural abuse.

To explore the differences between the Tresca and Von Mises yield criteria for loading-unloading-reloading plastic analyses, Ortega (1993) conducted a parametric study using finite element method. A program was written for the one dimensional, elastic plastic analysis of cylinders under positive internal and negative external pressure. An isotropic hardening condition was assumed. The results obtained from the analysis were then compared with the commercially available finite element analysis package - ANSYS 44A. The effect of the order of polynomials used to approximate the solution was studied, but the results were valid only for the one-dimensional finite element analysis of thick walled cylinders. Ortega found that the Von Mises yield criteria is very simple to apply and that the Tresca yield surface grows faster than the Von Mises surface. Thus, if a cylinder is subjected to pressure loading that causes yielding, the difference between the two criteria is decreased for the pure shear

condition. For uniaxial tension, the Tresca and VonMises criteria is equivalent, but after loading, these criteria diverge.

Alimi (1989) developed a numerical method to analyze thermal stresses and displacement in cylindrical shells. The thermal fatigue of a section of a heavy duty brake drum was studied to illustrate the application of the method developed. This study also included a custom program written in Fortran IV. Alimi proposed the use of a three layered (cast iron- copper- cast iron) composite tube rather than brake drums made of pure cast iron. This study demonstrated that the multilayer cylinder may reduce the thermal fatigue problem in brake drums and concluded that stainless steel would be a better material to use for outer layer, although the cost of stainless steel is much higher than that of cast iron.

Sirkis (1988) presented a two-dimensional hybrid experimental-numerical technique for elastic-plastic stress analysis, combining two techniques: the boundary element method and image processing. “Displacement Pattern Matching”, which is a pattern recognition scheme, determines the boundary conditions to be used in an elastic-plastic boundary element code. This is a very interesting study because boundary conditions are acquired from the actual specimen by comparing digitized images with a double exposure format. The results obtained using this method compared well with an ANSYS analysis and many experimental solutions like a perforated strip tensile test, V-notched specimen tensile test. However, this method works well only with static systems, i.e. when motion of the body is negligible. The specimen size used in this study was small, making it easier to process the image but if the sample size is large as

in a mold, which may be up to 30 feet long with a radius of between 8 inches to 60 inches, it is often very difficult to process the image and obtain the boundary conditions.

Hah (1997) studied the most proficient modeling techniques for moment resisting frames by applying nonlinear finite element techniques and the concept of parallel elasto-plastic material modeling into a nonlinear finite element analysis. The goal of this dissertation was to make the commercial nonlinear finite element application packages more practical, user friendly and economical. A simple cantilever beam with a concentrated tip load that is capable of producing a plastic hinge at the cantilever support was used as an example in the study. A special set of moment resisting frames, used to make up the skeleton of the structure to support a two floor facility was also examined. Hah concluded that to account for dynamic effects in the structure behavior, the number of elements should be sufficient to account for mass distribution. Parallel processing is advantageous for such problems because it reduces the effort needed to add the elements that account for material nonlinearity. Plates, shell buckling and snap-through problems may also benefit from parallel element techniques. The auto-stepping algorithm, used by most FEA packages proved to be very useful in the analysis.

Ruan (1990) investigated the solidification stage of casting, to produce results that may be useful in the design of solidification processes with a specific freezing front motion. Ruan presented a two-dimensional finite element model of the heat transfer and thermo mechanical behaviors associated with the solidification process, that is very useful in tracking the solid/liquid interface, allowing the and thermal and mechanical conditions to be modeled with ease. This work may be very useful in obtaining the

thermal load curve on the mold in the current study. However, while modeling the solidification process, the effect of air-gap formation was neglected, thus affecting the heat transfer and thermal stress.

White (1997) modeled multilayer thin film structures using analytical solution and hybrid finite element methods. Sharp edges and multimaterial wedges were included in this treatment. The hybrid finite element method formulates a special element containing a singularity to be employed in the region of the free edges, while regions beyond the free edges are represented by conventional elements. Combining classical techniques and finite element solutions helps to obtain the stress field with the least number of elements. Multilayer Structures (MLS) were used to provide solutions for both steady state and transient problems. MLS also assisted in predicting the location of crack initiation and adhesion failures between layers. A structure consisting of a thin film of AlN (substrate) of 0.64 mm (25mil) thickness, BCB (dielectric) of 10 μ m thickness, and copper (metallization) of thickness 5 μ m was modeled using MLS. The program developed for this study could be used to study the thin oxide layer formed on the inside surface of a cylindrical mold.

Okono (1978) used the finite element method to conduct a heat transfer analysis in solid propellant rocket motors modeled as long, hollow, circular cylinders subjected to a randomly varying temperature. For this analysis, the nonhomogeneous cylindrical structure was subdivided into homogeneous concentric regions and treated as thermorheologically simple viscoelastic rings. A probabilistic approach was used for the description of strength and induced thermal stress, since a random thermal response and a random material strength were produced by the random environmental temperature.

Using the assumption of a plane strain condition, the end effects were neglected. The probability of failure was calculated based on probability distributions of material strength and induced thermal stress using Maximum Stress Theory and the Maximum Strain Theory. A normal distribution was hypothesized and a chi-square test was performed to verify the normality assumption. The estimation of the service life was based on the assumption that the annual thermal history would be repetitive. Poisson's ratio was taken to be 0.49 which implies that material is slightly compressible. In this investigation, tangential stress was found to have a profound effect on the failure of the motor, although the method took a long time to conduct the stress analysis and to obtain the data needed for a meaningful failure prediction. Mechanical and thermal loads could not be combined by this method as it is only good for thermal loads and hence was limited in application.

Numerous studies have examined different aspects of the casting process. Numerical solutions have been obtained from custom programs, written in different computer languages, to analyze a cylinder subjected to thermal and mechanical loads. In order to incorporate new parameters the programs developed are generally very difficult to modify and moreover the codes are not widely available. However the thermal behavior of a cylindrical mold can be conveniently analyzed using the finite element method. In the past, the finite element method has been used to study pressure vessels (Given 1996), dies (Wang 2000), solid propellants in rocket motors (Okono 1978) and brake drums (Alimi 1989), all of which involved commercially available finite element modeling software. There are many commercial finite element modeling software packages available which can be used to analyze the permanent cylindrical mold, such

as ANSYS, ABACUS, NASTRAN and ALGOR to name a few. Finite element analysis of the cylindrical mold using any one of the commercially available packages will greatly simplify the otherwise complex computer programming need for this project. This study will make an effort to verify that the available finite element modeling packages have the capability to model complex material behavior with reasonable accuracy.

CHAPTER 3: ANSYS 9.0 FEATURES AND SYNTAX

ANSYS is a finite element modeling and analysis software package that can be used to analyze complex problems in mechanical structures, thermal processes, computational fluid dynamics, magnetics and electrical fields, to mention just a few of its applications. The capability to automate common tasks or even build a model in terms of the parameters using “ANSYS Parametric Design Language (APDL)”, makes it more flexible. APDL also encompasses a wide range of features such as repeating a command, macros, choice of parallel processing, if-then-else branching, do-loops, and scalar, vector and matrix operations. ANSYS provides a rich graphics capability that can be used to display the results of the analysis on a high-resolution graphics workstation. This chapter, which is mainly based on the material provided in ANSYS 9.0 documentation (2004), summarizes the equations used by ANSYS features (used in this study like rate independent plasticity, multilinear isotopic hardening (MISO), implementation and thermal boundary conditions) to formulate the system equation. This chapter also gives a brief overview of finite element method.

3.1 Finite Element Method

The finite element method is a numerical procedure for solving physics problems governed by a differential equation as an energy theorem. It has two characteristics that distinguish it from other numerical procedures (Huebner et al. 2001):

- 1). The method utilizes an integral formulation to generate a system of algebraic equations.
- 2). The method uses continuous piecewise smooth functions (interpolation) for approximating the unknown quantity or quantities.

The finite element method can be subdivided into four basic steps. These steps are listed here (Huebner et al. 2001).

1). Discretization of the region: This includes the location and numbering of the nodes, as well as specifying their co-ordinate values.

2). Specification of the approximation equation (interpolation function): The order of the approximation, whether linear or quadratic, must be written in terms of the unknown nodal values. An equation is written for each element. It is important to choose a proper interpolation function, which satisfies certain convergence requirements. Polynomials are the preferred approximating functions for the following reasons

- A polynomial of infinite order corresponds to the exact solution, but it is sufficient to obtain approximate solution using finite order polynomials.
- It is easy to perform differentiation and integration with polynomials, hence it is easier to formulate a model by using a polynomial function, which is highly compatible with the computer.
- It is possible to increase the accuracy of the solution by simply increasing the order of the polynomial.

3). Development of the system of equations: The weighting function for each of the unknown nodal values is defined and the weighted residual integral is evaluated.

This generates one equation for each unknown nodal value. In the potential formulation, the potential energy of the system is written in terms of the nodal displacement and then is minimized, which in turn gives one equation for each of the unknown displacements.

4). Calculation of the quantities of interest: These quantities are usually related to the derivative of the parameter and include the stress components, heat flow and fluid velocities.

3.2 ANSYS

3.2.1 Basic flow of ANSYS

- Pre-Processor
 - 1) Defines material properties and their behavior.
 - 2) Defines the geometry and the important features.
 - 3) Handles discretization (meshing).
 - 4) Defines load and boundary conditions.
- Processor (Solution): This component handles the analysis and preprocessing of data, which involves the computation of element properties, assemblage of elements and solution of equations of equilibrium.
- Post-Processor: Reviewing the result is probably the most important step in the analysis, because it helps the user to understand the affect of an applied load on the design, the quality of the finite element mesh, and so on. The post-processor accepts the results of the analysis, computes stress and handles post-processing of the results through the generation of graphs, tables and pictures. Two post-processors may be used to review the results: the general post-processor (POST 1), and the time-history post-processor (POST 26). The general post-processor allows the user to review the results

over the entire model at specific load steps and substeps or at specific time-points or frequencies. The time-history post-processor allows the user to review the results over time.

3.2.2 Analysis capabilities and range of applications

ANSYS is capable of performing structural, thermal, fluid, electromagnetic and coupled field (CF) analyses. The thermal and structural analysis, which is used in this study is described briefly.

- Structural Analysis

This type of analysis is the most common application of FEA and is used primarily for mechanical and civil engineering applications. Structural analysis is possible in the many areas, two of them are described briefly in this chapter.

- Static Analysis: This ignores the effect of time varying loads, although it can include a time-varying load by approximating it as a static equivalent load. Static analysis is used to determine displacements, stresses, strains and forces induced by loads that do not cause significant inertia and damping effects.

- Transient Dynamic Analysis: This analysis can be used to determine the time-varying displacements, strains, stresses, and forces in a structure as it responds to any combination of static, transient, and harmonic loads. The time scale of the loading is such that the inertia or damping effects are considered to be important. The basic equation of motion solved by a transient dynamic analysis is

$$(M)\{\ddot{u}\} + (C)\{\dot{u}\} + (K)\{u\} = \{F(t)\} \quad (3-1)$$

where:

(M) = mass matrix

(C) = damping matrix

(K) = stiffness matrix

$\{\ddot{u}\}$ = nodal acceleration vector

$\{\dot{u}\}$ = nodal velocity vector

$\{u\}$ = nodal displacement vector

$\{F(t)\}$ = load vector

- Thermal Analysis

This type of analysis is used to calculate the thermal gradients, temperature distribution, heat transfer and thermal flux of an object. The analysis can be performed using conduction, convection and radiation heat transfer modes. Here a thermal analysis is followed by stress analysis in order to calculate the thermal stresses caused by thermal expansions or contractions. The analysis can be performed in the following two areas.

- Steady-State Thermal Analysis: A steady-state thermal analysis calculates the effects of steady thermal loads on a system or component. Steady-state thermal analysis can be used to determine temperatures, thermal gradients, heat flow rates, and heat fluxes in an object that are caused by thermal loads that do not vary over time. A steady state condition allows varying heat storage effects over time to be ignored.

- Transient Thermal Analysis: Transient thermal analysis is used to determine temperatures and other thermal quantities that vary over time. Loads in a transient analysis are functions of time. Transient thermal analysis can be used to determine temperatures, thermal gradients, heat flow rates, and heat fluxes in an object that are caused by thermal loads that vary over time. To specify time-dependent loads, the function tool can be used to define an equation or function describing the curve and

then the function is either applied as a boundary condition, or the load-versus-time curve can be divided into load steps. In this study a time dependent load curve (described in chapter 4) is specified.

- Coupled-field analysis

A coupled-field analysis is an analysis that takes into account the interaction (coupling) between two or more disciplines (fields) of engineering. A thermal-stress analysis, for example, handles the interaction between the structural and thermal fields: it can be used to solve for the stress distribution due to applied temperature, or vice versa. Other examples of coupled-field analyses are piezoelectric analysis, thermal-electric analysis, and fluid-structure analysis.

3.2.3 Element library

The ANSYS element library consists of more than 100 different element formulations or types. An element type is identified by a name (8 characters maximum). An element is selected from the library for use in the analysis by selecting from a drop down menu or inputting its name in the element type command. Elements are connected to the nodes in a specific sequence and orientation. This connectivity can be defined by automatic meshing, or may be input directly by the user. Each element type has a degree of freedom set, which constitute the primary nodal unknowns to be determined by the analysis. These may be displacements, rotations, temperatures, pressures, voltages, etc. Derived results, such as stresses, heat flows, etc., are computed from these degree of freedom results.

The element used for this analysis was PLANE13. This element has a two-dimensional structural and thermal field capability with coupling between the fields. It

also has magnetic, electrical and piezoelectric capability. This element is defined by four nodes with four degrees of freedom per node. Figure 3.1 shows the geometry of the element. U_x , U_y , Temp, A_z and volts can be used as degree of freedom for the nodes, but as discussed earlier only four of these degrees of freedom can be used per node. It can have convection or heat flow as surface load, but not both. If both are applied on the same surface, convection supersedes heat flow. The element will accept temperature and heat generation as the body load. A special feature of this element is that it takes care of large deflection, large strain, stress stiffening and birth and death. The PLANE13 element can behave as plane strain, plane stress or axisymmetric element.

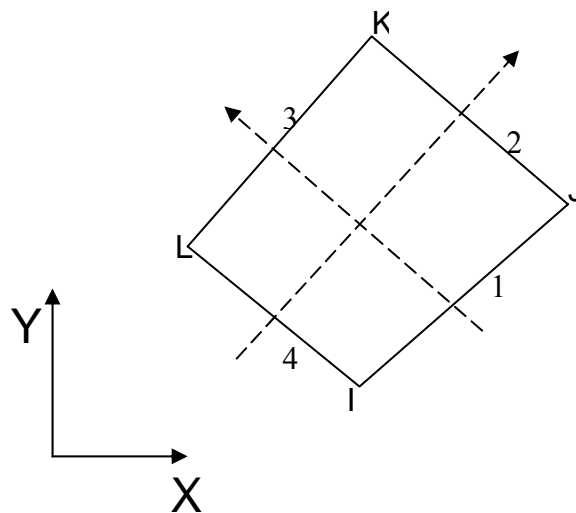


Figure 3.1: Geometry of PLANE13 element

3.2.4 Structures with Material Nonlinearities

Material nonlinearities arises due to the nonlinear relationship between stress and strain, that is, the stress is a nonlinear function of the strain. The relationship is also path dependent (except for the case of nonlinear elasticity and hyperelasticity), so that the stress depends on the strain history as well as the strain itself. The program can account for the material nonlinearities like rate-independent plasticity, creep,

hyperelasticity and viscoelasticity. In this study, rate independent plasticity, which is characterized by the irreversible straining that occurs in a material once a certain level of stress is reached, is used to account for material nonlinearities. The input for this feature is discussed in Chapter 4 and the formulation is described further in this chapter.

For the case of nonlinear materials, the elastic strain is given by:

$$\{\varepsilon^{el}\} = \varepsilon - \{\varepsilon^{th}\} - \{\varepsilon^{pl}\} - \{\varepsilon^{cr}\} - \{\varepsilon^{sw}\} \quad (3-2)$$

where:

ε^{el} = elastic strain vector

ε = total strain vector

ε^{th} = thermal strain vector

ε^{pl} = plastic strain vector

ε^{cr} = creep strain vector

ε^{sw} = swelling strain vector

And the total strain is :

$$\{\varepsilon^{tot}\} = \{\varepsilon^{pl}\} + \{\varepsilon^{th}\} + \{\varepsilon^{cr}\} \quad (3-3)$$

where:

ε^{tot} = component total strain

3.2.5 Rate-independent plasticity

Rate-independent plasticity is characterized by the irreversible straining that occurs in a material once a certain level of stress is reached. Plastic strains are assumed to develop instantaneously, independent of time. Plasticity theory provides a mathematical relationship that characterizes the elastoplastic response of materials.

There are three components involved in the rate-independent plasticity theory: the yield criterion, flow rule and the hardening rule. These will be discussed in detail below:

- Yield Criterion

The yield criterion determines the stress level at which yielding is initiated. For multi-component stresses, this is represented as a function of the individual components, $f(\{\sigma\})$, which can be interpreted as an equivalent stress σ_e :

$$\sigma_e = f(\{\sigma\}) \quad (3-4)$$

where:

$\{\sigma\}$ = stress vector

When the equivalent stress is equal to a material yield parameter σ_y ,

$$F(\{\sigma\}) = \sigma_y \quad (3-5)$$

the material will develop plastic strains. If σ_e is less than σ_y , the material is elastic and the stresses will develop according to the elastic stress-strain relationship.

- Flow Rule

The flow rule determines the direction of plastic strain and is given by:

$$\{d\epsilon^{pl}\} = \lambda \left\{ \begin{array}{c} \frac{\partial Q}{\partial \sigma} \end{array} \right\} \quad (3-6)$$

where:

λ = plastic multiplier (which determines the amount of plastic strain)

Q = a function of stress termed the plastic potential (which determines the direction of plastic strain)

- Hardening Rule

The hardening rule describes the change in the yield surface with progressive yielding, so that the conditions (i.e. stress states) for subsequent yielding can be established. Two hardening rules are possible in ANSYS: work (or isotropic) hardening and kinematic hardening. In work hardening, the yield surface remains centered about its initial centerline and expands in size as the plastic strains develop. For materials with isotropic plastic behavior, this is termed isotropic hardening and is shown in Figure 3.2 (a). Kinematic hardening assumes that the yield surface remains constant in size and the surface translates in stress space with progressive yielding, as shown in Figure 3.2 (b). The ANSYS program provides seven options with which to characterize different types of material behaviors. In this study, multilinear isotropic hardening rule “MISO” (Figure 3.3) was used to characterize the material behavior (refer to appendix A and appendix B for the input files for ANSYS). Table 3.1 summarizes the yield criterion, flow rule and hardening rule for multilinear isotropic plasticity option.

Name	Multilinear isotropic hardening
Yield Criterion	Von Mises/ Hill
Flow Rule	Associative
Hardening Rule	Work
Material	Multilinear

Table 3.1: Summary of multilinear isotropic plastic option

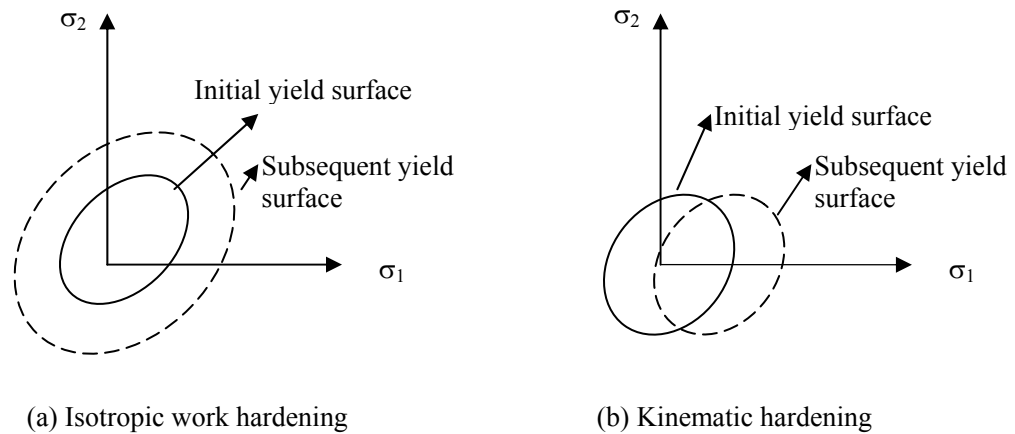


Figure 3.2: Types of hardening rules

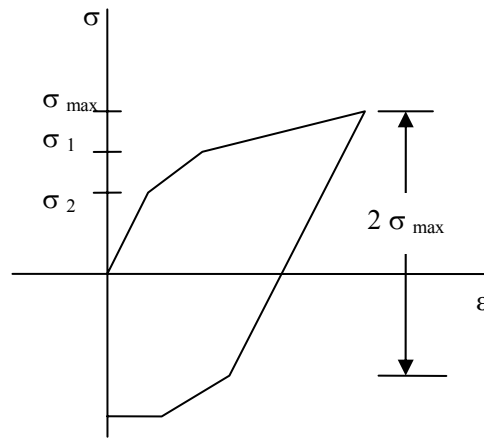


Figure 3.3 : Stress –strain curve for MISO behavior

3.2.6 Plastic strain increment

If the equivalent stress computed using elastic properties exceeds the material yield, then plastic straining must occur. Plastic strains reduce the stress state so that it satisfies the yield criterion given in, Equation 3-5. Based on the theory discussed earlier, the plastic strain increment is calculated. The hardening rule states that the yield criterion changes with work hardening and/or with kinematic hardening.

Incorporating these dependencies into Equation 3-5, and rearranging, we get:

$$F(\{\sigma\}, \kappa, \{\alpha\})=0 \quad (3-7)$$

where:

κ = plastic work

$\{\alpha\}$ = translation of yield surface

The plastic work is the sum of the plastic work done over the history of loading and expressed as:

$$\kappa = \int \{\sigma\}^T [M] \{d\varepsilon^{pl}\} \quad (3-8)$$

where:

$$[M] = \begin{bmatrix} 1 & 0 & 0 & 0 & 0 & 0 \\ 0 & 1 & 0 & 0 & 0 & 0 \\ 0 & 0 & 1 & 0 & 0 & 0 \\ 0 & 0 & 0 & 2 & 0 & 0 \\ 0 & 0 & 0 & 0 & 2 & 0 \\ 0 & 0 & 0 & 0 & 0 & 2 \end{bmatrix}$$

The translation (or shift) of the yield surface is also history dependent and is given as:

$$\{\alpha\} = \int C \{d\varepsilon^{pl}\} \quad (3-9)$$

where:

C = material parameter

Equation 3-7 can be differentiated so that the consistency condition is:

$$dF = \left\{ \frac{\partial F}{\partial \sigma} \right\}^T [M] \{d\sigma\} + \frac{\partial F}{\partial \kappa} d\kappa + \left\{ \frac{\partial F}{\partial \alpha} \right\}^T [M] \{d\alpha\} = 0 \quad (3-10)$$

from Equation 3-8 differential of plastic work is given as:

$$d\kappa = \{\sigma\}^T [M] \{d\varepsilon^{pl}\} \quad (3-11)$$

and from Equation 3-9 differential of translation is given as:

$$\{d\alpha\} = C\{d\varepsilon^{pl}\} \quad (3-12)$$

Then Equation 3-10 becomes

$$\left\{\frac{\partial F}{\partial \sigma}\right\}^T [M]\{d\sigma\} + \frac{\partial F}{\partial \kappa} \{\sigma\}^T [M]\{d\varepsilon^{pl}\} + C\left\{\frac{\partial F}{\partial \alpha}\right\}^T [M]\{d\varepsilon^{pl}\} = 0 \quad (3-13)$$

The stress increment can be computed via the elastic stress-strain relations

$$\{d\sigma\} = [D]\{d\varepsilon^{pl}\} \quad (3-14)$$

Where D is the stress-strain matrix

with

$$\{d\varepsilon^{el}\} = \{d\varepsilon\} - \{d\varepsilon^{pl}\} \quad (3-15)$$

since the total strain increment can be divided into an elastic and plastic part.

Substituting Equation 3-6 into Equation 3-13 and Equation 3-15 and combining Equation 3-13, Equation 3-14, and Equation 3-15 yields

$$\lambda = \frac{\left\{\frac{\partial F}{\partial \sigma}\right\}^T [M][D]\{d\varepsilon\}}{-\left\{\frac{\partial F}{\partial \kappa}\right\} \{\sigma\}^T [M]\left\{\frac{\partial Q}{\partial \sigma}\right\} - \left\{\frac{\partial F}{\partial \alpha}\right\}^T [M]\left\{\frac{\partial Q}{\partial \sigma}\right\} + \left\{\frac{\partial F}{\partial \sigma}\right\}^T [M][D]\left\{\frac{\partial Q}{\partial \sigma}\right\}} \quad (3-16)$$

The size of the plastic strain increment is therefore related to the total increment in strain, the current stress state, and the specific forms of the yield and potential surfaces. The plastic strain increment is then computed using Equation 3-6:

$$\{d\varepsilon^{pl}\} = \lambda \left\{\frac{\partial Q}{\partial \sigma}\right\} \quad (3-17)$$

3.2.7 Implementation

A Euler backward scheme is used to enforce the consistency condition in Equation 3-10. This ensures that the updated stress, strains and internal variables are all on the yield surface. The algorithm proceeds as follows:

1. The material parameter σ_y is determined for this time step (i.e. the yield stress at the current temperature).
2. The stresses are computed based on the trial strain $\{\varepsilon^{tr}\}$, which is the total strain minus the plastic strain from the previous time point.

$$\{\varepsilon_t^{pl}\} = \{\varepsilon_t\} - \{\varepsilon_{t-1}^{pl}\} \quad (3-18)$$

where the superscripts refer to the time point. The trial stress is

$$\{\sigma^{tr}\} = [D]\{\varepsilon^{tr}\} \quad (3-19)$$

3. The equivalent stress σ_e is evaluated at this stress level by Equation 3-4. If σ_e is less than σ_y the material is elastic and no plastic strain increment is computed.
4. If the stress exceeds the material yield, the plastic multiplier (λ) is determined as explained earlier.
5. Plastic strain increment ($\Delta\varepsilon^{pl}$) is computed via Equation 3-17.
6. The current plastic strain is updated

$$\{\varepsilon_t^{pl}\} = \{\varepsilon_{n-1}^{pl}\} - \{\nabla\varepsilon^{pl}\} \quad (3-20)$$

where:

$$\{\varepsilon_t^{pl}\} = \text{current plastic strains}$$

and the elastic strain computed

$$\{\varepsilon^{el}\} = \{\varepsilon^{tr}\} - \{\nabla\varepsilon^{pl}\} \quad (3-21)$$

where:

ε^{el} = elastic strains

The stress vector is:

$$\{\sigma\}=[D]\{\varepsilon^{el}\} \quad (3-22)$$

where:

$\{\sigma\}$ = stresses

7. The increments in the plastic work $\Delta\kappa$ and the center of the yield surface $\{\Delta\alpha\}$ are computed via Equation 3-11 and Equation 3-12 and the current values are updated

$$\kappa_t = \kappa_{t-1} - \Delta\kappa \quad (3-23)$$

and

$$\alpha_t = \alpha_{t-1} - \Delta\alpha \quad (3-24)$$

where the subscript t-1 refers to the values at the previous time point. For output

purposes, an equivalent plastic strain ($\varepsilon^{\wedge pl}$), equivalent plastic strain increment ($\Delta\varepsilon^{\wedge pl}$), equivalent stress parameter ($\sigma_e^{\wedge pl}$) are computed. The equivalent plastic strain increment is given by:

$$\Delta\varepsilon^{\wedge pl} = \left(\frac{2}{3} \{\Delta\varepsilon^{pl}\}^T [M] \{\Delta\varepsilon^{pl}\} \right)^{\frac{1}{2}} \quad (3-25)$$

Accumulated plastic strain is given by:

$$\varepsilon^{\wedge pl} = \sum \Delta\varepsilon^{\wedge pl} \quad (3-26)$$

3.2.8 Multilinear Isotropic Hardening

As explained earlier the multilinear isotropic hardening option uses the von Mises yield criterion with the associated flow rule and isotropic (work) hardening.

The equivalent stress Equation 3–4 is:

$$\sigma_e = \left(\frac{2}{3} \{S\}^T [M] \{S\} \right) \quad (3-27)$$

where $\{s\}$ is the deviatoric stress represented as:

$$\{S\} = \{\sigma\} - \sigma_m [1 \ 1 \ 1 \ 0 \ 0 \ 0]^T \quad (3-28)$$

When σ_e is equal to the current yield stress σ_k the material is assumed to yield.

The yield criterion is:

$$F = \left(\frac{2}{3} \{S\}^T [M] \{S\} \right) - \sigma_k = 0 \quad (3-29)$$

For work hardening, σ_k is a function of the amount of plastic work done. For the case of isotropic plasticity assumed here, σ_k can be determined directly from the equivalent plastic strain of Equation 3–29 and the uniaxial stress-strain curve in Figure 3.4. Here, σ_k is output as the equivalent stress parameter. For temperature-dependent curves with the MISO option, σ_k is determined by temperature interpolation of the input curves after they have been converted to stress-plastic strain format.

3.1.9 Thermal Analysis

The first law of thermodynamics states that thermal energy is conserved.

Applying this to a differential control volume:

$$\rho c \left\{ \frac{\partial T}{\partial t} + \{v\}^T \{L\} T \right\} + \{L\}^T \{q\} = \ddot{q} \quad (3-30)$$

where:

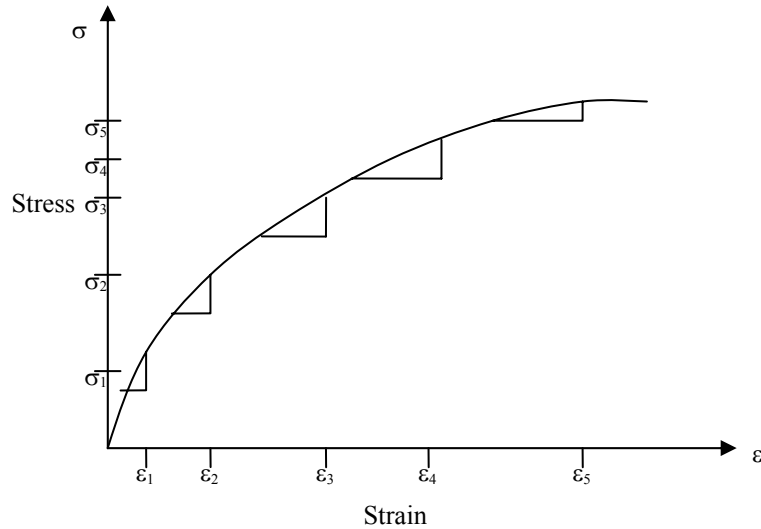


Figure 3.4: Uniaxial Behavior

ρ = density (input as DENS in ANSYS)

C = specific heat (input as C in ANSYS)

T = temperature ($T(x,y,z,t)$)

T = time

$\{q\}$ = heat flux vector (output as TFX, TFY, and TFZ)

\ddot{q} = heat generation rate per unit volume

$$\{L\} = \begin{Bmatrix} \frac{\partial}{\partial x} \\ \frac{\partial}{\partial y} \\ \frac{\partial}{\partial z} \end{Bmatrix} = \text{Vector operator}$$

$$\{v\} = \begin{Bmatrix} V_x \\ V_y \\ V_z \end{Bmatrix} = \text{Velocity vector for mass transport of heat.}$$

Next, Fourier's law is used to relate the heat flux vector to the thermal gradients:

$$\{q\} = -[D]\{L\}T \tag{3-31}$$

where:

$$D = \begin{bmatrix} K_{xx} & 0 & 0 \\ 0 & K_{yy} & 0 \\ 0 & 0 & K_{zz} \end{bmatrix}$$

K_{xx} , K_{yy} , K_{zz} = conductivity in the element x, y, and z directions, respectively

Combining Equation 3-30 and Equation 3-31,

$$\rho c \left\{ \frac{\partial T}{\partial t} + \{v\}^T \{L\} T \right\} = \{L\}^T ([D]) \{L\} T + \ddot{q} \quad (3-32)$$

Expanding Equation 3-32 to its more familiar form:

$$\rho c \left(\frac{\partial T}{\partial t} + V_x \frac{\partial T}{\partial X} + V_y \frac{\partial T}{\partial Y} + V_z \frac{\partial T}{\partial Z} \right) = \ddot{q} + \frac{\partial}{\partial X} \left(K_x \frac{\partial T}{\partial X} \right) + \frac{\partial}{\partial Y} \left(K_y \frac{\partial T}{\partial Y} \right) + \frac{\partial}{\partial Z} \left(K_z \frac{\partial T}{\partial Z} \right) \quad (3-33)$$

It will be assumed that all effects are in the global Cartesian system.

Three types of boundary conditions are considered.

1. Specified temperatures acting over surface S_1 :

$$T = T^* \quad (3-34)$$

where T^* is the specified temperature.

2. Specified heat flows acting over surface S_2 :

$$\{q\}^T \{\eta\} = -q^* \quad (3-35)$$

where:

$\{\eta\}$ = unit outward normal vector

Q^* = specified heat flow

3. Specified convection surfaces acting over surface S_3 (Newton's law of cooling):

$$\{q\}^T \{\eta\} = -h_f (T_S - T_B) \quad (3-36)$$

where:

h_f = convective film coefficient

T_B = bulk temperature of the adjacent fluid

T_S = temperature at the surface of the model

Combining Equation 3-31 with Equation 3-32 and Equation 3-36 yields

$$\{\eta\}^T [D] \{L\} T = q^* \quad (3-37)$$

$$\{\eta\}^T [D] \{L\} T = h_f (T_B - T) \quad (3-38)$$

Multiplying Equation 4-32 by a virtual change in temperature, integrating over the volume of the element, and combining with Equation 3-37, and Equation 3-38, yields:

$$\int_{vol} \left(\rho c \delta T \left(\frac{\partial T}{\partial t} + \{V\}^T \{L\} T \right) + \{L\}^T \delta T ([D] \{L\} T) \right) d(vol) = \int_{S_2} \delta T q^* d(S_2) + \int_{S_3} \delta T h_f (T_B - T) d(S_3) + \int_{vol} \delta T \ddot{q} d(vol) \quad (3-39)$$

where:

Vol = volume of the element

δT = an allowable virtual temperature = $\delta T(x, y, z, t)$

CHAPTER 4: METHODOLOGY, MODELS AND PARAMETERS

This chapter describes the overall methodology and then details the model including its geometry, load, boundary conditions, material properties, assumptions and solution options.

4.1 Methodology

The finite element method is used to deal with complex structures that are difficult to solve analytically. The finite difference method has been used in the past to study permanent cylindrical molds but the achievements and developments in the finite element technique have made it preferable for large-scale computations. The finite difference method is more suitable for moving boundary conditions, whereas the finite element method is suitable for solid structures such as permanent cylindrical mold, dies, pressure vessels and heat exchangers. The finite difference method uses an orthogonal mesh to represent the geometry. It is very difficult to model a thin-walled cylinder and obtain an acceptable solution, with a reasonable number of elements. Even the use of thousands of elements may not improve the analysis results. In contrast, the mesh in the finite element method can be non-orthogonal, generated by linear, triangular or quadrilateral elements. A thermal stress analysis of the mold can be performed with finite element method with no modification of the mesh. Thus, the finite element method is best suited for studying the mold. The finite element analysis used in this

study will provide information on the temperature distribution, stresses and strains in the mold. Only a single cycle of the thermal load is analyzed. By itself, the use of a single thermal cycle would not give adequate information to assess the life of the mold but the finite element analysis produces a result that is sufficient to estimate the life of mold by applying the Coffin-Manson equation. The Coffin-Manson equation uses plastic strain amplitude to estimate the life of a mold as discussed in Chapter 2. The plastic strain amplitude was obtained from the simulation results and substituted in the Coffin-Manson equation in order to calculate the life of the mold. The results obtained were validated against empirical industry data (i.e. the number of parts produced before the mold is discarded) and the mathematical model's results reported by Oliver (1988).

It is always economically desirable to improve the life of the mold. A sandwich (multilayer) model of steel-copper-steel has been suggested in the literature as a way to reduce the thermal gradient and stresses in mold or to improve the life of the mold (Oliver 1988, Alimi 1989). This multilayer cylindrical model was analyzed using the above mentioned finite element method and the results are discussed in Chapter 5.

4.2 Geometry and Boundary Conditions

The solid geometries of an actual mold and a multilayer cylinder are shown in Figures 4.1 and 4.2. Two models have been developed using an actual industrial geometry and a multi-layered cylinder of steel-copper-steel, which is the main focus of this study. This combination can lower the thermal gradient, provide dimensional stability and increase abrasion resistance. This design may be thought of as the thermal equivalent of the mechanical "I beam" (Oliver 1988). The outer and inner layer of steel

provides strength and stiffness, while the middle layer of copper provides a high conductivity path for heat flow.

For this analysis, the end effects are neglected. As shown in Figure 4.1 there are protruding and curved shapes on both ends of the mold, although most of the mold is cylindrical in shape. The effect of the ends (which are curved and protrude) will be different than that of the long symmetrical cylindrical shape. Even for a long symmetrical cylinder, the stresses at the ends are 25% higher than at points away from the end (Ugura 1999). However the mold must be discarded if the crack develops in the center, i.e. away from the ends. Figure 4.2 represents the 2-D geometry which was built in ANSYS for the analysis, which is a small part of cross section A-A shown in Figure 4.1. The inner gray layer is steel (thickness 6 mm), the middle orange layer is copper (thickness 18 mm) and the outer gray layer is steel (thickness 6 mm) in Figure 4.2. This is a two dimensional representation of a multilayered cylinder. The values for the cylinder dimensions noted in Figure 4.3, are:

$R_1 = 9.84$ in, cylinder inside radius.

$R_2 = 10.07$ in, outside radius of steel inner layer and inside radius of middle copper layer.

$R_3 = 10.69$ in, outside radius of middle copper layer and inside radius of outer steel layer.

$R_4 = 11.02$ in, cylinder outside radius.

$t = 1.18$ in, thickness of cylinder.

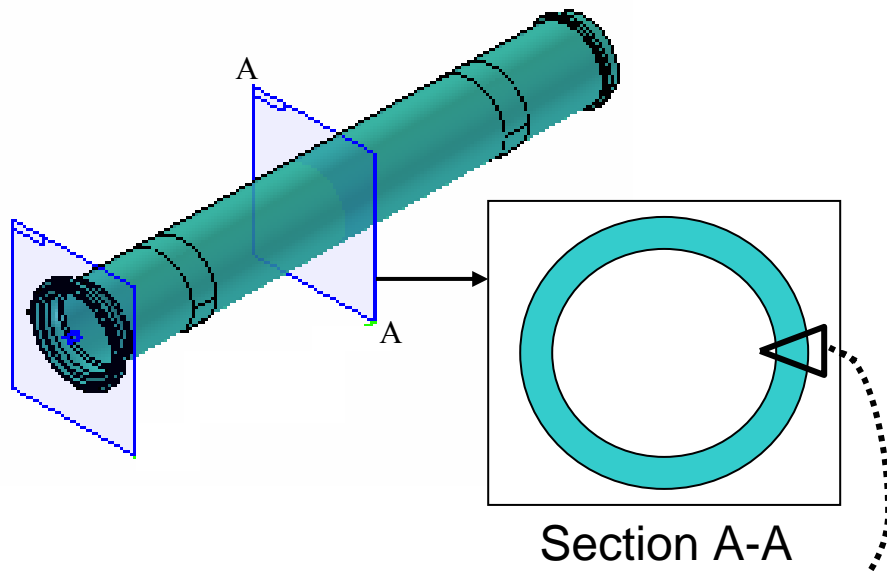


Figure 4.1: 30.00 foot long mold

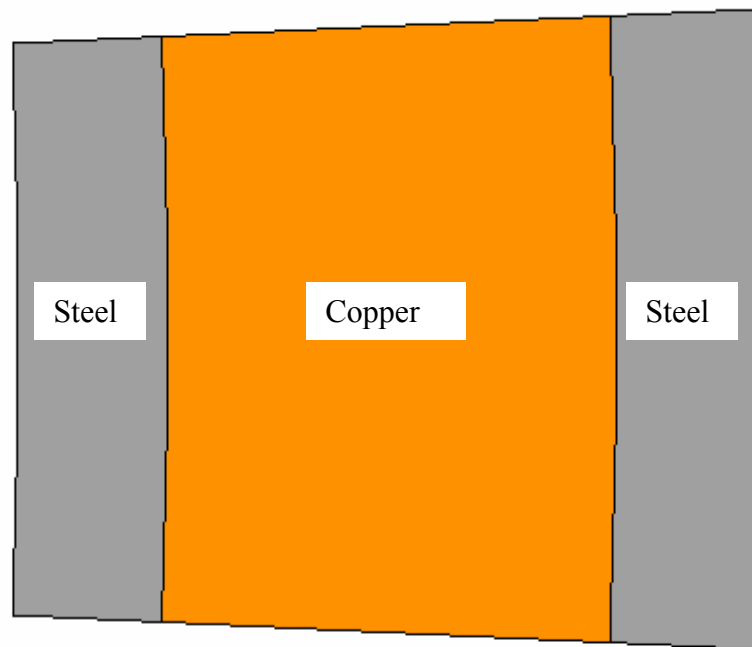


Figure 4.2: 2-D drawing of multilayer cylinder

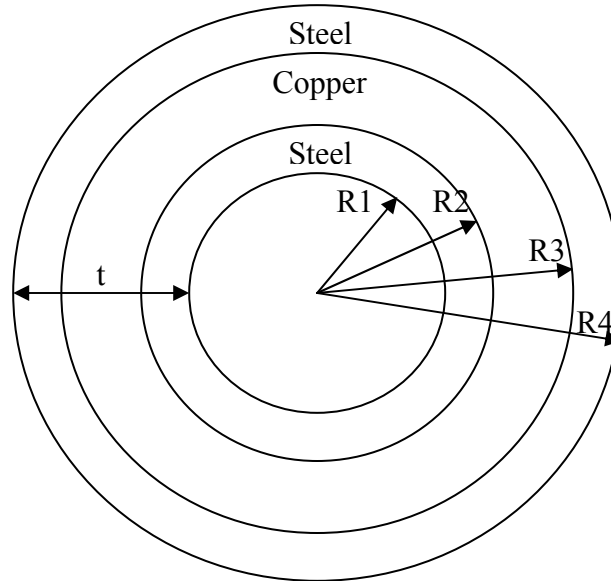


Figure 4.3: Cross section of cylinder showing dimensions

The thermal constraints imposed are:

1. The initial temperature of cylinder is 25° C.
2. The load is applied on the inner surface of the cylinder. The applied load curve is obtained by heating the inside surface of the cylinder by a flame for 10 seconds, after which the flame is turned off (Oliver 1988). The body is cooled by water at 25°C on the outer surface for next 25 seconds. The load curve obtained with this method is shown in Figure 4.4. The applied load curve replicates the phenomenon of pouring of the molten material (when the temperature of the mold inner surface rises considerably) and solidification of the material (when the temperature of the mold inner surface decreases).
3. The heat transfer coefficient on the outside surface is a function of the surface temperature. If the outer surface temperature is below 100° C, the heat transfer coefficient is 1575 watts/m², but if the surface temperature exceeds 100° C then the heat transfer coefficient is 3150 watts/m².

4. The total cycle time is 35 sec. First 10 sec is the heating phase and last 25 sec is the cooling phase.

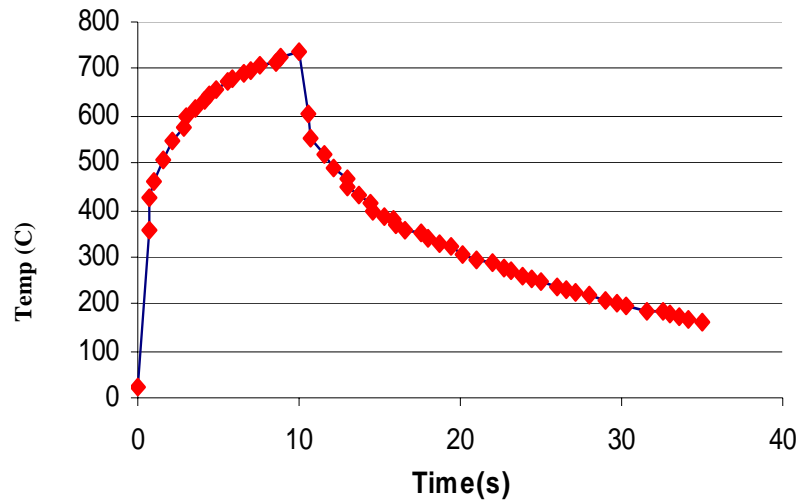


Figure 4.4: Load curve

The structural constraints are:

1. Plane strain.
2. Symmetrical boundary condition.

Figure 4.5 shows the load and boundary conditions applied to a multilayer cylinder. The inner layer is subjected to the thermal load curve shown in Figure 4.4, while the outer layer is subjected to convection cooling. The upper and lower layer are subjected to symmetrical boundary conditions. The thermal conductivity for steel and copper is defined in terms of the material properties and the mode of heat transfer is assumed to be mainly conduction and convection.

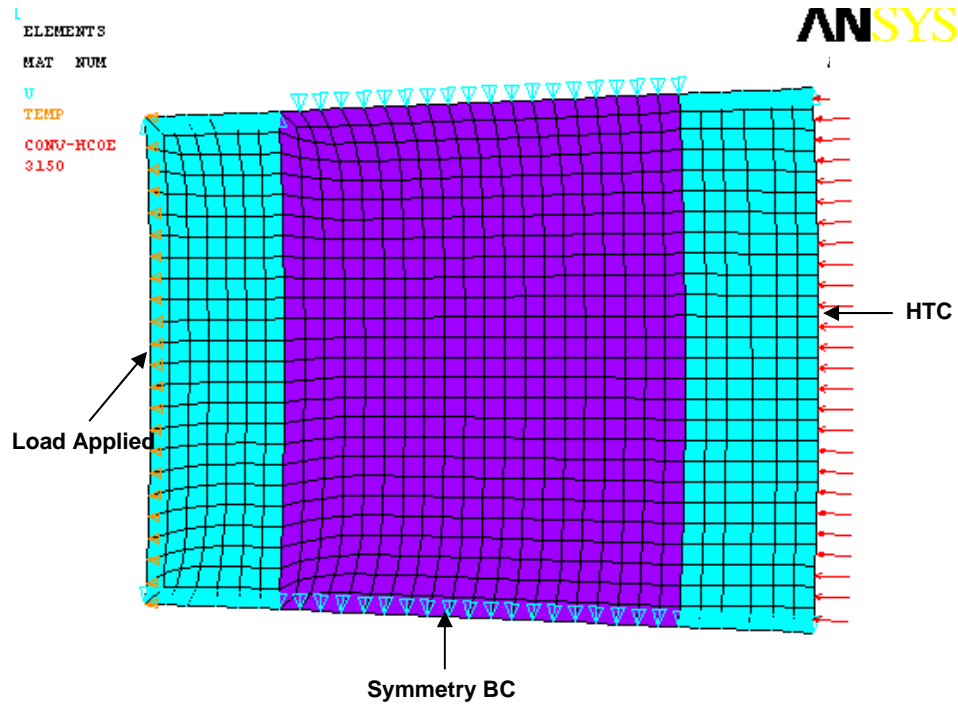


Figure 4.5: Load and boundary conditions

4.3 Material Properties

The material properties are a function of temperature except for Poisson's Ratio, which is assumed to be constant at all temperatures. Material number 1 is steel (2¼ % Cr 1% Mo) and material number 2 is oxygen free high conductivity (OFHC) copper. The material properties used are in SI units (MCS) and are listed below:

1. Density
2. Specific heat
3. Linear isotropic property
 - Elastic modulus
 - Poisson ratio
4. Thermal expansion
5. Thermal conductivity

6. Multilinear isotropic property (Stress- strain curve)

Appendix A contains a complete list of the material properties used in the analysis for steel and copper. Figures 4.7 and 5.8 are representative plots for material properties (refer to Appendix A, Figure A.1 – A.12 for other material properties). Figures 4.6 and 4.7 show the stress-strain curves (input for multilinear isotropic hardening) for steel and copper, respectively.

Fatigue life, defined as number of times molten material can be poured before crack initiates, was calculated for the inner surface, which is subjected to the highest load. As discussed earlier, this calculation is based on the Coffin-Manson equation (discussed in Chapter 2). In order to use this equation, fatigue ductility coefficients (the failure strain for a single load reversal and it is an empirical constant) and fatigue ductility exponent (slope of SN curve and it is also an empirical constant) are required, which are listed as below (Suresh 1991):

$$\epsilon_f \text{ (fatigue ductility coefficient)} = 0.73$$

$$C \text{ (fatigue ductility exponent)} = -0.62$$

4.4 Assumptions

1. Plane strain
2. Heat is transferred by conduction and convection. Radiation effects are neglected, because the outer surface is surrounded by a water jacket.
3. One thermal cycle lasts 35 sec, consisting of 10 seconds of heating followed by 25 second of cooling.
4. There is no heat abstraction by the air within the hollow cylinder.
5. No oxide layer is present on the inner surface of the mold.

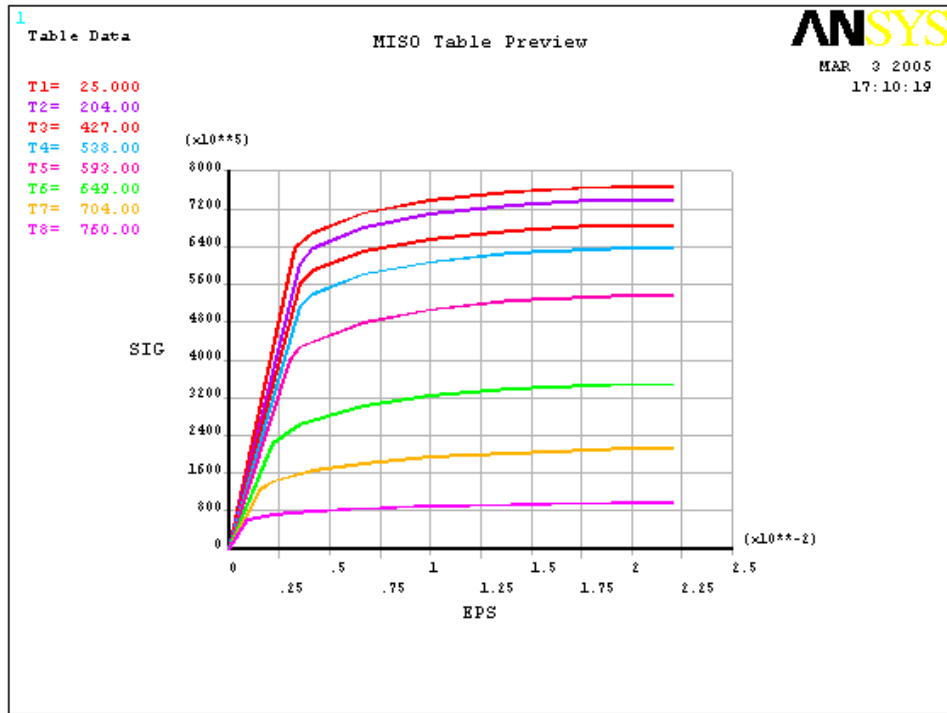


Figure 4.6: Stress-strain curve of steel (2¼ % Cr 1% Mo) at different temperature

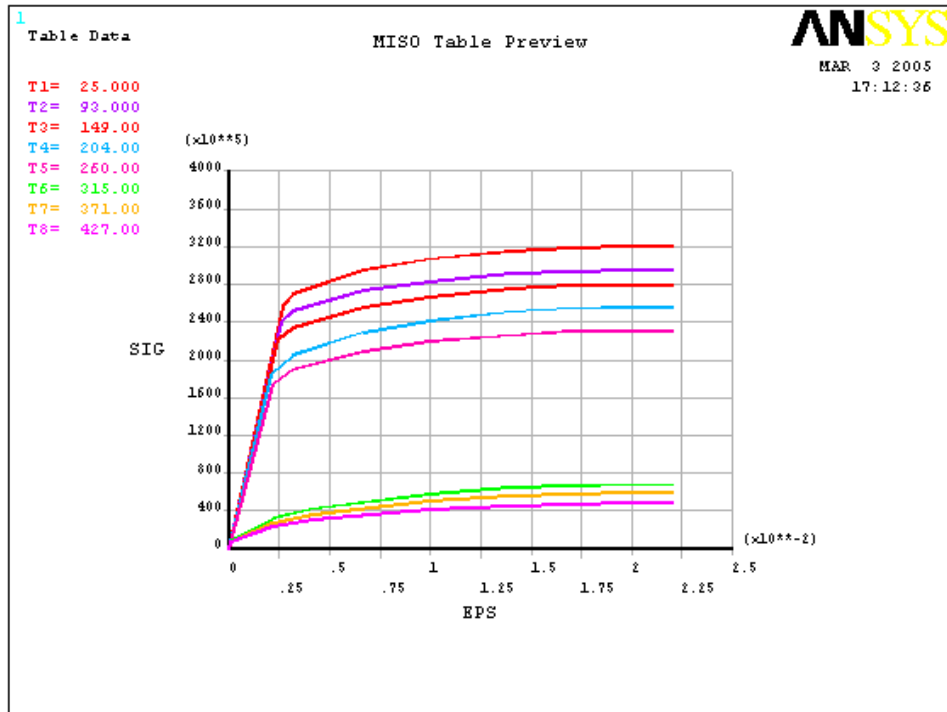


Figure 4.7: Stress-strain curve of oxygen free high conductivity copper at different temperature

6. There is no gaseous gap between the inner surface of the mold and the molten material.
7. Material properties are a function of temperature.
8. Contact surface (i.e. the interface between steel and copper) is always bonded.
9. Fatigue life is deterministic

4.5 Solution options

In order to obtain the solution, the following settings were invoked in ANSYS. The method used to introduce the settings is detailed earlier and also in Chapter 3. For example, to incorporate plastic material properties the stress strain curve is defined as input for multilinear isotropic hardening (MISO).

1. Problem Dimensionality2-D
2. Degree of Freedom.....U_x U_y Temp
3. Analysis Type.....Transient
4. Nonlinear Geometry Effects..... On
5. Units SI (MCS)
6. Plastic Material Properties IncludedYes (MISO)
7. Time at End of Load Step 35 sec
8. Time Step Size 0.25 sec

CHAPTER 5: RESULTS AND DISCUSSION

Finite element models of a multilayer cylindrical mold (steel–copper–steel) and two monolayer cylindrical molds (steel) were subjected to the load and boundary condition detailed in Chapter 4. The finite element analysis was performed with ANSYS Release 9.0. Analysis data was obtained for every time step but plotted only at critical time points i.e. time = 1 second (start of cycle), time = 10 seconds (end of heating phase and start of cooling phase) and time = 35 seconds (end of cycle). The time 1,10 and 35 seconds are also considered because the validation results are only available for the above mentioned time points.

The plots for the multilayer cylindrical mold – steel 2 ¼% Cr 1% Mo (thickness = 0.236 in), oxygen free high conductivity copper (thickness = 0.708 in), steel 2 ¼% Cr 1% Mo (thickness = 0.236 in) – are produced and discussed in this chapter. The results shown in this Chapter and the plots in Appendices are summarized in Tables 5.1, 5.2 and 5.3. The results produced and the validation status of each result is shown in the above mentioned tables. For example, X (Y) means that the result for the corresponding entity is mentioned in the respective appendix and it has also been validated against the result in Appendix E. Complete results from “An analytical method to optimize the thermal fatigue life of multilayered cylindrical shells” by Gene Oliver (1988) are given in Appendix E. As mentioned earlier, Oliver’s study was used for validation.

Sr. No.	Analysis Result	Time		
		1 second	10 second	35 second
1).	Radial temperature profile	X (Y)	X (Y)	X (Y)
2).	Radial stress	X (Y)	X (Y)	X (Y)
3).	Tangential stress	X (Y)	X (Y)	X (Y)
4).	Axial stress	X (Y)	X (Y)	X (Y)
5).	Equivalent stress	X (Y)	X (Y)	X (Y)
6).	Equivalent plastic strain	X (Y)	X (Y)	X (Y)
7).	Net displacement	X		
8).	Equivalent plastic strain over time	X (Y)		
9).	Total strain over time	X (Y)		
10).	Total strain difference over time	X (Y)		

Table 5.1: Results of multilayer cylinder analysis*

- X – Plot generated from data obtained by analysis performed in ANSYS, Y – Plot validated against (Oliver, 1988)

Sr. No.	Analysis Result	Time		
		1 second	10 second	35 second
1).	Radial temperature profile	X	X	X
2).	Radial stress	X	X	X
3).	Tangential stress	X	X	X
4).	Axial stress	X	X	X
5).	Equivalent stress	X	X	X
6).	Equivalent plastic strain	X	X	X
7).	Net displacement	X		
8).	Equivalent plastic strain over time	X		
9).	Total strain over time	X		
10).	Total strain difference over time	X		

Table 5.2: Results available in Appendix C*

- * X – Plot generated from data obtained by analysis performed in ANSYS, Y – Plot validated against (Oliver, 1988)

Sr. No.	Analysis Result	Time		
		1 second	10 second	35 second
1).	Radial temperature profile	X	X	X
2).	Radial stress	X	X	X
3).	Tangential stress	X	X	X
4).	Axial stress	X	X	X
5).	Equivalent stress	X	X	X
6).	Equivalent plastic strain	X	X	X
7).	Net displacement	X		
8).	Equivalent plastic strain over time	X		
9).	Total strain over time	X		
10).	Total strain difference over time	X		

Table 5.3: Results available in Appendix D *

* X – Plot generated from data obtained by analysis performed in ANSYS, Y – Plot validated against (Oliver, 1988)

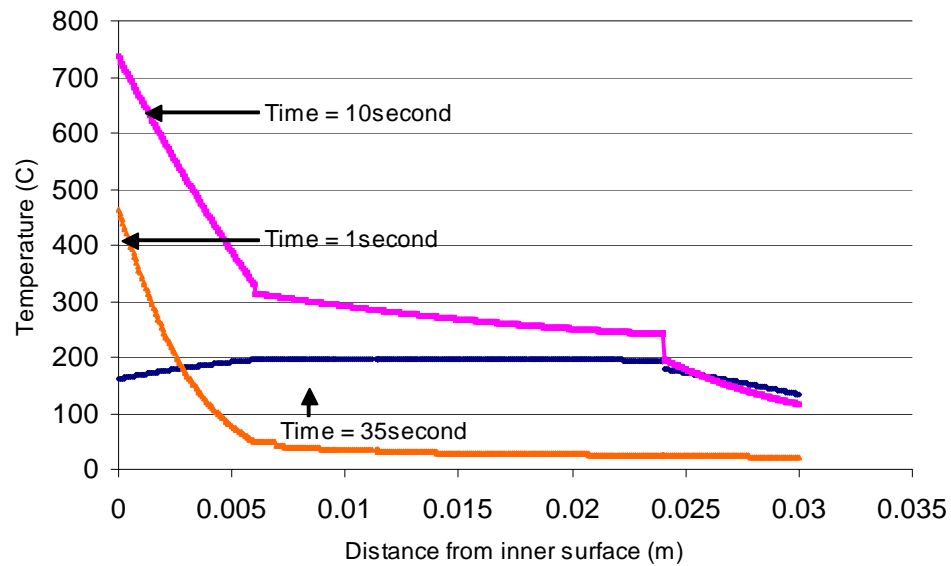


Figure 5.1: Radial temperature (C) distribution at time 1,10 and 35 second in multilayer cylinder (Steel-Cu-Steel)

Radial temperature distribution plotted in Figure 5.1 verifies that in First 10 seconds the temperature of the body is rising and in next 25 seconds the temperature of

the body decreases. At the end of the cycle i.e. at time 35 second the highest temperature is in the copper layer (middle section).

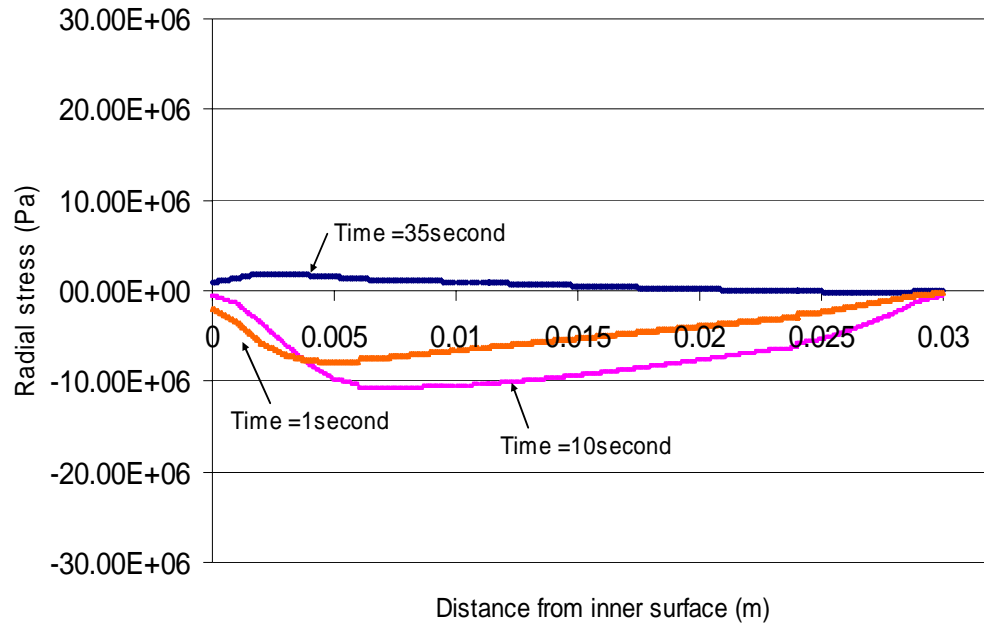


Figure 5.2: Radial stress (Pa) at time 1, 10 and 35 second in multilayer cylinder (steel-Cu-Steel)

The results from the finite element analysis were analyzed to determine how well they conformed to the criteria that must be satisfied. The conditions that must be met in order to give the model credibility are listed below:

1. The radial stress should be zero on inside and outside surface.
2. The radial stress distribution should be continuous.

The above mentioned conditions can be verified by examining the plots in Figure 5.2. The radial stress is zero on inside and outside surface and is significantly smaller than either the tangential stress (Figure 5.3) or the axial stress (Figure 5.4). The radial stress also appears to be continuous.

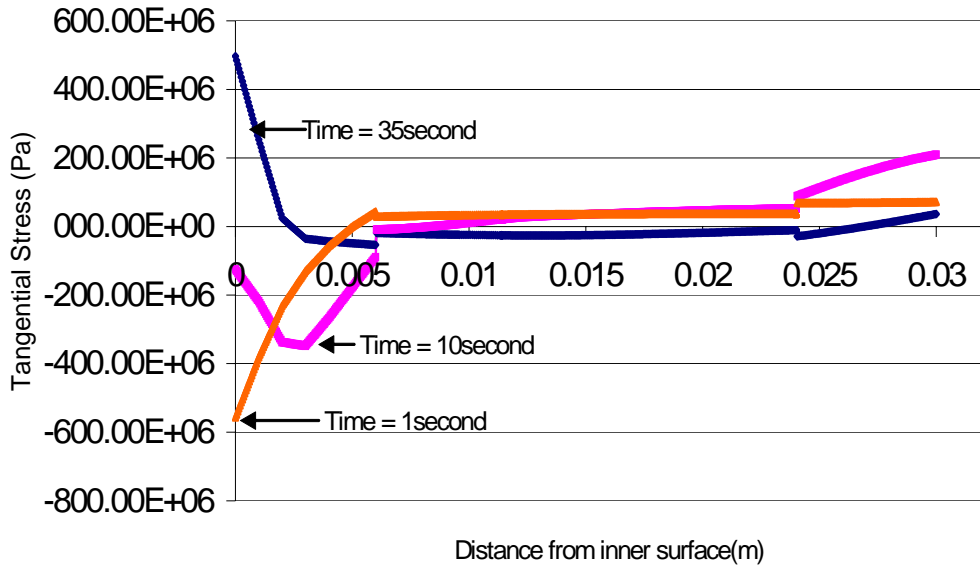


Figure 5.3: Tangential Stress (Pa) at time 1, 10 and 35 second in multilayer cylinder (Steel -Cu- Steel)

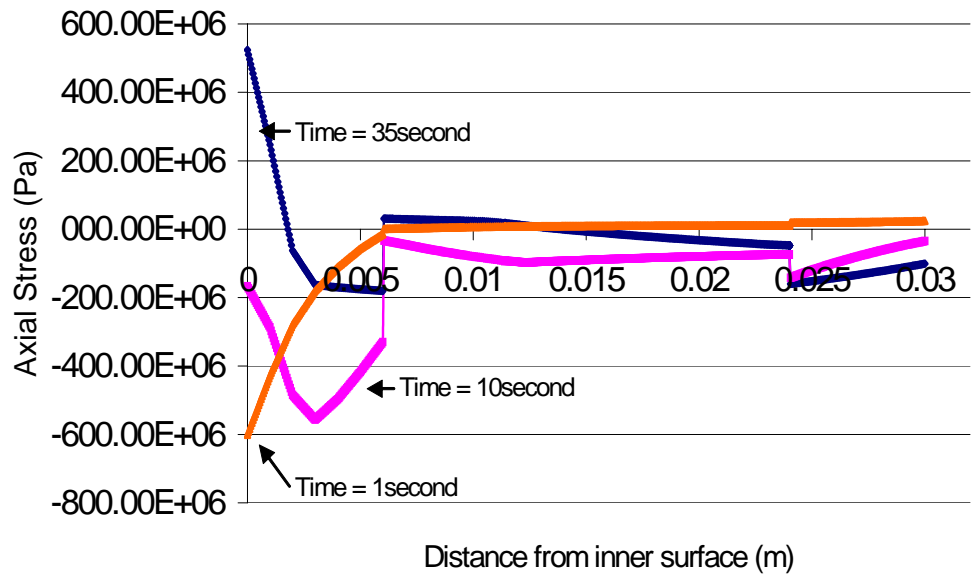


Figure 5.4: Axial Stress(Pa) at time 1, 10 and 35 second in multilayer cylinder (Steel-Cu-Steel)

The results from this study are generally in good agreement with the results in Appendix E but the tangential stress and axial stress are not equal. The model developed for this study assumes a plane strain condition, i.e. the displacement

component in the axial direction is zero and the other displacement components are independent of any displacement in the axial direction. For this condition the tangential stress is given by (Johns 1965):

$$\sigma_z = \nu (\sigma_r + \sigma_\theta) - E \alpha \Delta T \tag{5-1}$$

This shows that axial stress (σ_z) and tangential stress (σ_θ) will not be equal if no additional constraints have been imposed. From above equation the axial stress and tangential stress will be equal only if Poisson ratio (ν) is one and radial stress (σ_r), modulus of elasticity, coefficient of expansion and temperature difference is zero.

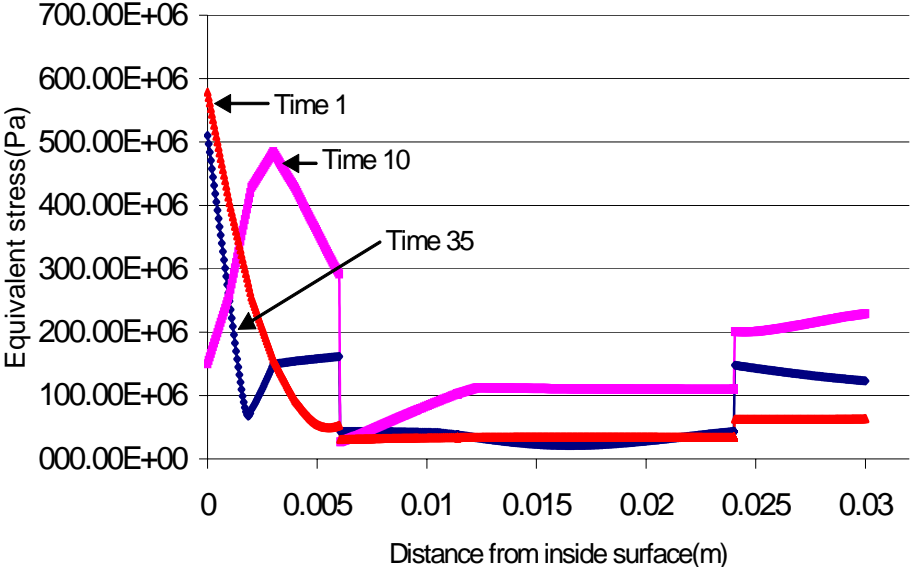


Figure 5.5: Equivalent stress (Pa) at time 1 ,10 and 35 second in multilayer cylinder (Steel-Cu-Steel)

Unlike the results in Appendix E, the location of the highest equivalent stress is on the inside surface rather than being slightly away from the inside surface (towards the outer surface). The method of defining the load cycle in this study may have contributed to this phenomenon. It is interesting to note that at the beginning of the cycle (i.e. at time = 1 second), the location of the highest equivalent stress is on the

inside surface (Figure 5.5), but as the cycle proceeds (i.e. at time = 10 seconds), the highest equivalent stress front has moved toward the outside surface, and at the end of the cycle (i.e. at time 35 seconds) it again regains its original position (Figure 5.5). This agrees with the results in Appendix E. The equivalent stress in this study is calculated as (ANSYS 9.0 documetation,2004)

$$\sigma_e = \left[\frac{1}{2} \left\{ (\sigma_r - \sigma_\theta)^2 + (\sigma_\theta - \sigma_z)^2 + (\sigma_z - \sigma_\theta)^2 + 6 * (\sigma_{r\theta}^2 + \sigma_{\theta z}^2 + \sigma_{\theta z}^2) \right\} \right]^{\frac{1}{2}} \quad (5-2)$$

It is clear from the Figure 5.5 that equivalent stresses are discontinuous in the multilayer model. Figure 5.6 (Equivalent plastic strain) show that yielding has occurred on the inside surface, hence it can be concluded that the equivalent stress at that location is above the yield stress or yield strength.

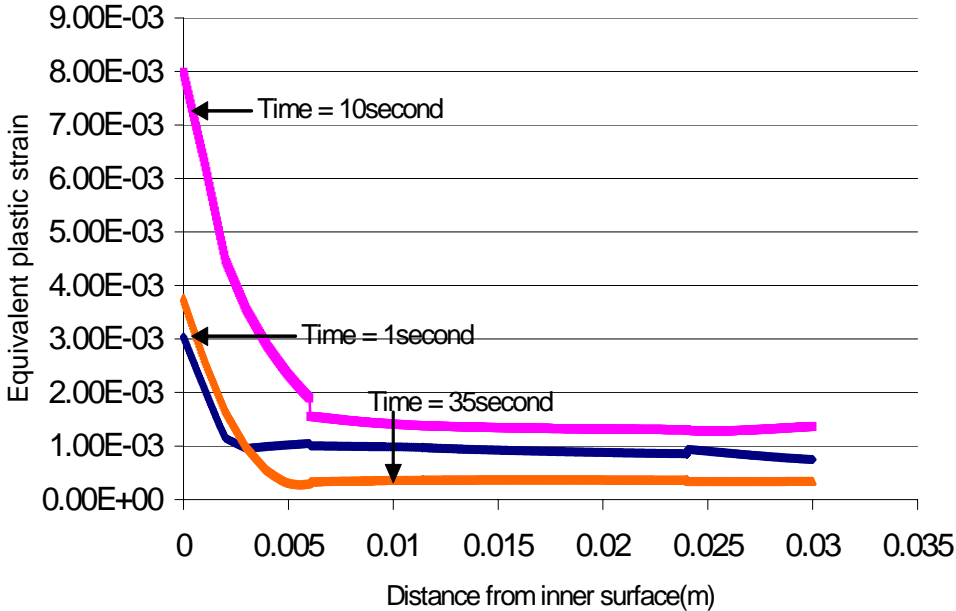


Figure 5.6: Equivalent plastic strain at time 1, 10 and 35 second in multilayer cylinder (Steel-Cu-Steel)

The magnitude of the equivalent stress in the outer layer is lower than the yield stress. The plot for plastic strain (Figures 5.6) indicates that there is no plastic strain in the outer layer of steel, hence the yield stress has not been exceeded.

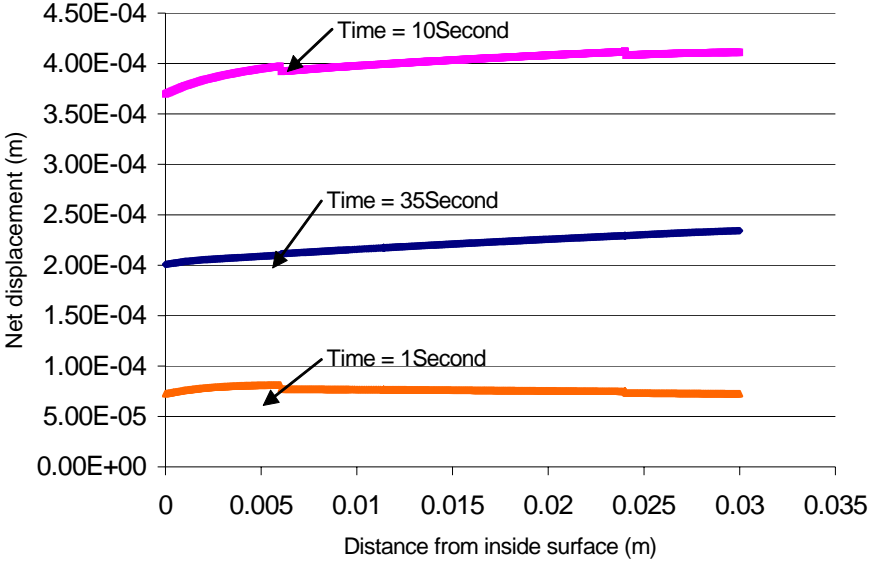
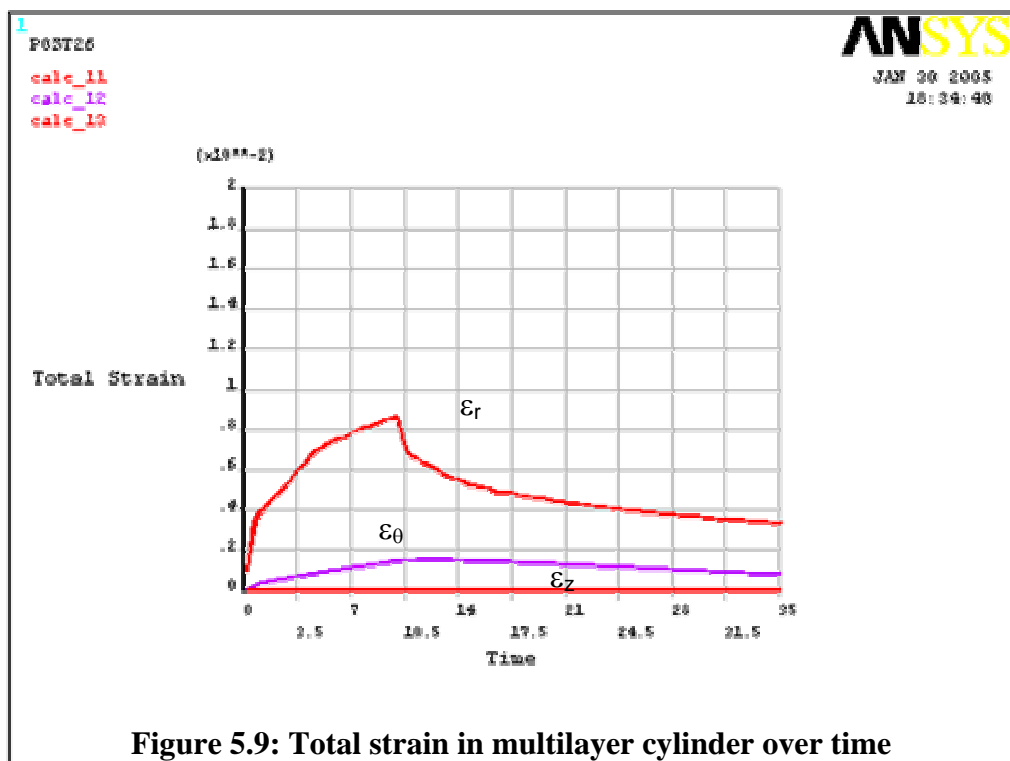
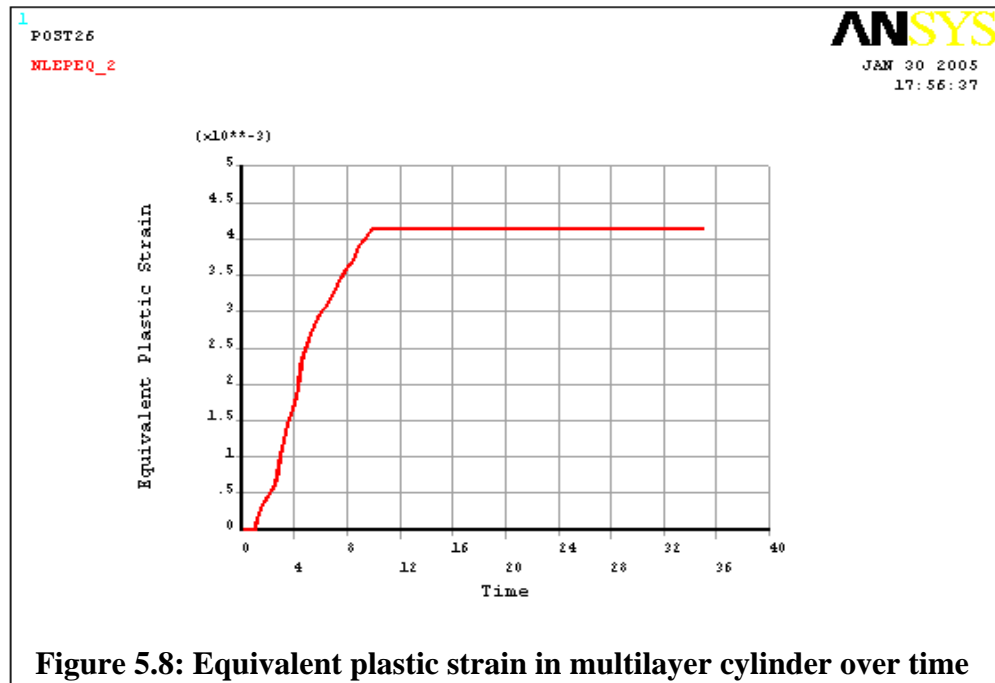


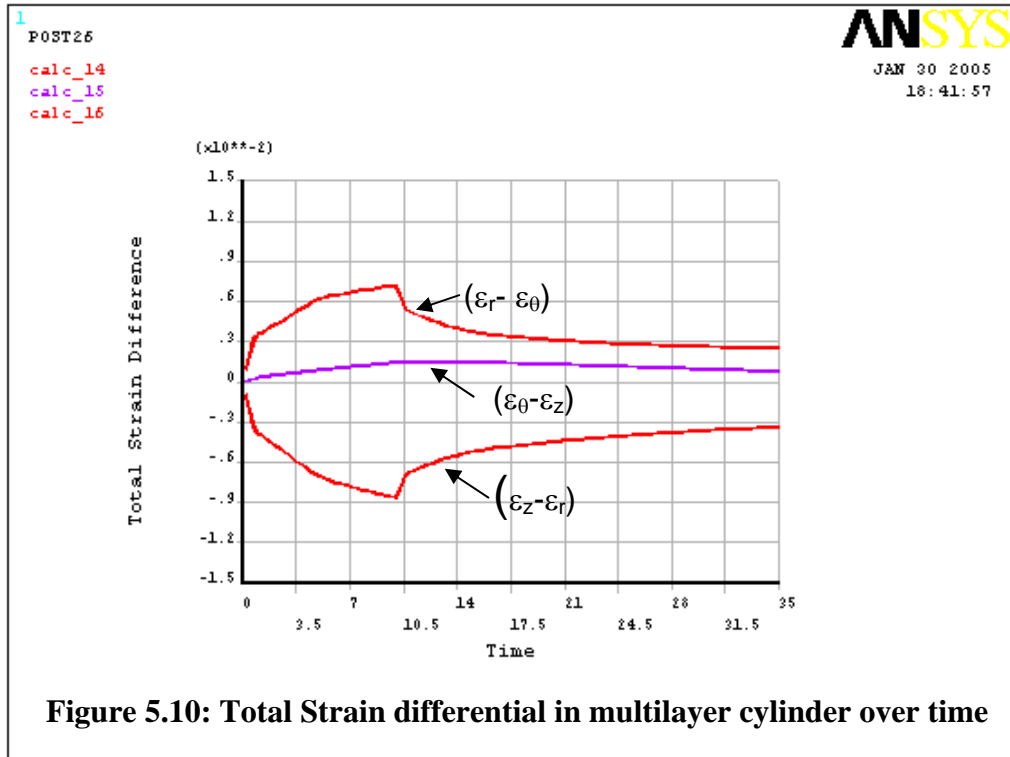
Figure 5.7: Net Displacement(m) at time 1, 10 and 35 second in multilayer cylinder (Steel-Cu-Steel)

Figure 5.7 shows the expansion and contraction of the multilayer cylinder. The body expands radially during heating phase i.e. from time 1 second to time 35 second and in cooling phase body tries to regain its original position but at the end of the cycle i.e. time 35 second as shown in plot the body does not regain its original position.

Figure 5.9 shows a graphical representation of radial strain, tangential strain and axial strain. One of the assumptions for this model is plane strain condition, which indicates that axial strain must be zero. It can be concluded from the figure that the axial strain is zero, which must be satisfied in order to give the model credibility. The total strain differential $((\epsilon_r - \epsilon_\theta), (\epsilon_\theta - \epsilon_z) \text{ and } (\epsilon_z - \epsilon_r))$ is plotted in Figure 5.10 and the data

obtained (Table 5.2) from the plot is used for fatigue life calculations for the cylindrical mold.





5.1 Fatigue Life

As discussed earlier in Chapter 2 the Coffin and Manson (Suresh 1991) studied low cycle fatigue, demonstrating that plastic strain is the major cause of low cycle fatigue failure. They gave an empirical formula to estimate the fatigue life (N_f) based on plastic strain approach, which is as below:

$$1/2 * \epsilon_p = \epsilon_f * (2N_f)^c \quad 5-3$$

Where ϵ_p (plastic strain amplitude) is calculated using following expression (Wang, 2000):

$$\epsilon_p = \frac{\sqrt{2}}{3} * \sqrt{[\epsilon_r - \epsilon_\theta]^2 + [\epsilon_\theta - \epsilon_z]^2 + [\epsilon_z - \epsilon_r]^2} \quad 5-4$$

Using Equations 5-2 and 5-3 the fatigue life (i.e. the number of pours before the first crack will develop) can be calculated. The calculated results and results obtained from the finite element analysis are summarized in Table 5.4.

Fatigue life is calculated using the Coffin-Manson equation, as discussed in Chapter 2. Table 5.4 shows the fatigue life obtained for different permanent cylindrical mold geometries.

Sr. No.	1	2	3
Material Combination	Steel-Cu-Steel	Steel	Steel
Inner Radius	9.84	3.42	6.69
Outer Radius	11.02	4.15	7.63
Thickness	1.12	0.52	0.94
ϵ_p (plastic strain amplitude) from ANSYS run	0.00588	0.00463	0.00544
# of Cycles (calculated)	3646	5361	4134
Actual industrial value	3800	5800	4300
Conservative Error (%)	4.0	7.5	3.8

Table 5.4: Calculation and validity of fatigue life

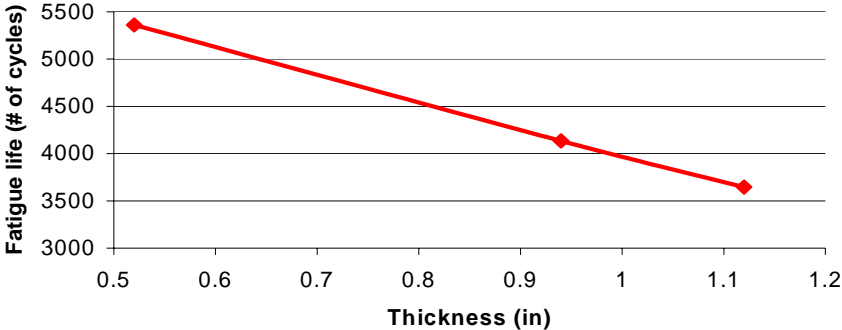


Figure 5.11: Fatigue life of the mold vs thickness of the mold

Increasing the thickness increases the distance involved in heat transfer, and if the cooling condition of the outer surface is kept constant, the body acts as a heat sink and the temperature is trapped between the inside surface and the outside surface. The temperature of the inside and outside surface is less than temperature between them (Figures 5.1, C.1 and D.1) at the end of the cycle i.e. at time 35 second. The use of the multilayer cylinder does reduce the stress level in the outer layer but the primary concern is to reduce the stress level on the inner surface, where the crack initiates. However, an increase in thickness may be accompanied by an increase in convection coefficient for more heat removal. For example spray cooling is commonly used to increase the convection coefficient, particularly in continuous casting and even for larger cylindrical molds for fast heat removal.

CHAPTER 6: CONCLUSIONS AND FUTURE WORK

As a result of this study, it was found that the permanent cylindrical mold could accurately be studied using a commercial FEA package, ANSYS. This reduces the dependency on expert programming skills in developing the numerical solutions. The model can be modified very easily to incorporate new parameters. The reduction in the time needed to perform two-dimensional analyses is an added advantage. It takes no longer than 15 minutes to obtain the solution for a significantly low time step (0.001 second) on a Celeron processor.

When these results were compared with the numerical results reported by earlier researchers, it was found that the stresses in the outer layer of steel were significantly different. This indicates the necessity of verifying the results experimentally. During this study it became clear that obtaining suitable material properties at high temperatures is a daunting task. Very few expressions relating material properties and temperature were found in the literature. An extensive study of material properties at elevated temperatures (in the range of 1000°C - 2000°C) should be conducted. This should further improve the accuracy of the Coffin-Manson approach

In this work, the interface between the steel and copper was assumed to be always bonded. However, due to differences in the coefficients of thermal expansion and the temperature distribution, this assumption may not be valid. An initial stress

condition or incorporating the glue (bonding material to hold the steel and copper together) property, would help to better understand the model. A detailed investigation of contact surface between layers will be a step forward.

In real molds an oxide layer is formed on the inside surface of cylinder, acting as an insulating medium between molten material and mold. A study of this layer and its properties would help to define the thermal load that is applied at the inner surface when subjected to different pouring conditions.

As discussed earlier spray cooling is a viable option for larger cylindrical molds to increase the heat transfer coefficient. Spray cooling is widely used in continuous casting. There have been few studies to understand the effect of nozzle design and fluid velocity on the distribution of heat transfer coefficient in continuous casting. The parts produced by continuous casting are mainly flat slabs. Because of cylindrical shape of the mold, problems such as “out of roundness” and “problems while pulling the solidified pipe” are often encountered in industry while introducing the spray cooling. The effect of spray cooling on permanent cylindrical mold should thus be studied.

REFERENCES AND BIBLIOGRAPHY

1. Alimi M. H. 1989. A simplified analysis of thermal fatigue in cylindrical shells, Ph.D. diss., The University of Alabama, Tuscaloosa.
2. Ansys Inc., 2004. Ansys Release 9.0 documentation.
3. Black J T, R. A. Kohser, E. P. Degarmo 1997. Materials and Processes in Manufacturing, 8th edition, Prentice Hall.
4. Coffin L.F. Jr. and Schenectady N. Y. 1954. A study of effects of cyclic thermal stress on a ductile metal, ASME, vol.76, p.923
5. Duhamel J.M.C. 1838. “Memories per Divens Sarrot”, vol 5, p440, Paris, France.
6. Gao J. W. and C. Y. Wang 1999. Modeling the solidification of functionally graded materials by centrifugal casting, Materials Science and Engineering, A292, p207-215.
7. Givens P. C. 1996. Finite element analysis of large pressurized vessel and laminated cylindrical vessel, MSc., University Of Alberta, Canada.
8. Hah J. 1997. Nonlinear finite element analysis of ductile elasto-plastic structures, Ph.D. diss., University of California, Los Angels.
9. Hanson R.S. 1958. Solutions of two plasticity problems by the deformation and incremental theories, Ph.D. diss., Iowa state university.

10. Hattel J. H. and P. N. Hansen 1994. A 1-D Analytical model for the thermally induced stress in the mold surface during die casting, *Appl. Math. Modelling*, Vol. 18. p550-559.
11. Huebner K. H., Dewhirst D. L. and Smith D. E., Ted G. Byrom 2001. *The Finite Element Method for Engineers*, 4th edition, John Wiley & Sons, Inc.
12. Janco N. 1988. *Centrifugal Casting*, American Foundrymen's Society, Inc.
13. Johns D. J. 1965. *Thermal Stress Analysis*, Pergamon Press Ltd., 1st edition.
14. Lin J. Y. and H.T. Chen, 1994. Numerical solution of hyperbolic heat conduction in cylindrical and spherical systems, *Appl. Math Modelling*, Vol. 18, p384-390.
15. Logan D. L. 1986. *A First Course in the Finite Element Method*, PWS Engineering.
16. Manson S.S. and Robert E. 1981. *Thermal Stress and Low-cycle Fatigue*, Krieger Publishing Company, Florida pp. 224-240.
17. Mendelson A. and Manson S.S. October 1956. Practical solution of plastic deformation problems in elastic range ASME, Paper No. 56-A-202.
18. Okono A. J. 1978. Thermal stress analysis and life prediction of a time-temperature-dependent viscoelastic hollow cylinder subjected to a time-dependent temperature, Ph.D. diss., Virginia Polytechnique and State University.
19. Oliver G. L. 1988. An analytical method to optimize the thermal fatigue life of multilayered cylindrical shells, Ph.D. diss. The University of Alabama at Birmingham.
20. Ortega R. 1993. Finite element analysis of a thick-walled cylinder elastic-plastic behavior, MSE, The University of Alabama in Huntsville.

21. Park J. K., B. G. Thomas, I. V. Samarasekera and U. S. Yoon 2002. Thermal and Mechanical behavior of copper molds during thin-slab casting: mold crack formation, Metallurgical and Materials Transaction, Vol 33B, p426-436.
22. Ruan Y. 1990. Analysis of temperature fields and thermal stresses in solidifying bodies using the finite element method, Ph.D. diss., The University of Minnesota.
23. S. Suresh 1991. Fatigue of Material 2nd edition, Cambridge University Press.
24. Serajzadeh S. 2004. Modeling of temperature history and phase transformation during cooling of steel, Journal of Materials Processing Technology 146, p311-317.
25. Simo, J. C. and Taylor, R. L. 1985. Consistent Tangent Operators for Rate-Independent Elastoplasticity, Computer Methods in Applied Mechanics and Engineering, Vol. 48, pp. 101-118.
26. Sirikis J. S. 1988. A two-dimensional hybrid experimental-numerical technique for elasto-plastic stress analysis, Ph.D. diss., University of Florida.
27. Sirinterlikci A., 2000. Thermal management and prediction of heat checking in die casting, Ph.D. diss., The Ohio State University.
28. Tanaka M., T. Matusmoto and Q. F. Y. Shinshu 1994. Time-stepping boundary element method applied to 2-D transient heat conduction problems, Appl. Math Modelling, Vol 18, p569-576.
29. Timoshenko S.P. and Goodier J.N. 1970. Theory of Elasticity 3rd edition, McGraw-Hill Publications.
30. Trovent M. and S. Argyropoulos 1998. The implementation of a mathematical model to characterize mold metal interface effects in metal casting, Canadian Metallurgical Quarterly, Vol 37, p185-196.

31. Ugura A. C. 1999. Stresses in Plates and Cylinders, 2nd edition, WCB/McGraw-Hill.
32. Wang B. December 2000. The prediction of low cycle fatigue for die casting with FEM, MEng, Carleton University, Ottawa, Canada.
33. White D. Y. 1997. Stress analysis in multilayer structures, Ph.D. diss., The Florida State University.

APPENDIX A
(MATERIAL PROPERTIES)

APPENDIX A

This appendix contains plots of material properties for steel (Figures A.1 – A.6) and copper (Figures A.7 – A.12)

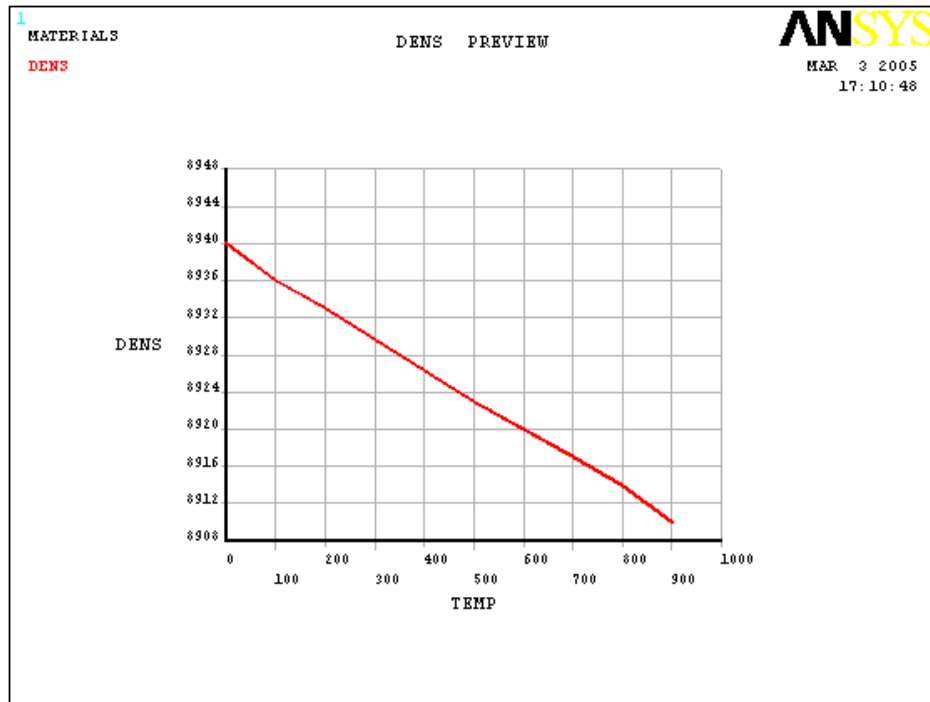


Figure A.1: Density of steel (2¼ % Cr 1% Mo) vs temperature

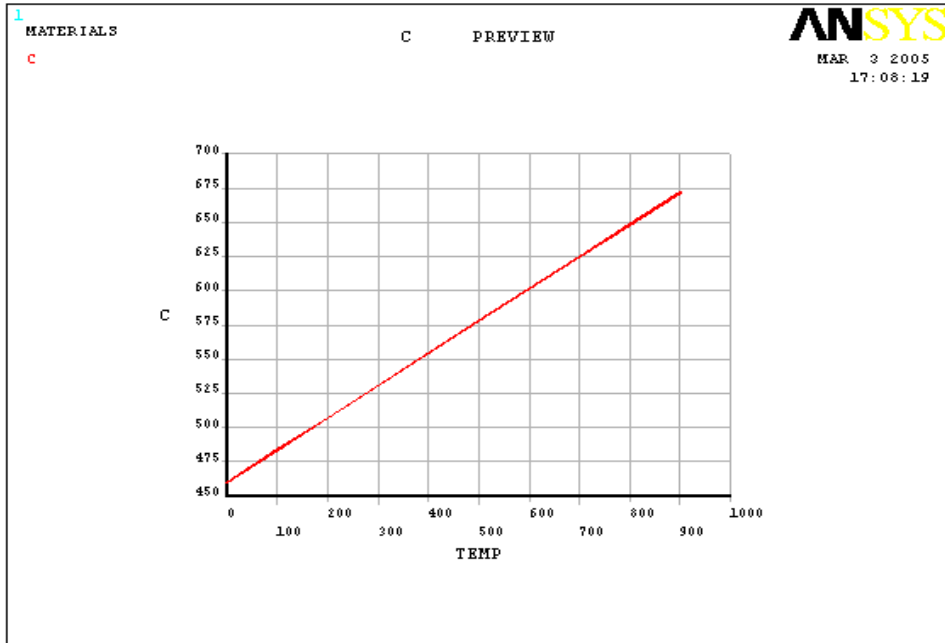


Figure A.2: Specific heat of steel (2¼ % Cr 1% Mo) vs temperature

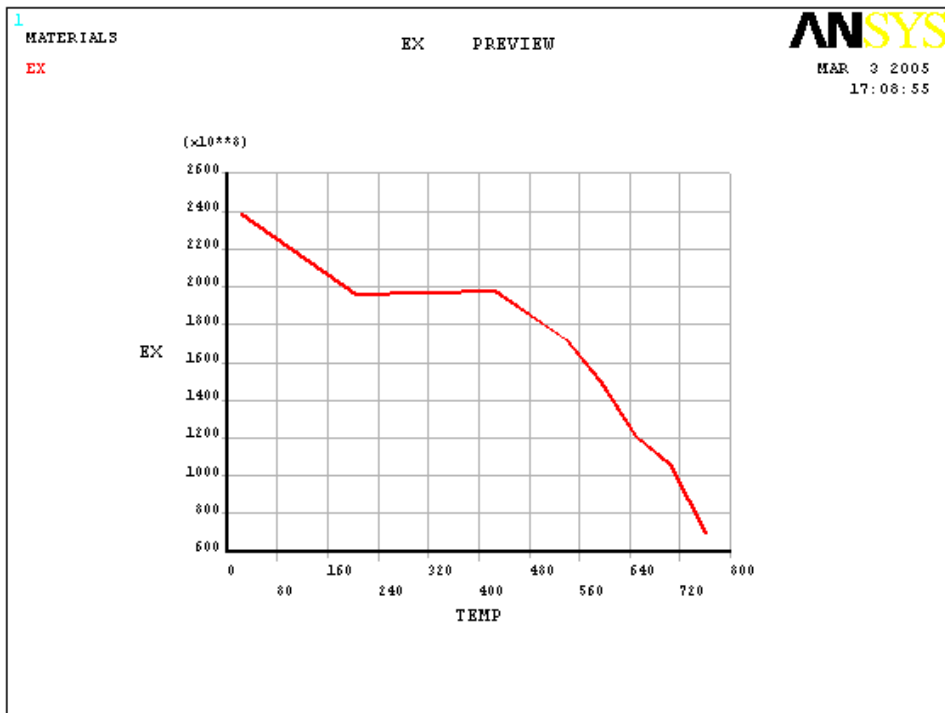


Figure A.3: Elastic modulus of steel (2¼ % Cr 1% Mo) vs temperature

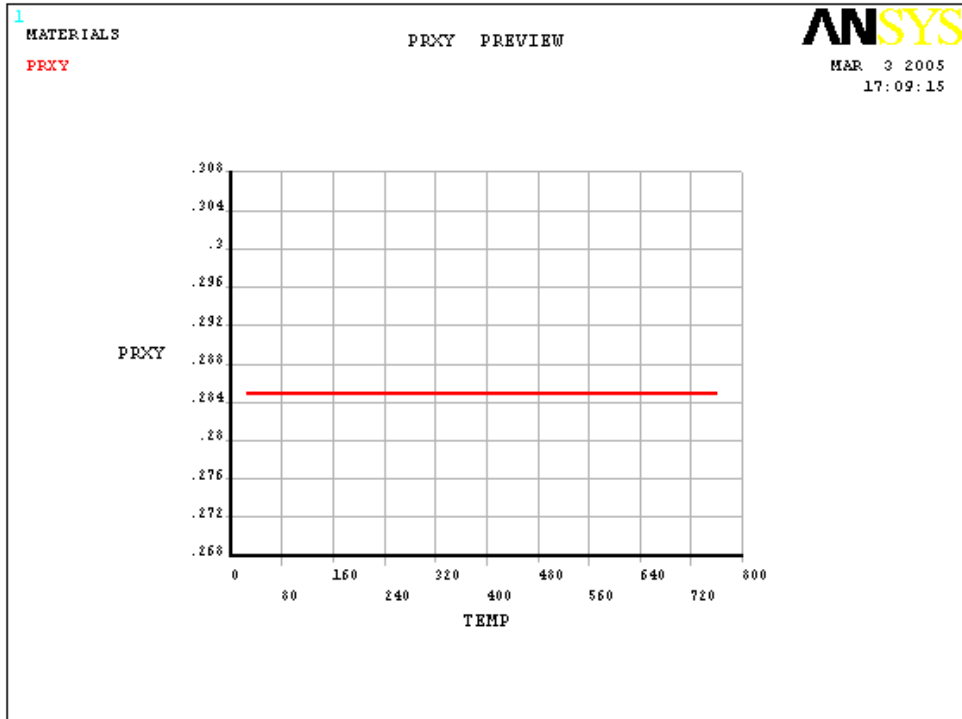


Figure A.4: Poisson ratio of steel (2¼ % Cr 1% Mo) vs temperature

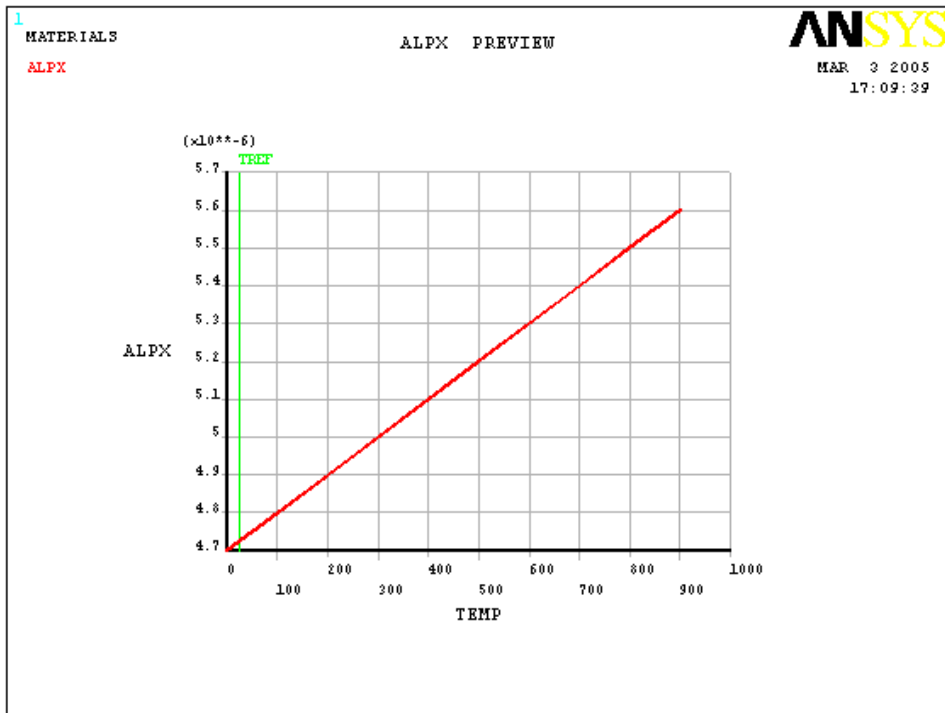


Figure A.5: Coefficient of expansion of steel (2¼ % Cr 1% Mo) vs temperature

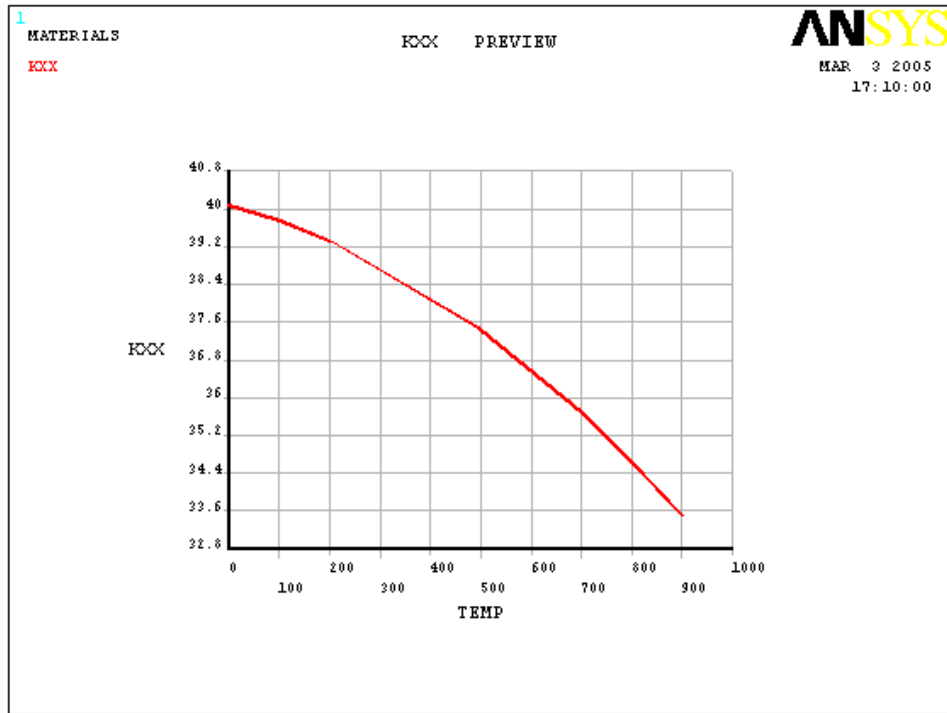


Figure A.6: Thermal conductivity of steel (2¼ % Cr 1% Mo) vs temperature

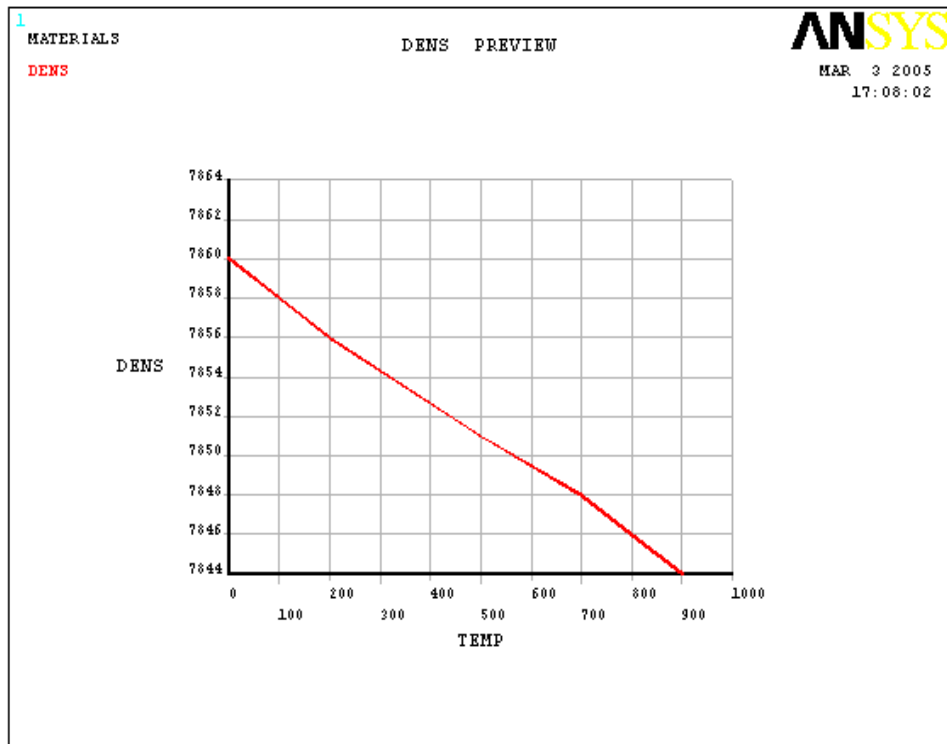


Figure A.7: Density of copper vs temperature

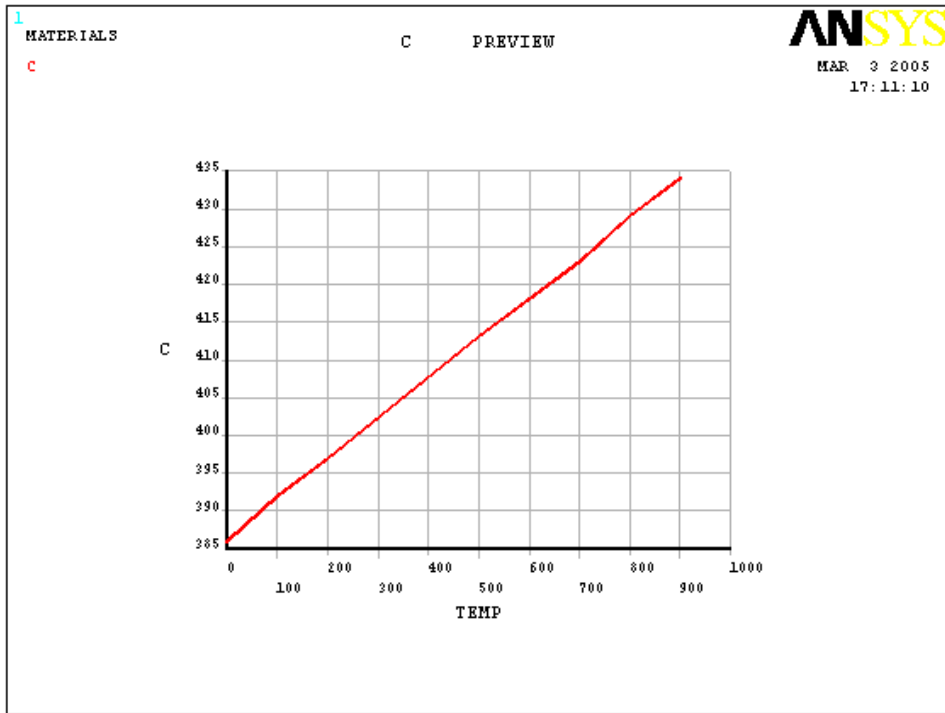


Figure A.8: Specific heat of copper vs temperature

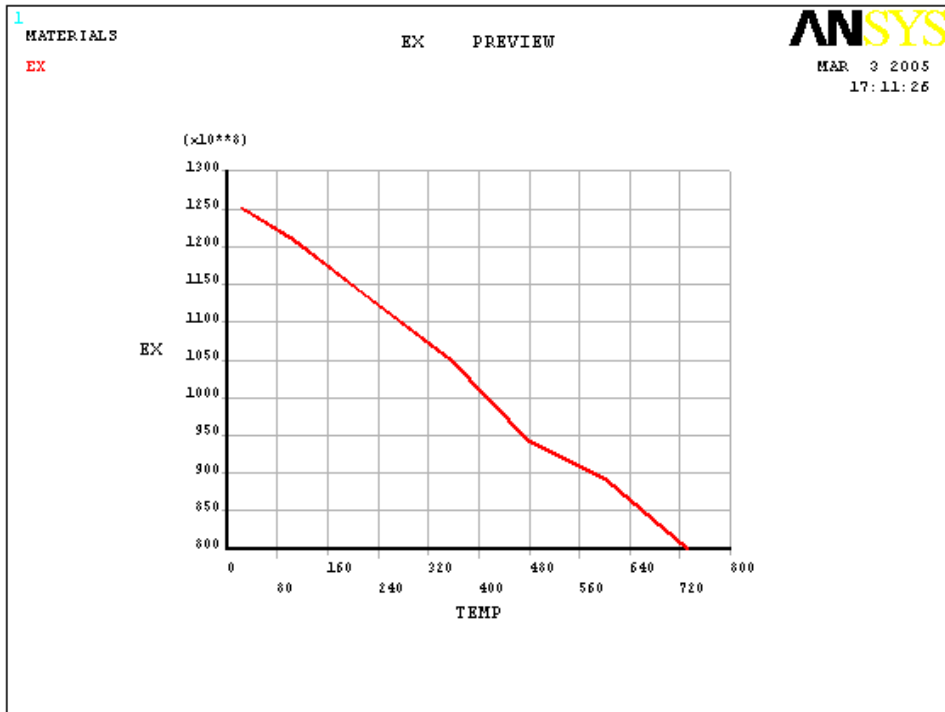


Figure A.9: Elastic Modulus of copper vs temperature

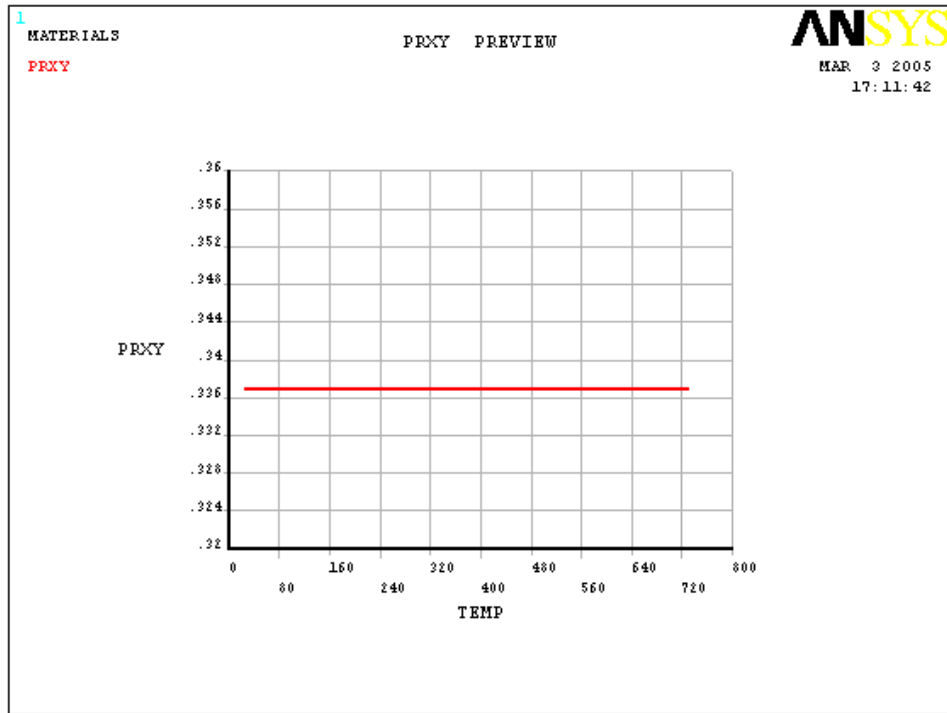


Figure A.10: Poisson ratio of copper vs temperature

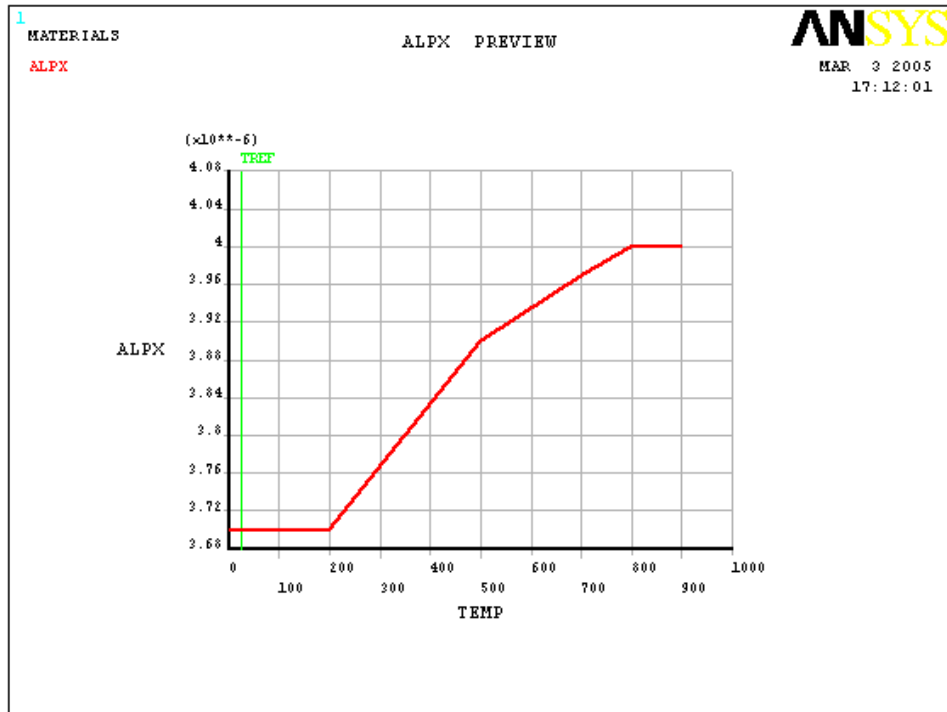


Figure A.11: Coefficient of expansion of copper vs temperature

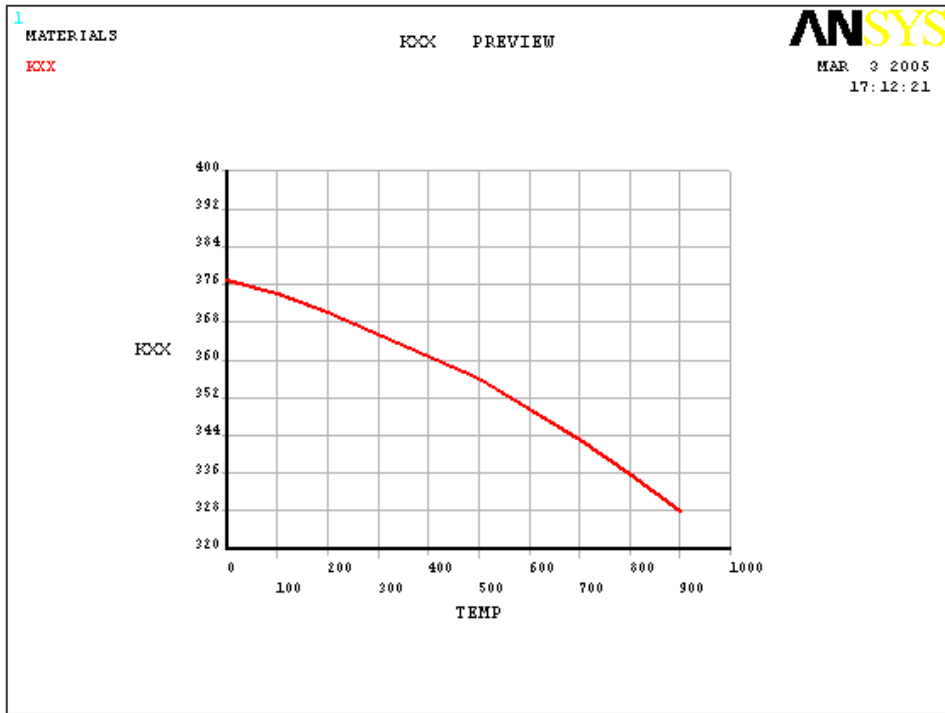


Figure A.12: Thermal conductivity of copper vs temperature

APPENDIX B

(INPUT FILE (ANSYS) FOR FINITE ELEMENT ANALYSIS)

APPENDIX B

This appendix contains the log file generated by ANSYS to define elements, create the geometry, define the material properties, assign attributes to the geometry, mesh the geometry, define loads and boundary conditions and define solution options such as time steps, data output and convergence control. This input file is for pre processing and defining solution options. Once the model has been created and solution option has been defined, the user is expected to check the solution options and start to solve the current load set. After obtaining the solution, the user can postprocess any results of interest.

```
/BATCH
/COM,ANSYS RELEASE 9.0  UP20021010   10:12:51  03/16/2005
/input,menust,tmp,",,,,,,,,,,,,,,1
/GRA,POWER
/GST,ON
/PLO,INFO,3
/GRO,CURL,ON
/REPLOT,RESIZE
/PREP7
!*
```

/ BUILD GEOMMETRY (CHAPTER 4.2)

```
CSYS,1
ET,1,PLANE13
K,1,0.25,-2.5,0,
K,2,0.256,-2.5,0,
K,3,0.256,2.5,0,
K,4,0.25,2.5,0,
K,5,0.256,-2.5,0,
```

K,6,0.274,-2.5,0,
K,7,0.274,2.5,0,
K,8,0.256,2.5,0,
K,9,0.274,-2.5,0,
K,10,0.28,-2.5,0,
K,11,0.28,2.5,0,
K,12,0.274,2.5,0,
L, 1, 2
L, 2, 3
L, 3, 4
L, 4, 1
L, 5, 6
L, 6, 7
L, 7, 8
L, 8, 5
L, 9, 10
L, 10, 11
L, 11, 12
L, 12, 9
FLST,2,4,4
FITEM,2,1
FITEM,2,2
FITEM,2,3
FITEM,2,4
AL,P51X
FLST,2,4,4
FITEM,2,5
FITEM,2,6
FITEM,2,7
FITEM,2,8
AL,P51X
FLST,2,4,4
FITEM,2,9
FITEM,2,10
FITEM,2,11
FITEM,2,12
AL,P51X
FLST,5,4,4,ORDE,4
FITEM,5,1
FITEM,5,3
FITEM,5,9
FITEM,5,11
FLST,5,2,5,ORDE,2
FITEM,5,1
FITEM,5,3

/ DEFINE MATERIAL PROPERTIES (CHAPTER 4.5)

TOFFST,273
MPTEMP
MPTEMP,1,25,204,427,538,593
MPTEMP,6,649,704,760,
MPDATA,EX,1,1,193e9,172e9,160.34e9,146.49e9,133.14e9
MPDATA,EX,1,6,101.8e9,79.8e9,66.2e9,
MPTEMP
MPTEMP,1,25,204,427,538,593
MPTEMP,6,649,704,760,
MPDATA,NUXY,1,1,0.285,0.285,0.285,0.285,0.285
MPDATA,NUXY,1,6,0.285,0.285,0.285,
MPTEMP
MPTEMP,1,0,100,200,500,700
MPTEMP,6,800,900,
MPDATA,ALPX,1,1,0.47e-5,0.48e-5,0.49e-5,0.52e-5,0.54e-5
MPDATA,ALPX,1,6,0.55e-05,0.56e-5,
MPTEMP
MPTEMP,1,0,100,200,500,700
MPTEMP,6,800,900,
MPDATA,DENS,1,1,8940,8936,8933,8923,8917
MPDATA,DENS,1,6,8914,8910,
MPTEMP
MPTEMP,1,25,
MPDATA,MU,1,1,1,
MPTEMP
MPTEMP,1,0,100,200,500,700
MPTEMP,6,800,900,
MPDATA,KXX,1,1,40.08,39.76,39.33,37.44,35.68
MPDATA,KXX,1,6,34.65,33.51,
MPTEMP
MPTEMP,1,0,100,200,500,700
MPTEMP,6,800,900,
MPDATA,C,1,1,460,484,507,578,625
MPDATA,C,1,6,648,672,
MPTEMP
MPTEMP,1,25,204,427,538,593
MPTEMP,6,649,704,760,
MPDATA,PRXY,1,1,0.285,0.285,0.285,0.285,0.285
MPDATA,PRXY,1,6,0.285,0.285,0.285,
MPTEMP
MPTEMP,1,0,100,200,500,700
MPTEMP,6,800,900,
MPDATA,REFT,1,1,25,25,25,25,25
MPDATA,REFT,1,6,25,25,
MPTEMP

MPTEMP,1,25,93,150,204,260
 MPTEMP,6,315,371,427,605,730,
 MPDATA,EX,2,1,95.3e9,92.4e9,92.1e9,87.79e9,79.13e9
 MPDATA,EX,2,6,80e9,80e9,80e9,80e9,80e9
 MPTEMP
 MPTEMP,1,0,100,200,500,700
 MPTEMP,6,800,900,
 MPDATA,ALPX,2,1,0.37e-5,0.37e-5,0.37e-5,0.39e-5,0.397e-5
 MPDATA,ALPX,2,6,0.40e-5,0.40e-5,
 MPTEMP
 MPTEMP,1,0,100,200,500,700
 MPTEMP,6,800,900,
 MPDATA,DENS,2,1,7860,7858,7856,7851,7848
 MPDATA,DENS,2,6,7846,7844,
 MPTEMP
 MPTEMP,1,25,
 MPDATA,MU,2,1,1,
 MPTEMP
 MPTEMP,1,0,100,200,500,700
 MPTEMP,6,800,900,
 MPDATA,KXX,2,1,376.85,374,370,356,343
 MPDATA,KXX,2,6,336,328,
 MPTEMP
 MPTEMP,1,0,100,200,500,700
 MPTEMP,6,800,900,
 MPDATA,C,2,1,386,392,397,413,423
 MPDATA,C,2,6,429,434,
 MPTEMP
 MPTEMP,1,25,93,150,204,260
 MPTEMP,6,315,371,427,605,730,
 MPDATA,PRXY,2,1,0.337,0.337,0.337,0.337,0.337
 MPDATA,PRXY,2,6,0.337,0.337,0.337,0.337,0.337,
 MPTEMP
 MPTEMP,1,0,100,200,500,700
 MPTEMP,6,800,900,
 MPDATA,REFT,2,1,25,25,25,25,25
 MPDATA,REFT,2,6,25,25,

/ DEFINE STRESS-STRAIN CURVE FOR MULTILINEAR ISOTROPIC HARDENING BEHAVIOR (CHAPTER 3.1.4 AND CHAPTER 4.5)

TB,MISO,1,8,7,
 TBTEMP,25
 TBPT,,0.0033,637.35e6
 TBPT,,0.0042,670.97e6
 TBPT,,0.0067,711.22e6

TBPT,,0.01,737.63e6
TBPT,,0.014,755.03e6
TBPT,,0.018,764.93e6
TBPT,,0.02,766.18e6
TBTEMP,204
TBPT,,0.0035,602.43e6
TBPT,,0.0042,638.28e6
TBPT,,0.0067,679.84e6
TBPT,,0.01,708.49e6
TBPT,,0.014,727.16e6
TBPT,,0.018,737.42e6
TBPT,,0.02,739.5e6
TBTEMP,427
TBPT,,0.0035,561.18e6
TBPT,,0.0042,591e6
TBPT,,0.0067,629.93e6
TBPT,,0.01,656.39e6
TBPT,,0.014,673.84e6
TBPT,,0.018,682.79e6
TBPT,,0.020,684.94e6
TBTEMP,538
TBPT,,0.0035,512.74e6
TBPT,,0.0042,541.3e6
TBPT,,0.0067,581.47e6
TBPT,,0.01,606.68e6
TBPT,,0.014,625.35e6
TBPT,,0.018,634.29e6
TBPT,,0.02,636.45e6
TBTEMP,593
TBPT,,0.003,399.44e6
TBPT,,0.0035,426.65e6
TBPT,,0.0067,479.63e6
TBPT,,0.01,506.06e6
TBPT,,0.014,524.73e6
TBPT,,0.018,534e6
TBPT,,0.020,537.04e6
TBTEMP,649
TBPT,,0.0022,224.13e6
TBPT,,0.0035,264.21e6
TBPT,,0.0067,303e6
TBPT,,0.01,323.05e6
TBPT,,0.014,338.25e6
TBPT,,0.018,345e6
TBPT,,0.020,347.96e6
TBTEMP,704
TBPT,,0.0016,127.72e6

TBPT,,0.0022,143e6
TBPT,,0.0042,165e6
TBPT,,0.0067,182e6
TBPT,,0.01,195.79e6
TBPT,,0.018,210.5e6
TBPT,,0.02,212.18e6
TBTEMP,760
TBPT,,0.00093,61.57e6
TBPT,,0.0022,72.59e6
TBPT,,0.0042,78.5e6
TBPT,,0.0067,85.5e6
TBPT,,0.01,90.32e6
TBPT,,0.018,96.123e6
TBPT,,0.020,98.19e6
TB,MISO,2,8,7,
TBTEMP,25
TBPT,,0.0027,257.28e6
TBPT,,0.0032,269.56e6
TBPT,,0.0067,294.96e6
TBPT,,0.01,306.97e6
TBPT,,0.014,315.58e6
TBPT,,0.017,319.02e6
TBPT,,0.02,320.03e6
TBTEMP,93
TBPT,,0.0026,240.26e6
TBPT,,0.0032,251.98e6
TBPT,,0.0067,273.75e6
TBPT,,0.01,283.34e6
TBPT,,0.014,291e6
TBPT,,0.017,294.25e6
TBPT,,0.02,295.25e6
TBTEMP,149
TBPT,,0.0024,222.02e6
TBPT,,0.0032,234e6
TBPT,,0.0067,256.1e6
TBPT,,0.01,266.37e6
TBPT,,0.014,275e6
TBPT,,0.017,278.4e6
TBPT,,0.02,279.4e6
TBTEMP,204
TBPT,,0.0021,184.36e6
TBPT,,0.0032,204.71e6
TBPT,,0.0067,229.5e6
TBPT,,0.01,241.52e6
TBPT,,0.014,251.34e6
TBPT,,0.017,254.76e6

```

TBPT,,0.02,256.37e6
TBTEMP,260
TBPT,,0.0022,174.1e6
TBPT,,0.0032,190e6
TBPT,,0.0067,209.5e6
TBPT,,0.01,219.1e6
TBPT,,0.014,226e6
TBPT,,0.017,230e6
TBPT,,0.02,230.9e6
TBTEMP,315
TBPT,,0.0001,8e6
TBPT,,0.0022,32.05e6
TBPT,,0.0042,42.7e6
TBPT,,0.01,58.485e6
TBPT,,0.014,64.667e6
TBPT,,0.017,67.0e6
TBPT,,0.02,67.883e6
TBTEMP,371
TBPT,,0.0001,8e6
TBPT,,0.0022,28.01e6
TBPT,,0.0042,37.153e6
TBPT,,0.01,50.607e6
TBPT,,0.014,56e6
TBPT,,0.017,58.4e6
TBPT,,0.02,59.4e6
TBTEMP,427
TBPT,,0.0001,8e6
TBPT,,0.0022,23.76e6
TBPT,,0.0042,30.49e6
TBPT,,0.01,41.517e6
TBPT,,0.014,45.88e6
TBPT,,0.017,47.68e6
TBPT,,0.02,48.5e6

```

/ DEFINE ATTRIBUTE TO THE LAYERS (CHAPTER 4.5)

```

CM,_Y,AREA
ASEL, , , ,P51X
CM,_Y1,AREA
CMSEL,S,_Y
!*
CMSEL,S,_Y1
AATT, 1, , 1, 0,
CMSEL,S,_Y
CMDELE,_Y
CMDELE,_Y1

```

```

!*
CM,_Y,AREA
ASEL, , , , 2
CM,_Y1,AREA
CMSEL,S,_Y
!*
CMSEL,S,_Y1
AATT, 2, , 1, 0,
CMSEL,S,_Y
CMDELE,_Y
CMDELE,_Y1

```

/ DESCRITIZE THE CONTINUUM (CHAPTER 4.3)

```

FLST,5,4,4,ORDE,4
FITEM,5,1
FITEM,5,3
FITEM,5,9
FITEM,5,11
CM,_Y,LINE
LSEL, , , ,P51X
CM,_Y1,LINE
CMSEL,,_Y
!*
LESIZE,_Y1, , ,12,1, , , ,1
!*
FLST,5,2,4,ORDE,2
FITEM,5,5
FITEM,5,7
CM,_Y,LINE
LSEL, , , ,P51X
CM,_Y1,LINE
CMSEL,,_Y
!*
LESIZE,_Y1, , ,36,1, , , ,1
!*
FLST,5,6,4,ORDE,6
FITEM,5,2
FITEM,5,4
FITEM,5,6
FITEM,5,8
FITEM,5,10
FITEM,5,12
CM,_Y,LINE
LSEL, , , ,P51X
CM,_Y1,LINE

```

```

CMSEL,,_Y
!*
LESIZE,_Y1,,0.5,,1,,,1
!*
MSHAPE,0,2D
MSHKEY,0
!*
FLST,5,3,5,ORDE,2
FITEM,5,1
FITEM,5,-3
CM,_Y,AREA
ASEL,,,,P51X
CM,_Y1,AREA
CHKMSH,'AREA'
CMSEL,S,_Y
!*
AMESH,_Y1
!*
CMDELE,_Y
CMDELE,_Y1
CMDELE,_Y2
!*
/UI,MESH,OFF
SAVE
!*
!*

```

/ DEFINE THAT CONTACT SURFACE IS ALWAYS BONDED(CHAPTER 4.6)

```

/COM, CONTACT PAIR CREATION - START
CM,_NODECM,NODE
CM,_ELEMCM,ELEM
CM,_KPCM,KP
CM,_LINECM,LINE
CM,_AREACM,AREA
CM,_VOLUCM,VOLU
/GSAV,cwz,gsav,,temp
MP,MU,2,1.0
MAT,2
MP,EMIS,2,
R,3
REAL,3
ET,2,169
ET,3,172
R,3,,,0.5,0.1,0,
RMORE,0.1,0.1,1.0E20,0.0,1.0,0.5

```

```

RMORE,0.0,340,1.0,,1.0,0.5
RMORE,0,1.0,1.0,0.0,,1.0
KEYOPT,3,3,0
KEYOPT,3,4,0
KEYOPT,3,5,1
KEYOPT,3,7,2
KEYOPT,3,8,0
KEYOPT,3,9,0
KEYOPT,3,10,1
KEYOPT,3,11,0
KEYOPT,3,12,5
KEYOPT,3,2,0
KEYOPT,3,1,1
! Generate the target surface
LSEL,S,,2
CM,_TARGET,LINE
TYPE,2
NSLL,S,1
ESLN,S,0
ESURF,ALL
CMSEL,S,_ELEMCM
! Generate the contact surface
LSEL,S,,8
CM,_CONTACT,LINE
TYPE,3
NSLL,S,1
ESLN,S,0
ESURF,ALL
ALLSEL
ESEL,ALL
ESEL,S,TYPE,,2
ESEL,A,TYPE,,3
ESEL,R,REAL,,3
/PSYMB,ESYS,1
/PNUM,TYPE,1
/NUM,1
EPLOT
ESEL,ALL
ESEL,S,TYPE,,2
ESEL,A,TYPE,,3
ESEL,R,REAL,,3
CMSEL,A,_NODECM
CMDEL,_NODECM
CMSEL,A,_ELEMCM
CMDEL,_ELEMCM
CMSEL,S,_KPCM

```

```

CMDEL,_KPCM
CMSEL,S,_LINECM
CMDEL,_LINECM
CMSEL,S,_AREACM
CMDEL,_AREACM
CMSEL,S,_VOLUCM
CMDEL,_VOLUCM
/GRES,cwz,gsav
CMDEL,_TARGET
CMDEL,_CONTACT
/COM, CONTACT PAIR CREATION - END
CWZDELE,3,1,"
!*
!*
/COM, CONTACT PAIR CREATION - START
CM,_NODECM,NODE
CM,_ELEMCM,ELEM
CM,_KPCM,KP
CM,_LINECM,LINE
CM,_AREACM,AREA
CM,_VOLUCM,VOLU
/GSAV,cwz,gsav,,temp
MP,MU,2,1
MAT,2
MP,EMIS,2,0
R,4
REAL,4
ET,4,169
ET,5,175
R,4,,,0.5,0.1,0,
RMORE,0.1,0.1,1.0E20,0.0,1.0,0.5
RMORE,0.0,340,1.0,,1.0,0.5
RMORE,0,1.0,1.0,0.0,,1.0
RMORE,10.0
KEYOPT,5,3,0
KEYOPT,5,4,0
KEYOPT,5,5,1
KEYOPT,5,7,2
KEYOPT,5,8,0
KEYOPT,5,9,0
KEYOPT,5,10,1
KEYOPT,5,11,0
KEYOPT,5,12,5
KEYOPT,5,2,0
KEYOPT,5,1,1
! Generate the target surface

```

```

LSEL,S,,,2
CM,_TARGET,LINE
TYPE,4
NSLL,S,1
ESLN,S,0
ESURF,ALL
CMSEL,S,_ELEMCM
! Generate the contact surface
LSEL,S,,,8
CM,_CONTACT,LINE
TYPE,5
NSLL,S,1
ESLN,S,0
ESURF,ALL
ALLSEL
ESEL,ALL
ESEL,S,TYPE,,4
ESEL,A,TYPE,,5
ESEL,R,REAL,,4
/PSYMB,ESYS,1
/PNUM,TYPE,1
/NUM,1
EPLOT
ESEL,ALL
ESEL,S,TYPE,,4
ESEL,A,TYPE,,5
ESEL,R,REAL,,4
CMSEL,A,_NODECM
CMDEL,_NODECM
CMSEL,A,_ELEMCM
CMDEL,_ELEMCM
CMSEL,S,_KPCM
CMDEL,_KPCM
CMSEL,S,_LINECM
CMDEL,_LINECM
CMSEL,S,_AREACM
CMDEL,_AREACM
CMSEL,S,_VOLUCM
CMDEL,_VOLUCM
/GRES,cwz,gsav
CMDEL,_TARGET
CMDEL,_CONTACT
/COM, CONTACT PAIR CREATION - END
!*
!*
/COM, CONTACT PAIR CREATION - START

```

```

CM,_NODECM,NODE
CM,_ELEMCM,ELEM
CM,_KPCM,KP
CM,_LINECM,LINE
CM,_AREACM,AREA
CM,_VOLUCM,VOLU
/GSAV,cwz,gsav,,temp
MP,MU,1,1.0
MAT,1
MP,EMIS,1,
R,5
REAL,5
ET,6,169
ET,7,175
R,5,,0.5,0.1,0,
RMORE,0.1,0.1,1.0E20,0.0,1.0,0.5
RMORE,0.0,40,1.0,,1.0,0.5
RMORE,0,1.0,1.0,0.0,,1.0
RMORE,10.0
KEYOPT,7,3,0
KEYOPT,7,4,0
KEYOPT,7,5,1
KEYOPT,7,7,2
KEYOPT,7,8,0
KEYOPT,7,9,0
KEYOPT,7,10,1
KEYOPT,7,11,0
KEYOPT,7,12,5
KEYOPT,7,2,0
KEYOPT,7,1,1
! Generate the target surface
LSEL,S,,6
CM,_TARGET,LINE
TYPE,6
NSLL,S,1
ESLN,S,0
ESURF,ALL
CMSEL,S,_ELEMCM
! Generate the contact surface
LSEL,S,,12
CM,_CONTACT,LINE
TYPE,7
NSLL,S,1
ESLN,S,0
ESURF,ALL
ALLSEL

```

```

ESEL,ALL
ESEL,S,TYPE,,6
ESEL,A,TYPE,,7
ESEL,R,REAL,,5
/PSYMB,ESYS,1
/PNUM,TYPE,1
/NUM,1
EPLT
ESEL,ALL
ESEL,S,TYPE,,6
ESEL,A,TYPE,,7
ESEL,R,REAL,,5
CMSEL,A,_NODECM
CMDEL,_NODECM
CMSEL,A,_ELEMCM
CMDEL,_ELEMCM
CMSEL,S,_KPCM
CMDEL,_KPCM
CMSEL,S,_LINECM
CMDEL,_LINECM
CMSEL,S,_AREACM
CMDEL,_AREACM
CMSEL,S,_VOLUCM
CMDEL,_VOLUCM
/GRES,cwz,gsav
CMDEL,_TARGET
CMDEL,_CONTACT
/COM, CONTACT PAIR CREATION - END
/MREP,EPLT
SAVE
!*

```

/ DEFINE LOAD AND BOUNDARY CONDITIONS (CHAPTER 4.2)

```

ANTYPE,4
!*
TRNOPT,FULL
LUMPM,0
!*
FLST,2,385,1,ORDE,2
FITEM,2,1
FITEM,2,-385
IC,P51X,TEMP,25, ,
FLST,2,6,4,ORDE,6
FITEM,2,1
FITEM,2,3

```

```

FITEM,2,5
FITEM,2,7
FITEM,2,9
FITEM,2,11
DL,P51X, ,SYMM
FLST,2,1,4,ORDE,1
FITEM,2,4
SAVE
*DIM,Load,TABLE,58,1,1,time, ,
!*
*DIM,conv,TABLE,3,1,1,time, ,
!*
*SET,LOAD(1,0,1) , 0
*SET,LOAD(1,1,1) , 25
*SET,LOAD(2,0,1) , 0.7
*SET,LOAD(2,1,1) , 357.28
*SET,LOAD(3,0,1) , 0.76
*SET,LOAD(3,1,1) , 425
*SET,LOAD(4,0,1) , 1
*SET,LOAD(4,1,1) , 462.5
*SET,LOAD(5,0,1) , 1.52
*SET,LOAD(5,1,1) , 506.45
*SET,LOAD(6,0,1) , 2.16
*SET,LOAD(6,1,1) , 544.27
*SET,LOAD(7,0,1) , 2.8
*SET,LOAD(7,1,1) , 573.3
*SET,LOAD(8,0,1) , 3.2
*SET,LOAD(8,1,1) , 598.5
*SET,LOAD(9,0,1) , 3.5
*SET,LOAD(9,1,1) , 615.32
*SET,LOAD(10,0,1) , 4.2
*SET,LOAD(10,1,1) , 632.12
*SET,LOAD(11,0,1) , 4.37
*SET,LOAD(11,1,1) , 646.64
*SET,LOAD(12,0,1) , 4.9
*SET,LOAD(12,1,1) , 658.09
*SET,LOAD(13,0,1) , 5.5
*SET,LOAD(13,1,1) , 671.83
*SET,LOAD(14,0,1) , 5.8
*SET,LOAD(14,1,1) , 680.23
*SET,LOAD(15,0,1) , 6.5
*SET,LOAD(15,1,1) , 688.61
*SET,LOAD(16,0,1) , 7
*SET,LOAD(16,1,1) , 697
*SET,LOAD(17,0,1) , 7.6
*SET,LOAD(17,1,1) , 707

```

*SET,LOAD(18,0,1) , 8.5
*SET,LOAD(18,1,1) , 715.3
*SET,LOAD(19,0,1) , 8.9
*SET,LOAD(19,1,1) , 723.7
*SET,LOAD(20,0,1) , 10
*SET,LOAD(20,1,1) , 735.5
*SET,LOAD(21,0,1) , 10.5
*SET,LOAD(21,1,1) , 602
*SET,LOAD(22,0,1) , 10.75
*SET,LOAD(22,1,1) , 552
*SET,LOAD(23,0,1) , 11.5
*SET,LOAD(23,1,1) , 518.7
*SET,LOAD(24,0,1) , 12.2
*SET,LOAD(24,1,1) , 489.63
*SET,LOAD(25,0,1) , 12.95
*SET,LOAD(25,1,1) , 463.62
*SET,LOAD(26,0,1) , 13.07
*SET,LOAD(26,1,1) , 446.79
*SET,LOAD(27,0,1) , 13.67
*SET,LOAD(27,1,1) , 429.96
*SET,LOAD(28,0,1) , 14.4
*SET,LOAD(28,1,1) , 412.34
*SET,LOAD(29,0,1) , 14.55
*SET,LOAD(29,1,1) , 398.6
*SET,LOAD(30,0,1) , 15.25
*SET,LOAD(30,1,1) , 384.79
*SET,LOAD(31,0,1) , 15.85
*SET,LOAD(31,1,1) , 378.65
*SET,LOAD(32,0,1) , 16
*SET,LOAD(32,1,1) , 369.5
*SET,LOAD(33,0,1) , 16.5
*SET,LOAD(33,1,1) , 357.2
*SET,LOAD(34,0,1) , 17.5
*SET,LOAD(34,1,1) , 349.5
*SET,LOAD(35,0,1) , 18
*SET,LOAD(35,1,1) , 338.8
*SET,LOAD(36,0,1) , 18.75
*SET,LOAD(36,1,1) , 328.09
*SET,LOAD(37,0,1) , 19.4
*SET,LOAD(37,1,1) , 319.66
*SET,LOAD(38,0,1) , 20.1
*SET,LOAD(38,1,1) , 307.4
*SET,LOAD(39,0,1) , 21
*SET,LOAD(39,1,1) , 294.3
*SET,LOAD(40,0,1) , 22
*SET,LOAD(40,1,1) , 285.17

```
*SET,LOAD(41,0,1) , 22.7
*SET,LOAD(41,1,1) , 274
*SET,LOAD(42,0,1) , 23.2
*SET,LOAD(42,1,1) , 269
*SET,LOAD(43,0,1) , 23.8
*SET,LOAD(43,1,1) , 261.4
*SET,LOAD(44,0,1) , 24.4
*SET,LOAD(44,1,1) , 255
*SET,LOAD(45,0,1) , 25
*SET,LOAD(45,1,1) , 248.36
*SET,LOAD(46,0,1) , 26
*SET,LOAD(46,1,1) , 238.39
*SET,LOAD(47,0,1) , 26.5
*SET,LOAD(47,1,1) , 233.02
*SET,LOAD(48,0,1) , 27.2
*SET,LOAD(48,1,1) , 226.1
*SET,LOAD(49,0,1) , 28
*SET,LOAD(49,1,1) , 218.4
*SET,LOAD(50,0,1) , 29
*SET,LOAD(50,1,1) , 209.2
*SET,LOAD(51,0,1) , 29.75
*SET,LOAD(51,1,1) , 203.8
*SET,LOAD(52,0,1) , 30.3
*SET,LOAD(52,1,1) , 196.1
*SET,LOAD(53,0,1) , 31.5
*SET,LOAD(53,1,1) , 186
*SET,LOAD(54,0,1) , 32.6
*SET,LOAD(54,1,1) , 181.6
*SET,LOAD(55,0,1) , 33
*SET,LOAD(55,1,1) , 176
*SET,LOAD(56,0,1) , 33.6
*SET,LOAD(56,1,1) , 172.38
*SET,LOAD(57,0,1) , 34.1
*SET,LOAD(57,1,1) , 167.7
*SET,LOAD(58,0,1) , 35
*SET,LOAD(58,1,1) , 161
*SET,CONV(1,0,1) , 0
*SET,CONV(1,1,1) , 1575
*SET,CONV(2,0,1) , 6.5
*SET,CONV(2,1,1) , 3150
*SET,CONV(3,0,1) , 35
*SET,CONV(3,1,1) , 3150
SAVE
!*
!*
/GO
```

```
DL,P51X, ,TEMP, %LOAD%
FLST,2,1,4,ORDE,1
FITEM,2,10
/GO
!*
!*
SFL,P51X,CONV, %CONV% , ,100,
SAVE
FINISH
```

/DEFINE SOLUTION OPTIONS (CHAPTER 5)

```
/SOL
!*
ANTYPE,4
!*
TRNOPT,FULL
LUMPM,0
!*
ANTYPE,4
NLGEOM,1
DELTIM,0.25,0,0.25
OUTRES,ERASE
OUTRES,ALL,1
KBC,0
NCNV,0,0,0,0,0
TIME,35
/GST,1,0
!*
OUTRES,ALL,ALL,
!*
SOLCONTROL,ON,1,
!*
!*
TIME,35
AUTOTS,-1
DELTIM,0.25,0,0.25,1
KBC,0
!*
/PNUM,KP,0
/PNUM,LINE,1
/PNUM,AREA,1
/PNUM,VOLU,0
/PNUM,NODE,0
/PNUM,TABN,0
/PNUM,SVAL,0
```

```
/NUMBER,1  
!*  
/PNUM,MAT,1  
/REPLOT  
  
!*  
TSRES,ERASE  
/STATUS,SOLU
```

APPENDIX C

RESULTS FOR MONOLAYER CYLIDRICAL MOLD (IR = 3.42'', OR = 4.15'',
THICKNESS = 0.52'')

APPENDIX C

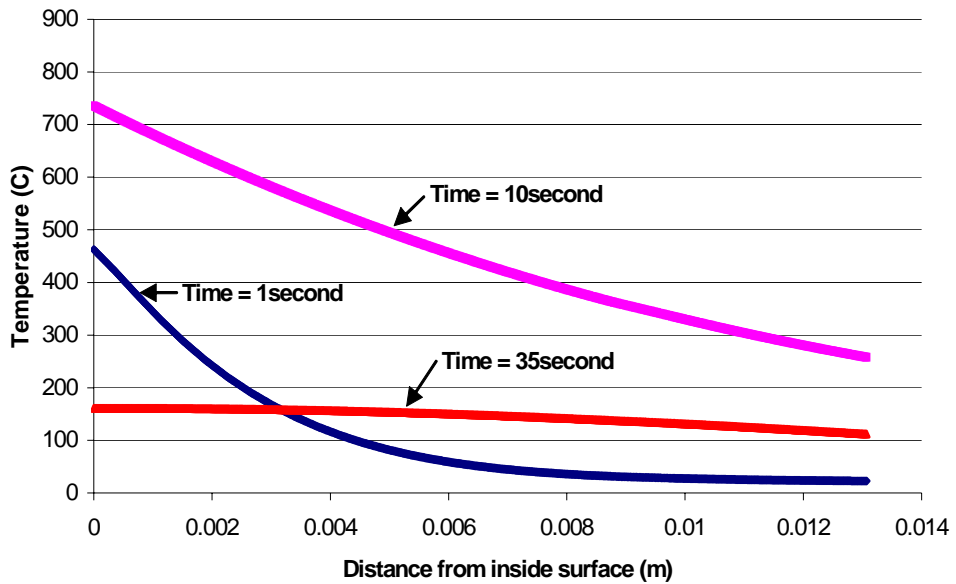


Figure C.1: Radial temperature (C) in monolayer cylinder at time 1,10 and 35 second

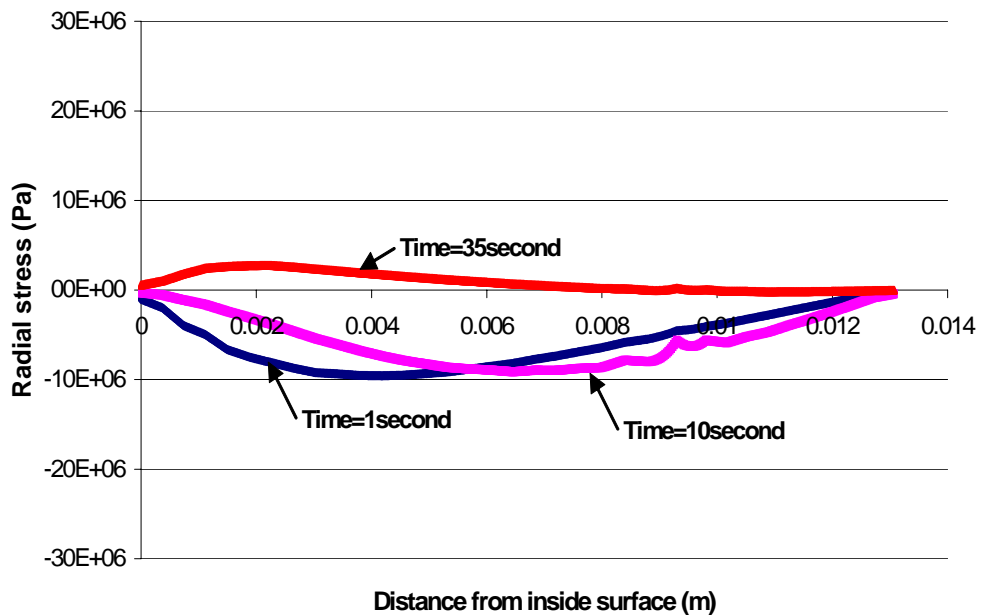


Figure C.2: Radial stress (Pa) in monolayer cylinder at time 1,10 and 35 second

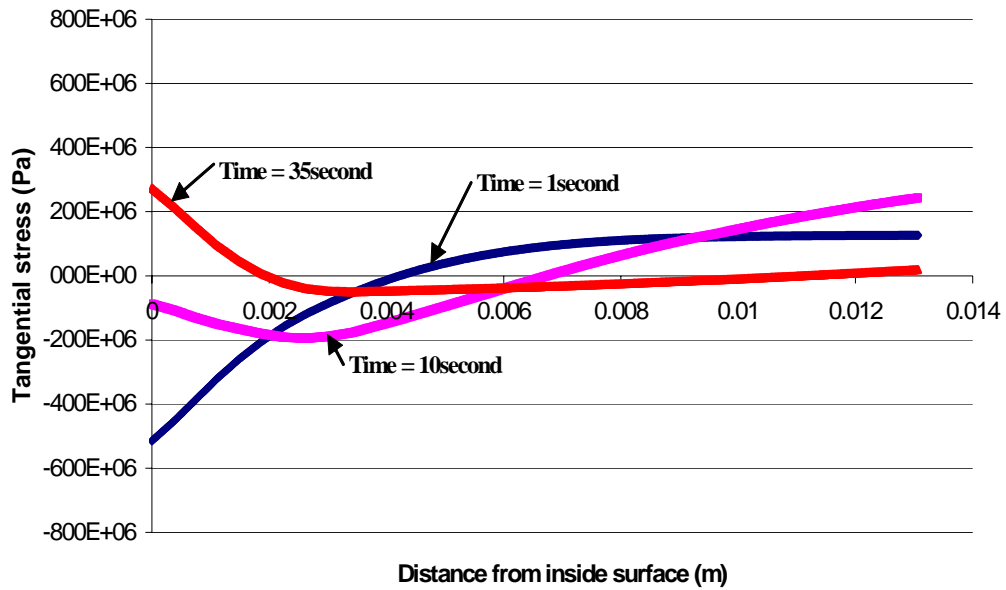


Figure C.3: Tangential stress (Pa) in monolayer cylinder at time 1,10 and 35 second

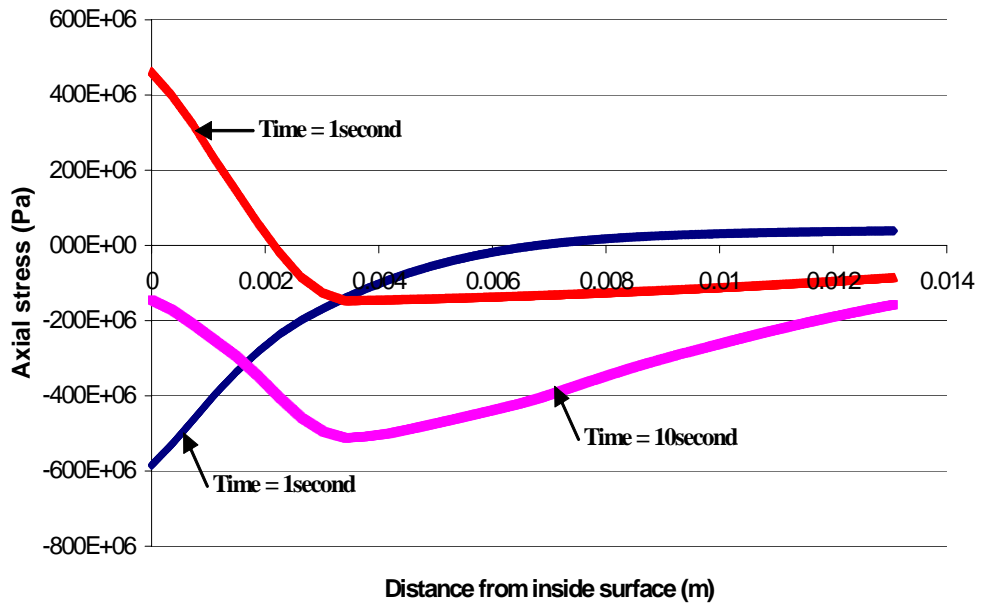


Figure C.4: Axial stress (Pa) in monolayer cylinder at time 1,10 and 35 second

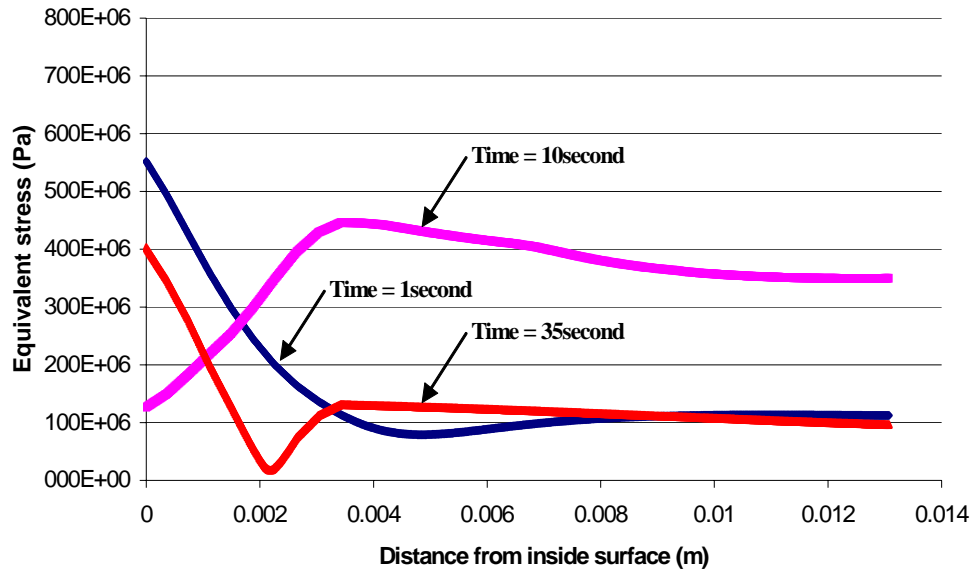


Figure C.5: Equivalent stress in monolayer cylinder at time 1,10 and 35 second

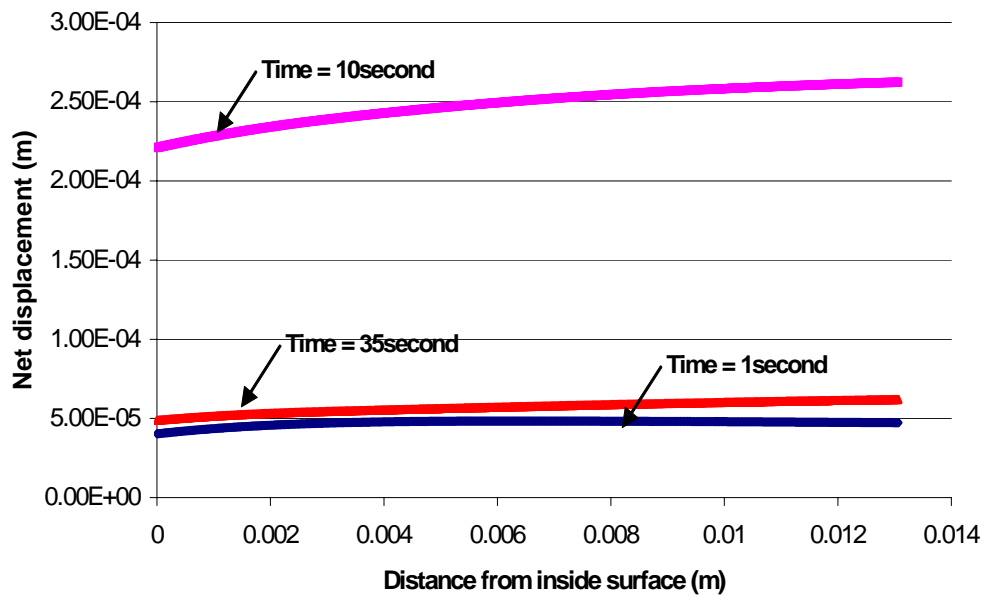


Figure C.6: Net displacement (m) in monolayer cylinder at time 1,10 and 35 second

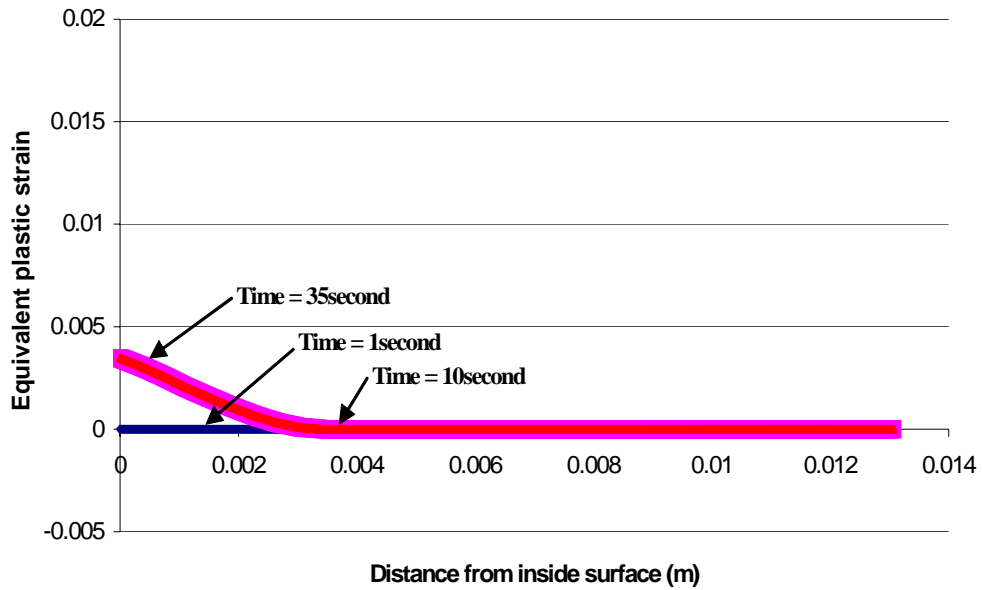


Figure C.6: Equivalent plastic strain in monolayer cylinder at time 1,10 and 35 second

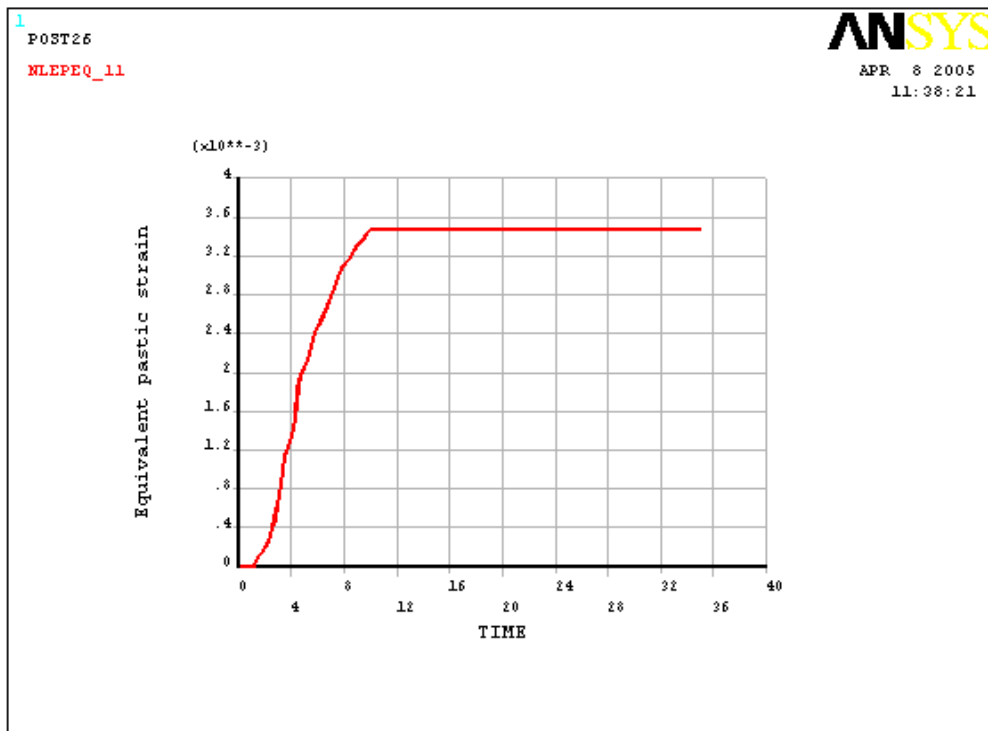


Figure C.8: Equivalent plastic strain in monolayer cylinder over time

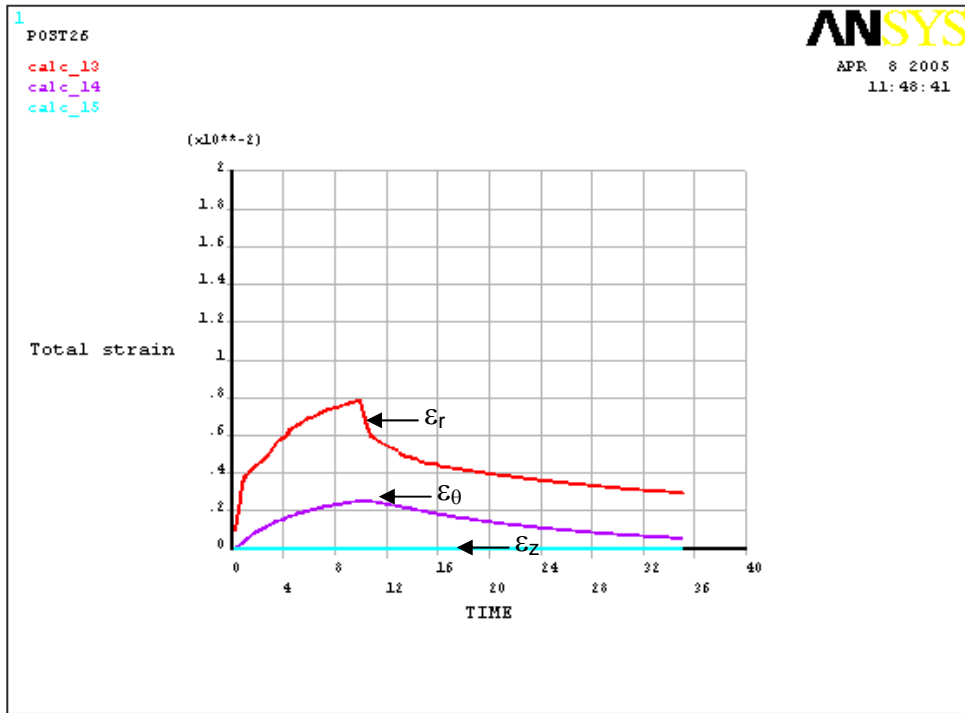


Figure C.9: Total strain in monolayer cylinder over time

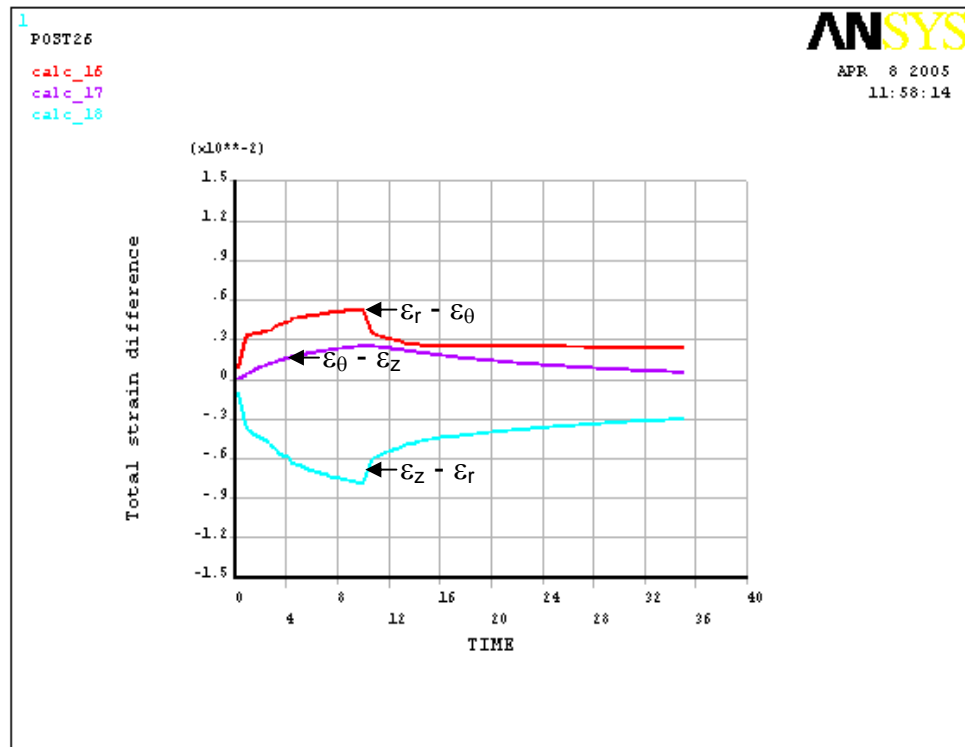


Figure C.10: Total strain difference in monolayer cylinder over time

APPENDIX D

RESULTS FOR MONOLAYER CYLIDRICAL MOLD (IR = 6.69'', OR = 7.63'',
THICKNESS = 0.95'')

APPENDIX D

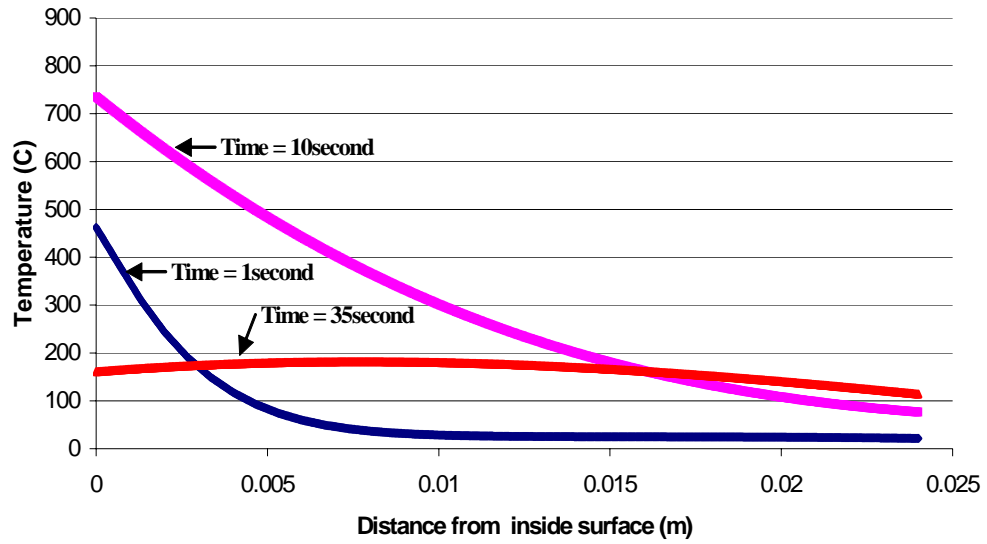


Figure D.1: Radial temperature (C) profile in monolayer cylinder at time 1,10 and 35 second

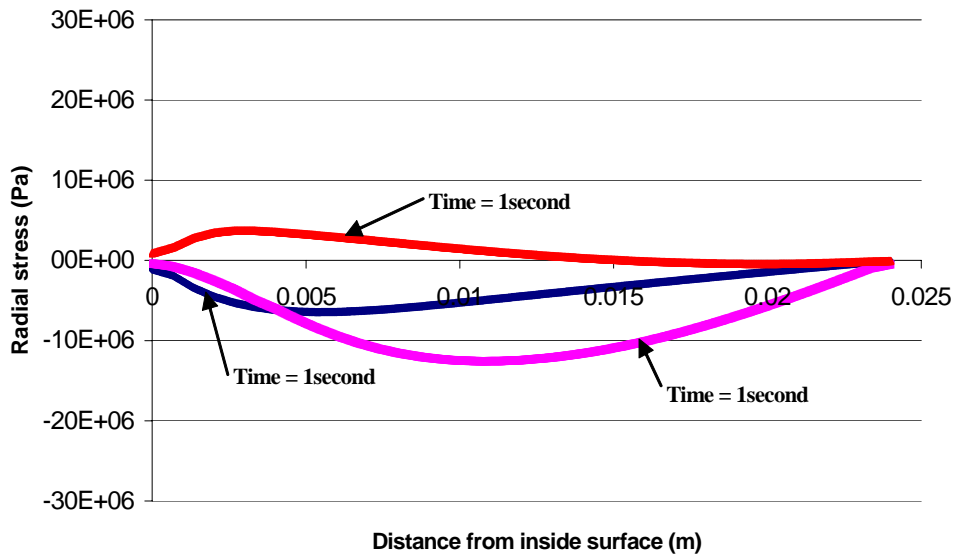


Figure D.2: Radial stress (Pa) in monolayer cylinder at time 1,10 and 35 second

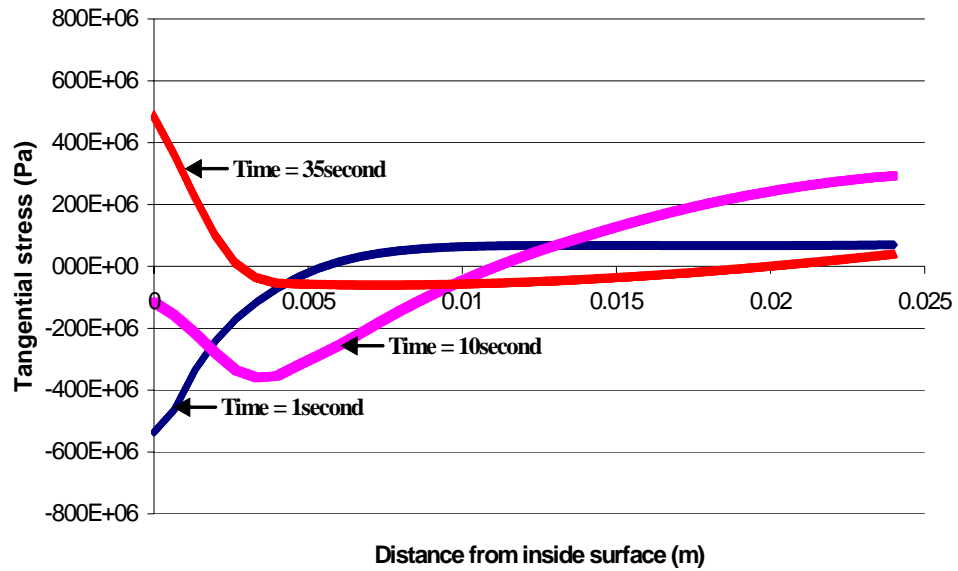


Figure D.3: Tangential stress (Pa) in monolayer cylinder at time 1,10 and 35 second

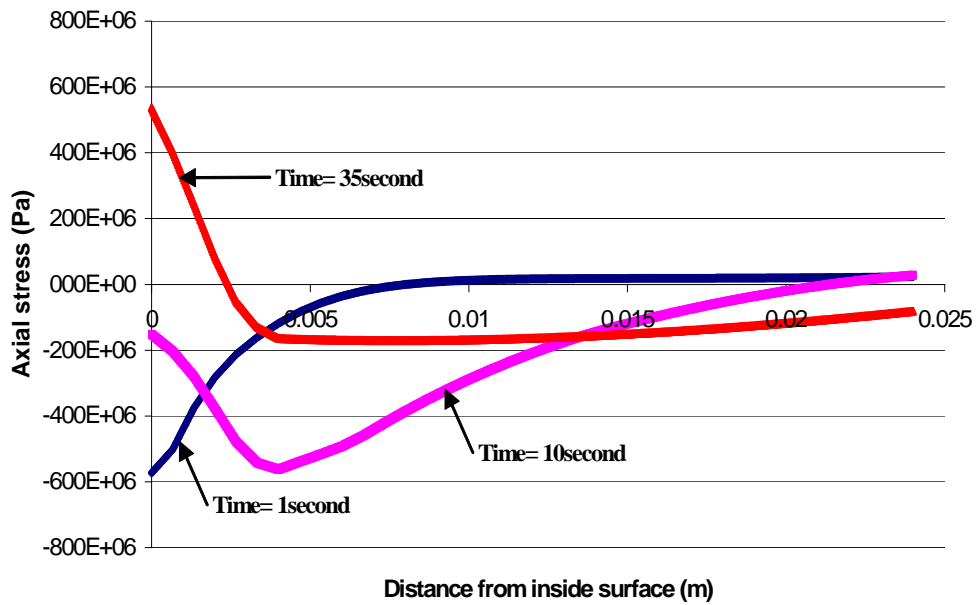


Figure D.4: Axial stress (Pa) in monolayer cylinder at time 1,10 and 35 second

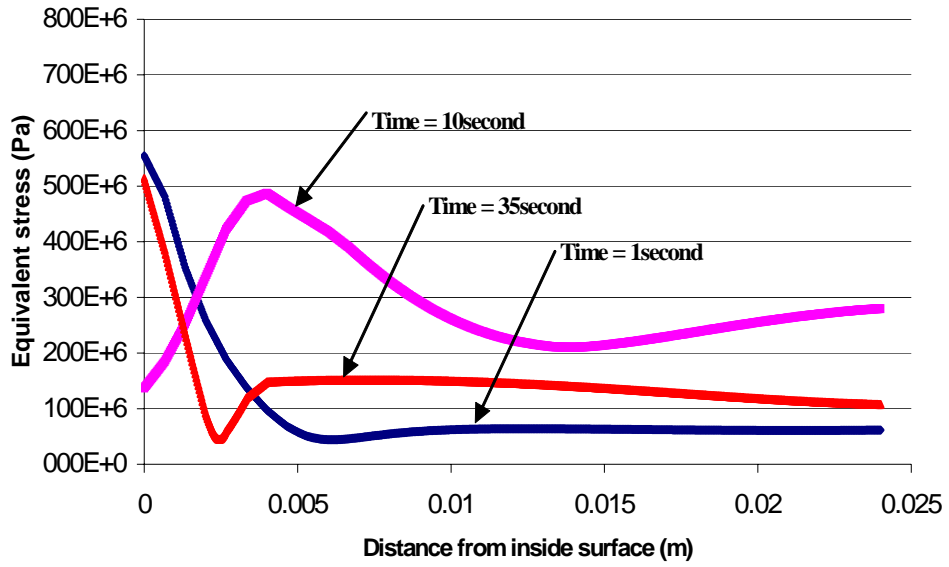


Figure D.5: Equivalent stress (Pa) in monolayer cylinder at time 1,10 and 35 second

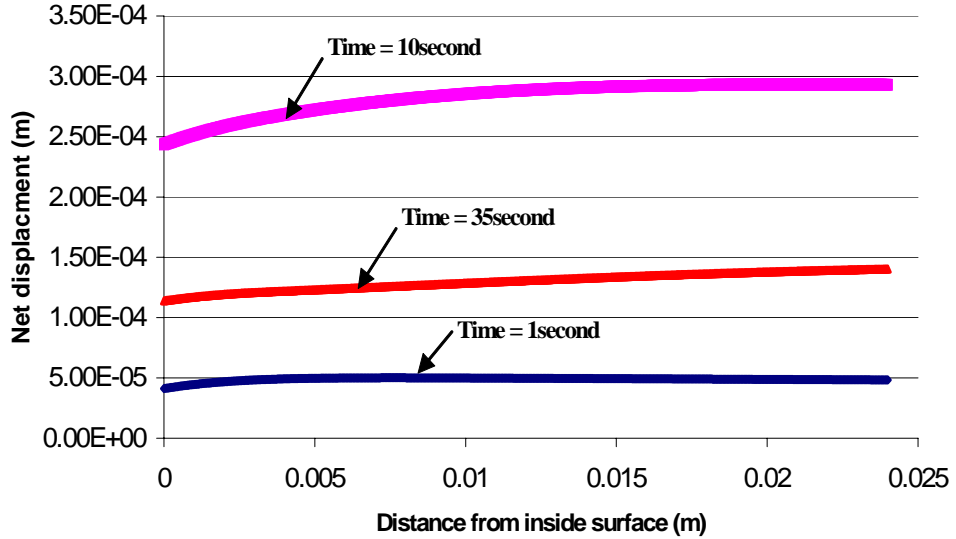


Figure D.6: Net displacement(m) in monolayer cylinder at time 1,10 and 35 second

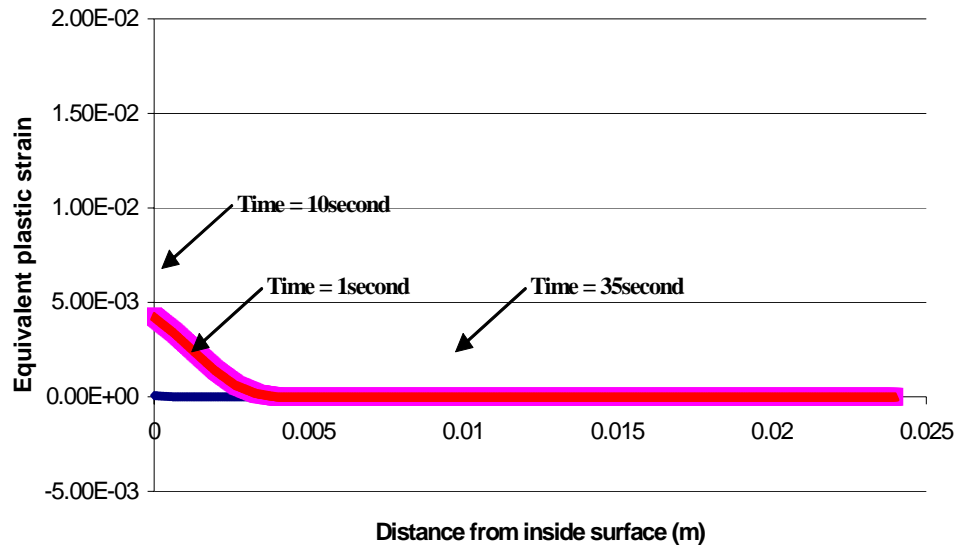


Figure D.7: Equivalent plastic strain in monolayer cylinder at time 1,10 and 35 second

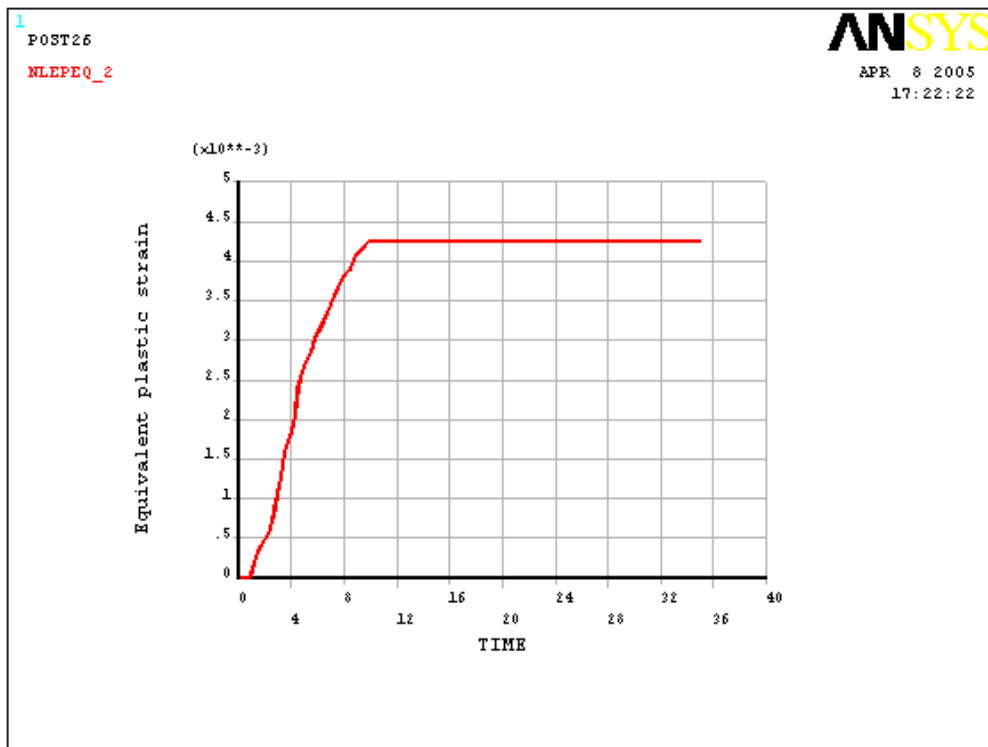


Figure D.8: Equivalent plastic strain in monolayer cylinder over time

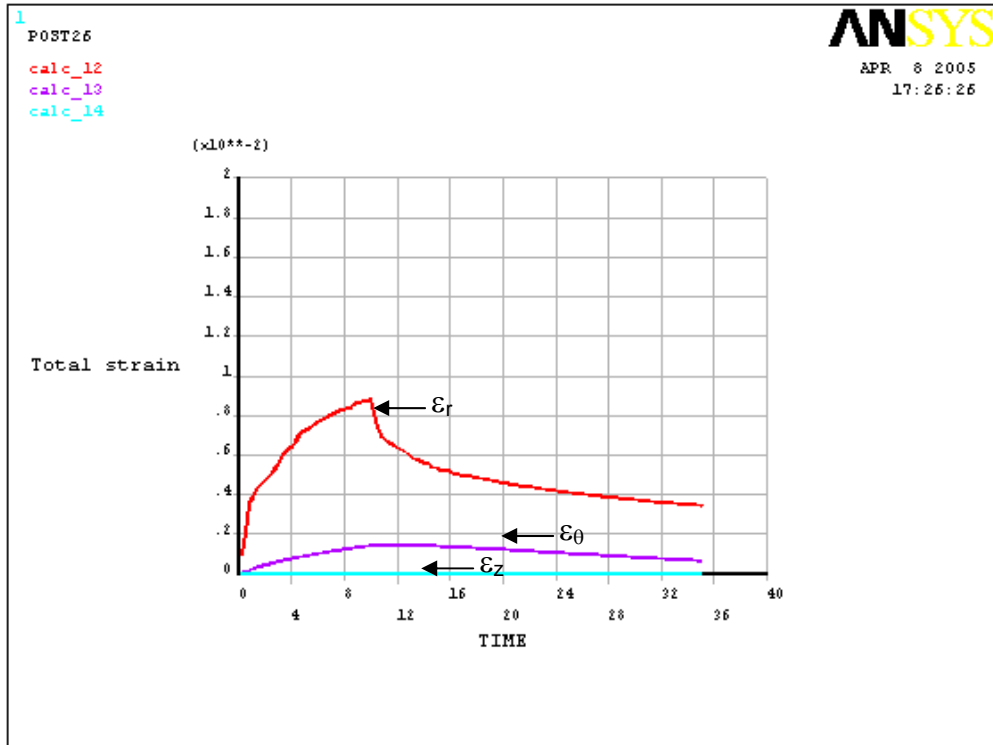


Figure D.9: Total strain in monolayer cylinder over time

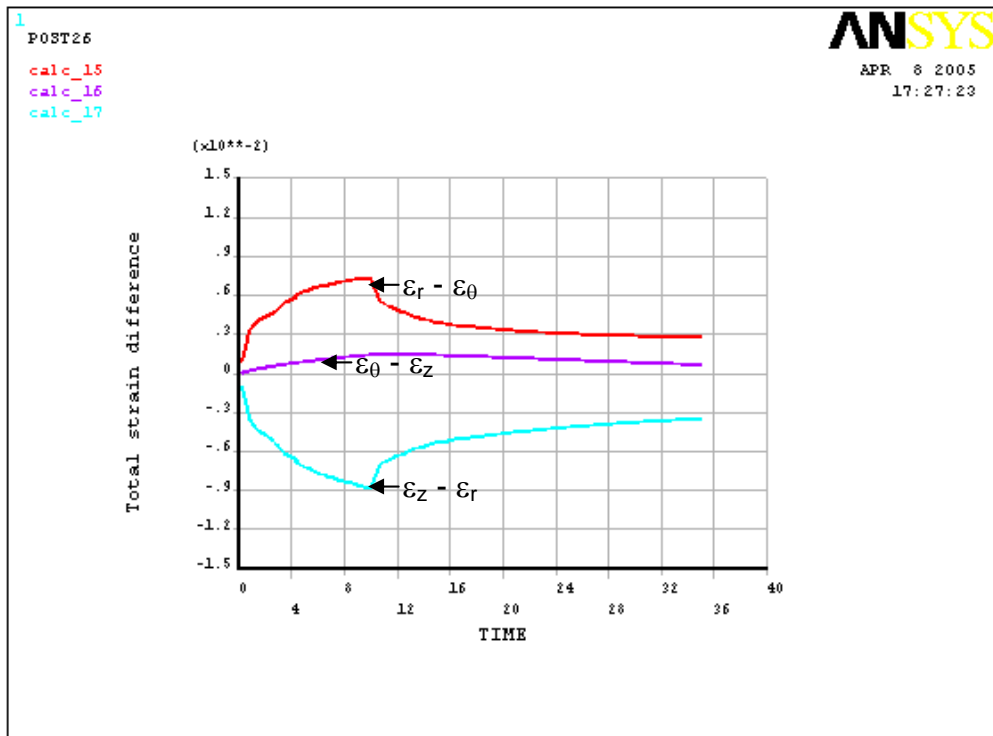


Figure D.10: Total strain difference in monolayer cylinder over time

APPENDIX E
RESULT FOR VALIDATION [12]

APPENDIX E

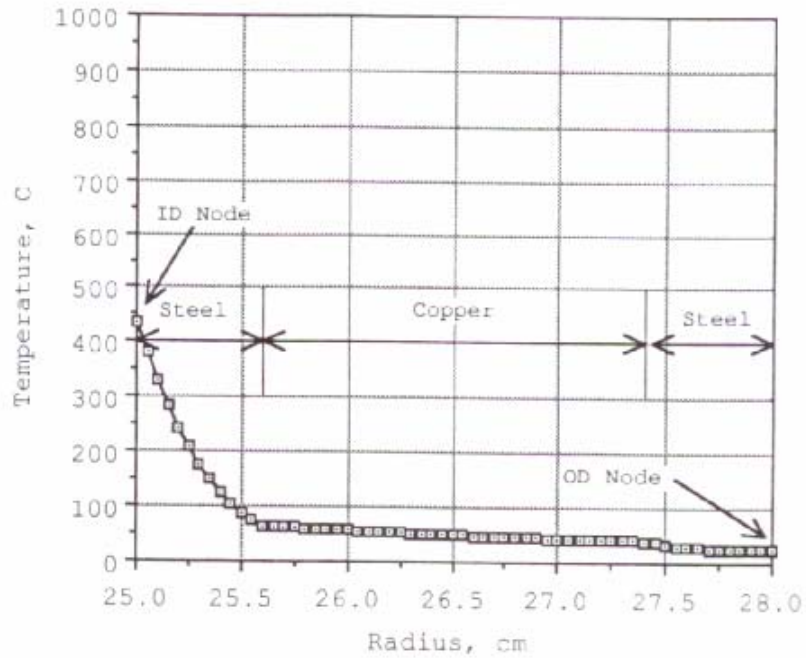


Figure E.1: Radial temperature profile in a composite tube with a 6 mm Steel OD layer – 18 mm Cu middle layer – 6 mm Steel ID Layer at 1second (Oliver, 1988)

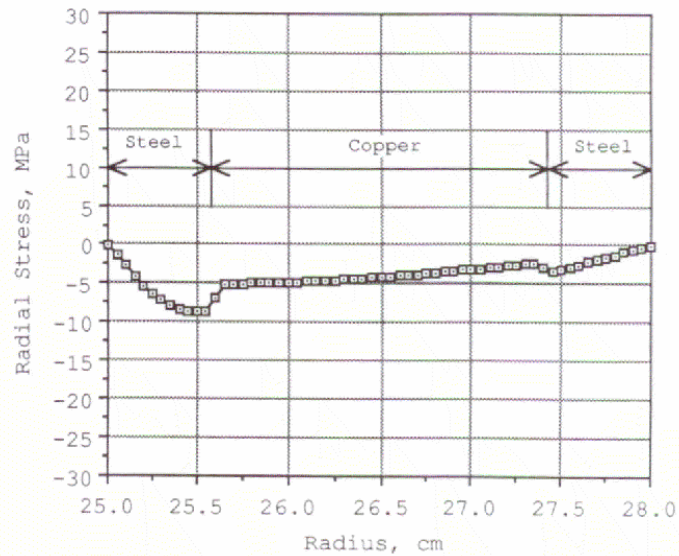


Figure E.2: Radial stress in a composite tube with a 6 mm Steel OD layer – 18 mm Cu middle layer – 6 mm Steel ID Layer at 1second (Oliver, 1988)

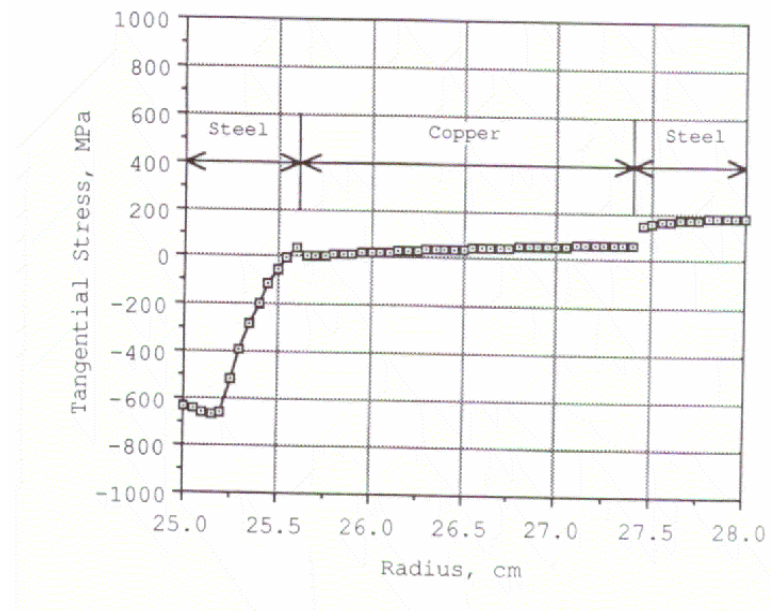


Figure E.3: Tangential stress in a composite tube with a 6 mm Steel OD layer – 18 mm Cu middle layer – 6 mm Steel ID Layer at 1second (Oliver, 1988)

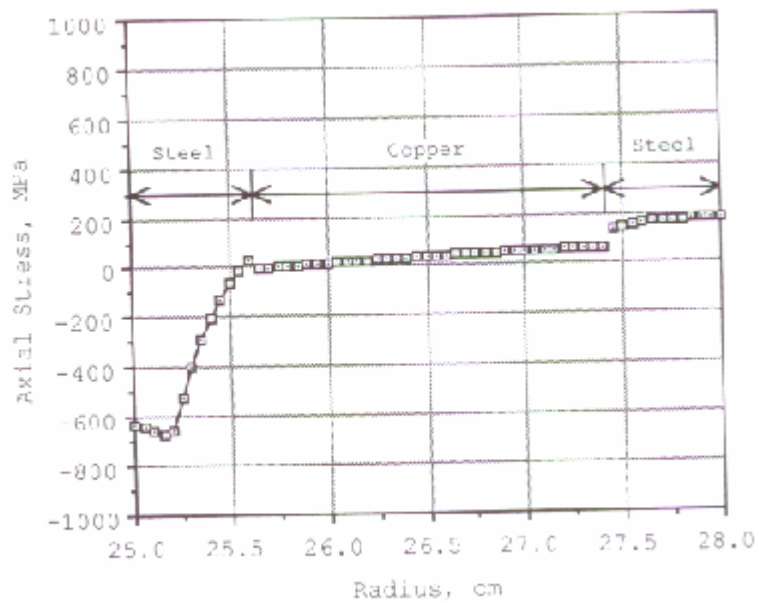


Figure E.4: stress in a composite tube with a 6 mm Steel OD layer – 18 mm Cu middle layer – 6 mm Steel ID Layer at 1 second (Oliver, 1988)

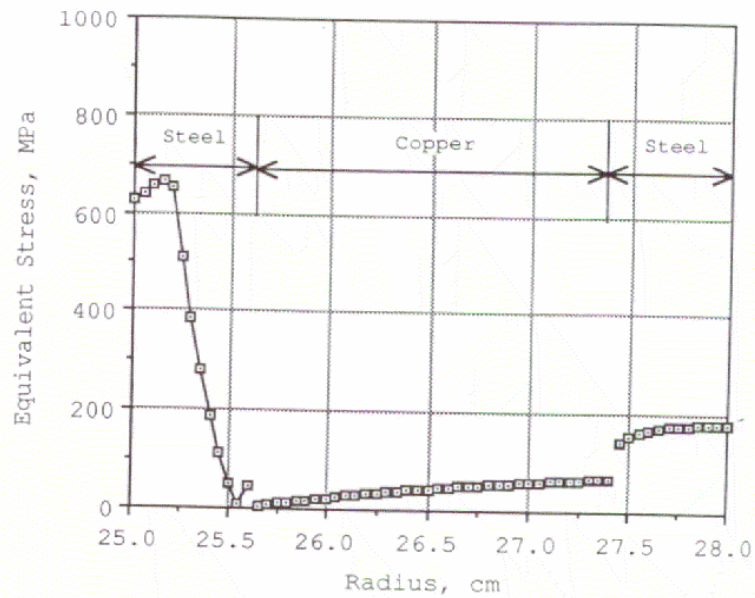


Figure E.5: Equivalent stress in a composite tube with a 6 mm Steel OD layer – 18 mm Cu middle layer – 6 mm Steel ID Layer at 1 second (Oliver, 1988)

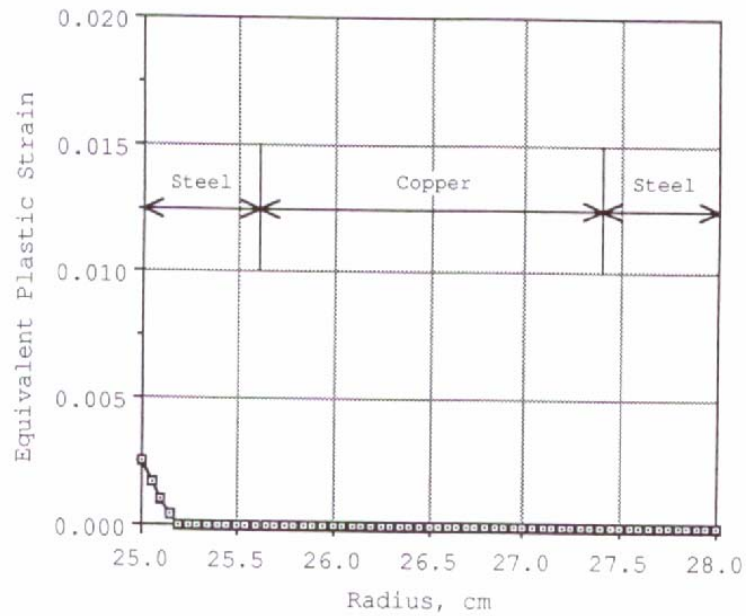


Figure E.6: Equivalent plastic strain in a composite tube with a 6 mm Steel OD layer – 18 mm Cu middle layer – 6 mm Steel ID Layer at 1 second (Oliver, 1988)

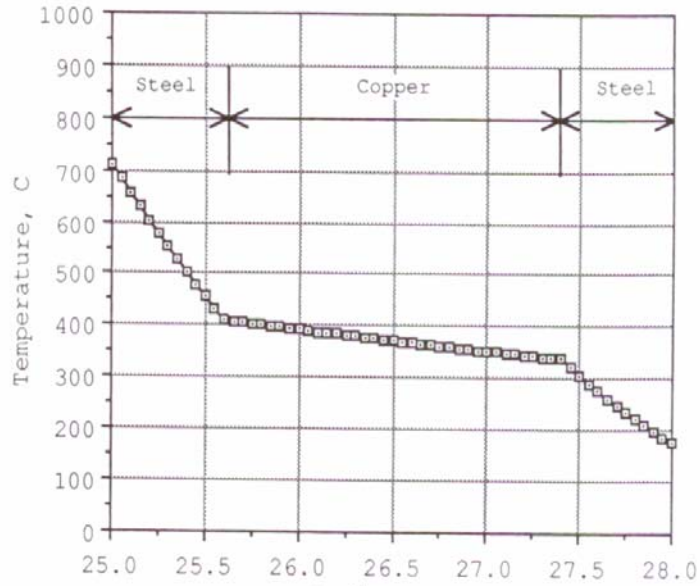


Figure E.7: Radial temperature profile in a composite tube with a 6 mm Steel OD layer – 18 mm Cu middle layer – 6 mm Steel ID Layer at 10 second (Oliver, 1988)

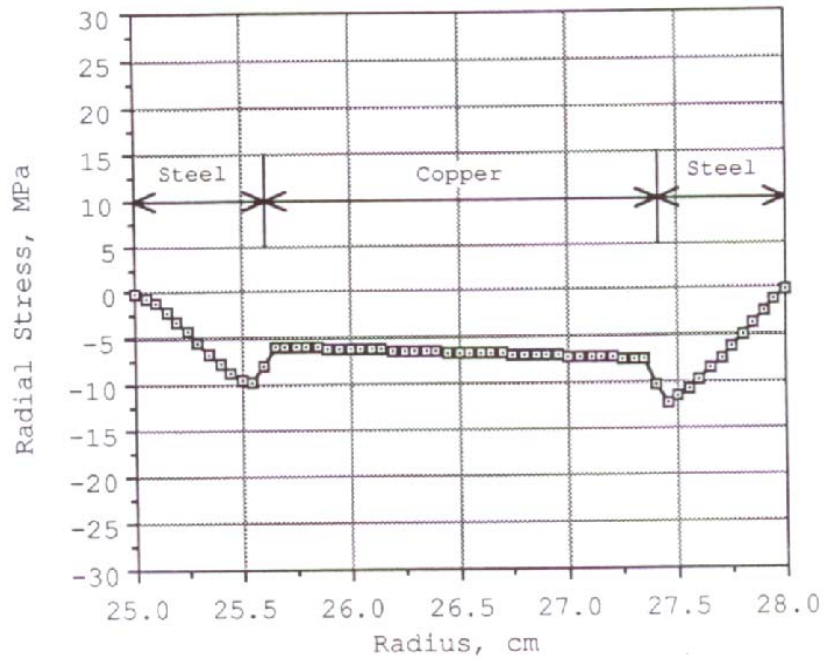


Figure E.8: Radial stress in a composite tube with a 6 mm Steel OD layer – 18 mm Cu middle layer – 6 mm Steel ID Layer at 10 second (Oliver, 1988)

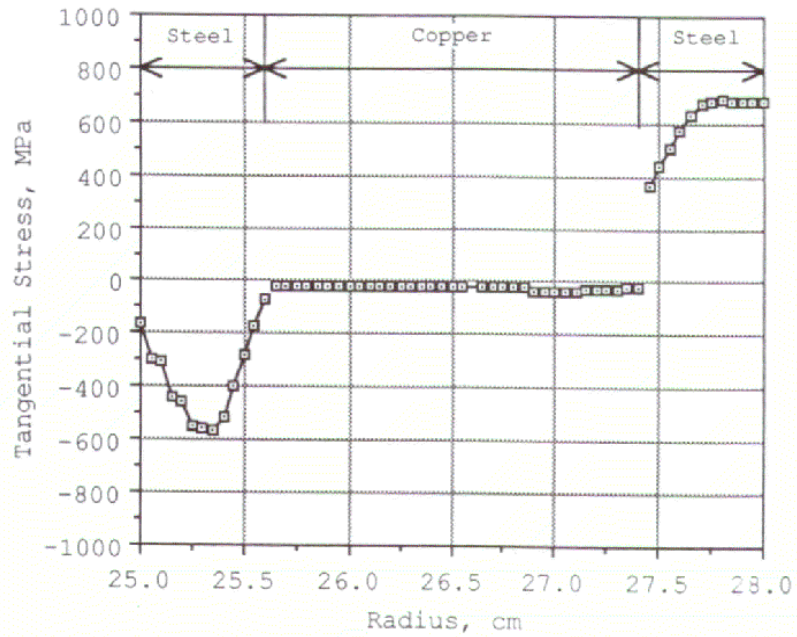


Figure E.9: Tangential stress in a composite tube with a 6 mm Steel OD layer – 18 mm Cu middle layer – 6 mm Steel ID Layer at 10 second (Oliver, 1988)

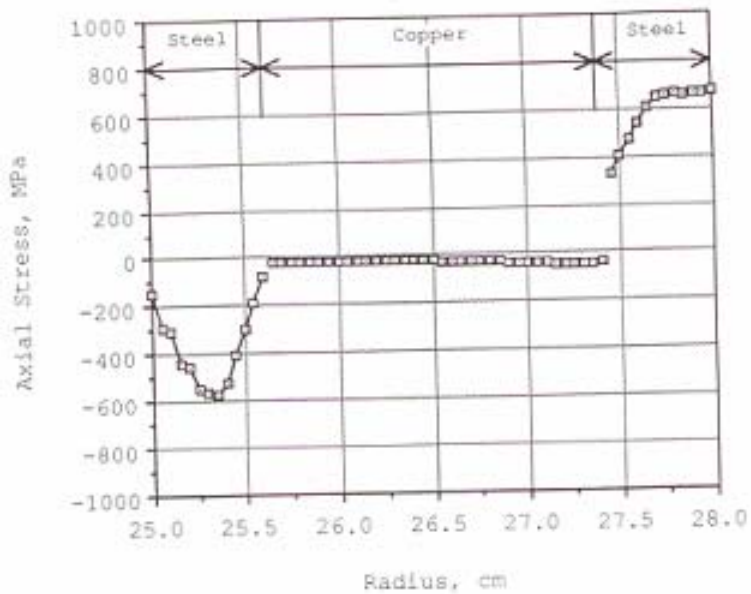


Figure E.10: Axial stress in a composite tube with a 6 mm Steel OD layer – 18 mm Cu middle layer – 6 mm Steel ID Layer at 10 second (Oliver, 1988)

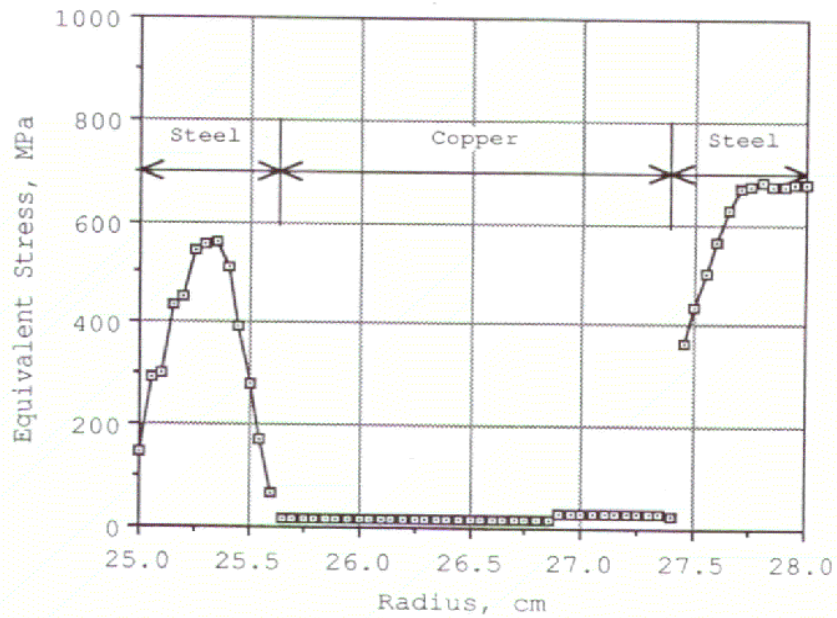


Figure E.11: Equivalent stress in a composite tube with a 6 mm Steel OD layer – 18 mm Cu middle layer – 6 mm Steel ID Layer at 10 second (Oliver, 1988)

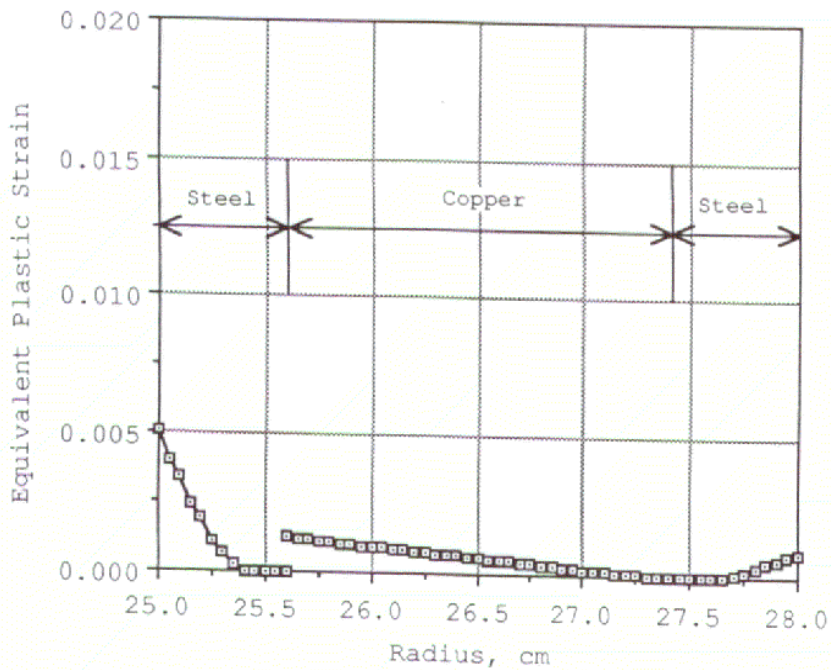


Figure E.12: Equivalent plastic strain in a composite tube with a 6 mm Steel OD layer – 18 mm Cu middle layer – 6 mm Steel ID Layer at 10 second (Oliver, 1988)

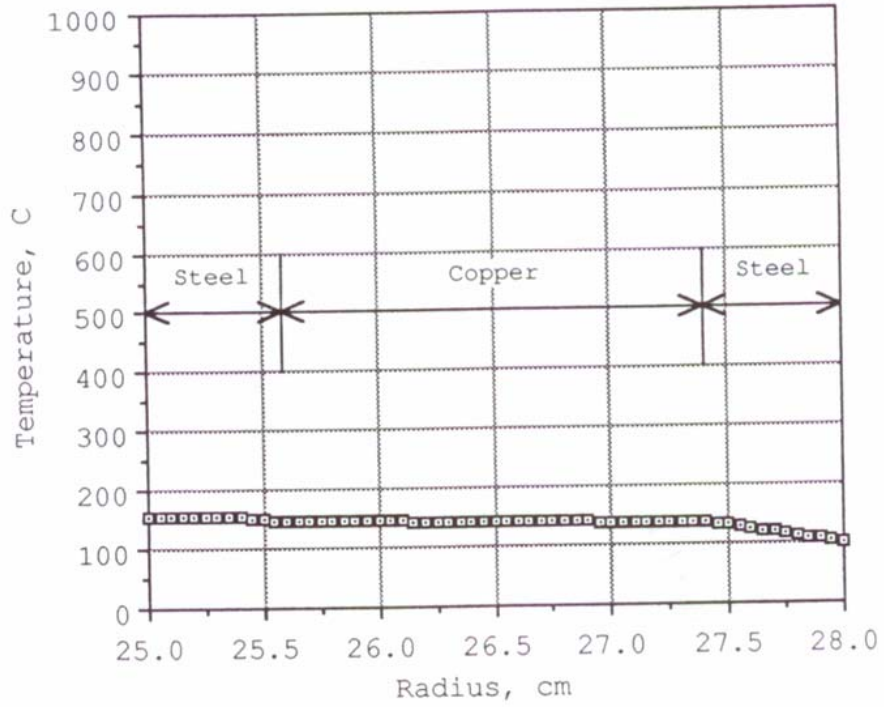


Figure E.13: Radial temperature profile in a composite tube with a 6 mm Steel OD layer – 18 mm Cu middle layer – 6 mm Steel ID Layer at 35 second (Oliver, 1988)

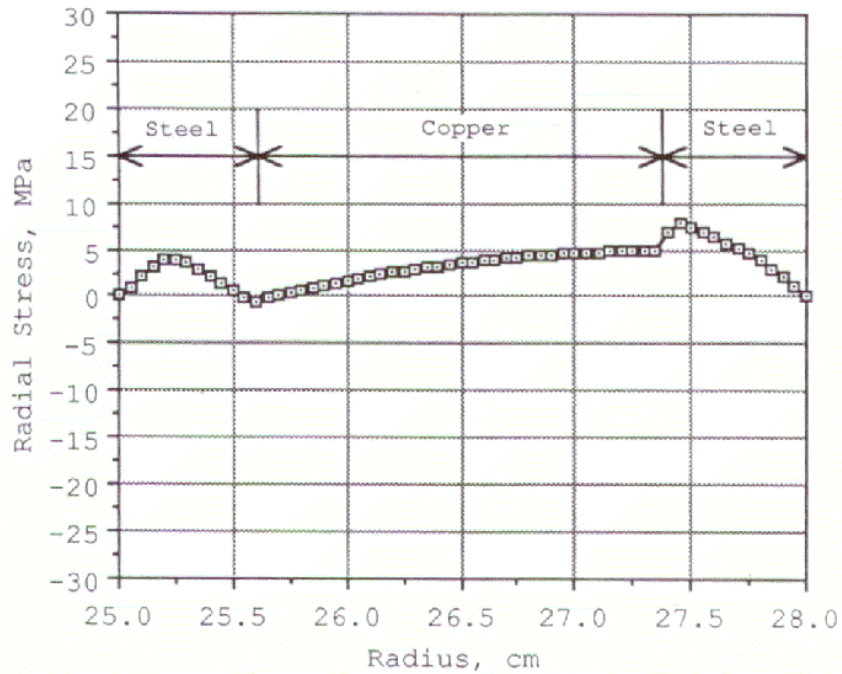


Figure E.14: Radial stress in a composite tube with a 6 mm Steel OD layer – 18 mm Cu middle layer – 6 mm Steel ID Layer at 35 second (Oliver, 1988)

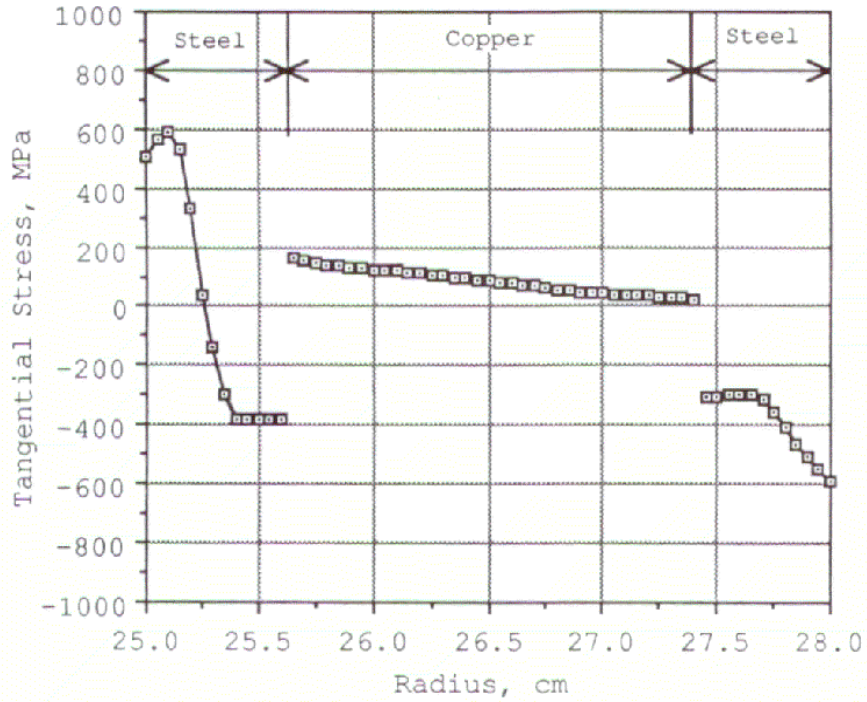


Figure E.15: Tangential stress in a composite tube with a 6 mm Steel OD layer – 18 mm Cu middle layer – 6 mm Steel ID Layer at 35 second (Oliver, 1988)

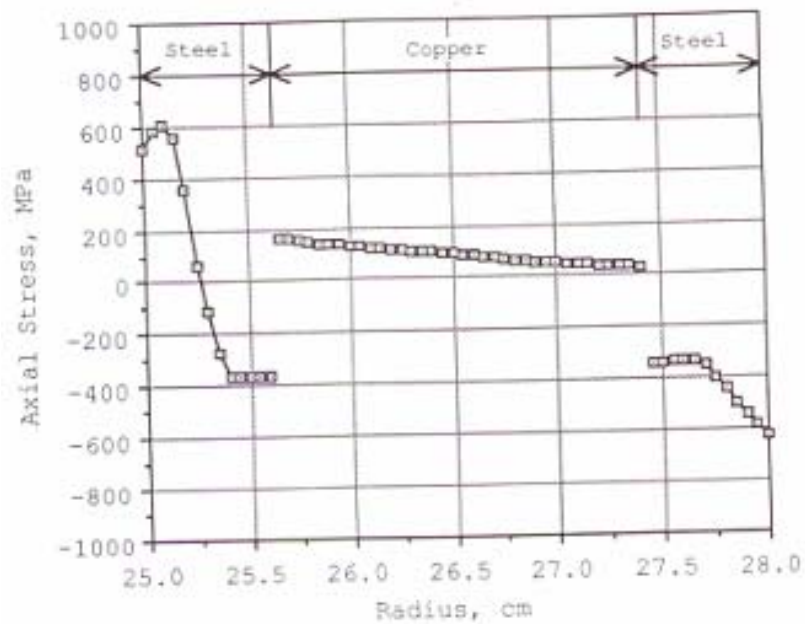


Figure E.16: Axial stress in a composite tube with a 6 mm Steel OD layer – 18 mm Cu middle layer – 6 mm Steel ID Layer at 35 second (Oliver, 1988)

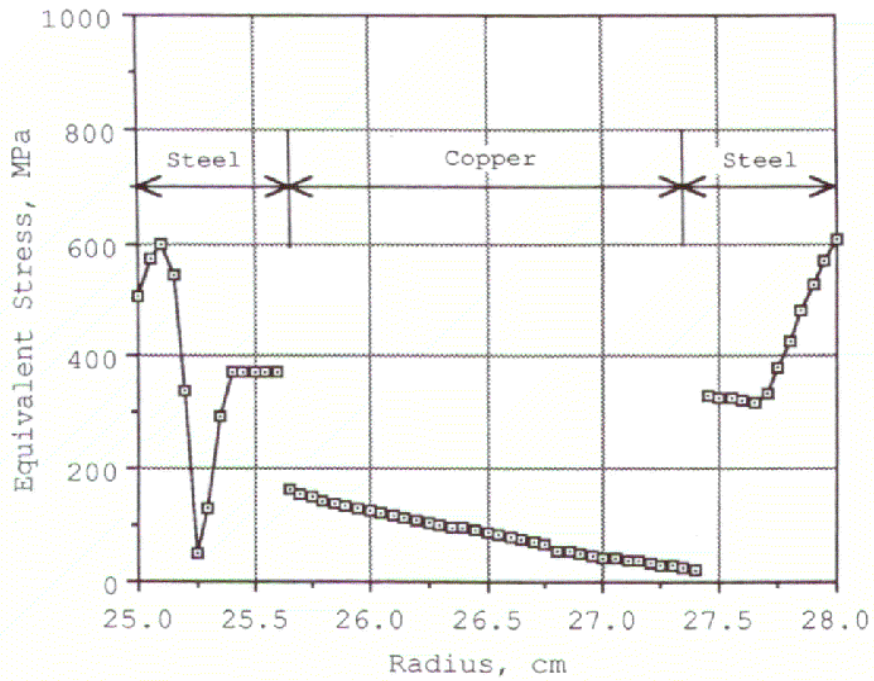


Figure E.17: Equivalent stress in a composite tube with a 6 mm Steel OD layer – 18 mm Cu middle layer – 6 mm Steel ID Layer at 35 second (Oliver, 1988)

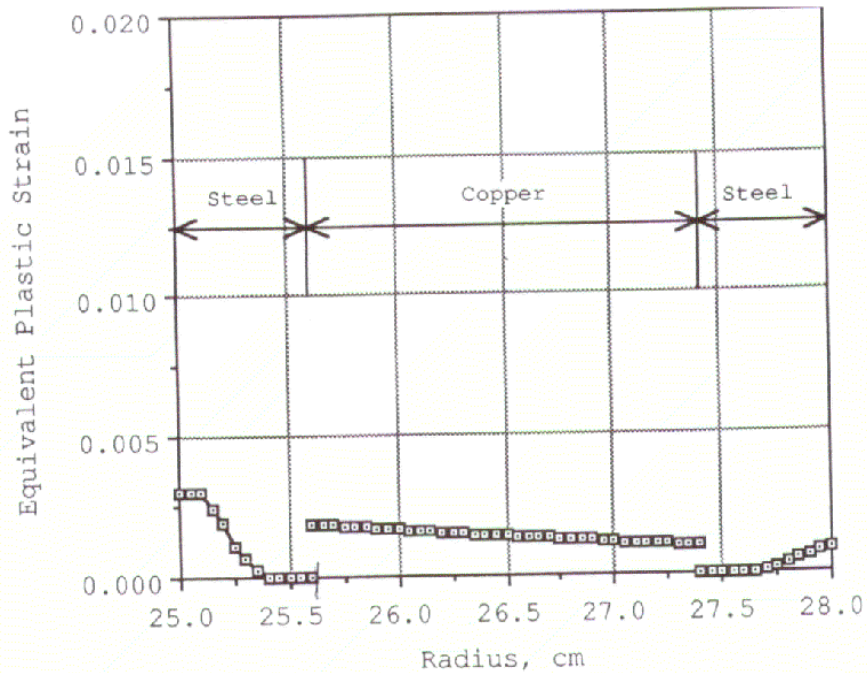


Figure E.18: Equivalent plastic strain in a composite tube with a 6 mm Steel OD layer – 18 mm Cu middle layer – 6 mm Steel ID Layer at 10 second (Oliver, 1988)

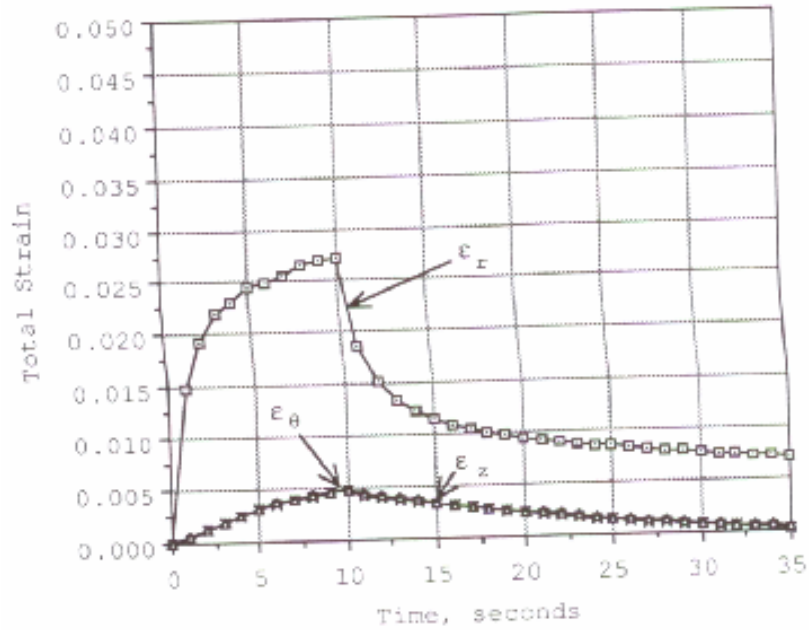


Figure E.19: Total strain in a composite tube with a 6 mm Steel OD layer – 18 mm Cu middle layer – 6 mm Steel ID Layer over time (Oliver, 1988)

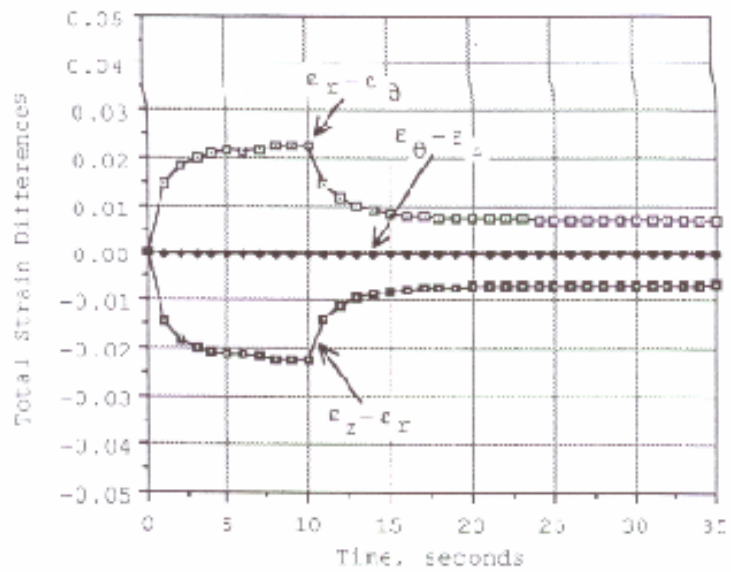


Figure E.20: Total strain difference in a composite tube with a 6 mm Steel OD layer – 18 mm Cu middle layer – 6 mm Steel ID Layer over time (Oliver, 1988)